



UNIVERSITY OF BERGAMO

School of Doctoral Studies

Doctoral Degree in Engineering and Applied Sciences

XXIX Cycle

SSD: ING-IND/10

**TITLE:**

**HYBRID THERMOSYPHON/PULSATING HEAT  
PIPE FOR GROUND AND SPACE APPLICATIONS**

**A novel two-phase passive heat transfer device**

Supervisor:

Chiar.mo Prof. Marco Marengo

Tutor:

Chiar.mo Prof. Elvio Cossali

Co-supervisor:

Dr. Mauro Mameli

The Chair of the Doctoral Program:

Chiar.mo Prof. Valerio Re

Doctoral Thesis

Daniele MANGINI

Student ID 1002675

Academic year 2015/16

*“Discovery consists of looking at the same thing as everyone else and  
thinking something different.”*

**Albert Szent-Györgyi**





---

## Abstract

---

**P**ulsating heat pipes (PHP) are very promising passive

heat transfer devices, simply made of a capillary tube and characterized by high thermal performance and extraordinary space adaptability. One of the main advantages with respect to Thermosyphons (TS) is that PHPs can work also without gravity assistance, making such technology interesting also for space applications. Nevertheless, the global heat power input that they can absorb is limited due to the capillary dimensions of the tube. The actual literature shows that it would be theoretically possible to build a hybrid TS/PHP with an Inner Diameter larger than the capillary limit, evaluated in normal gravity conditions, that works indeed as a loop thermosyphon on ground and switches to the typical PHP slug/plug operation when microgravity occurs. The aim of the present work is to prove the feasibility of such hybrid two-phase passive heat transfer device concept by means of a complete multi-parametric experimental campaign.

Therefore, during the first year of the doctoral thesis, a fully equipped hybrid TS/PHP experiment is designed and built at the Thermal Physics Laboratories of the University of Bergamo. Then, such device is tested both on ground and in hyper-micro gravity conditions during the 61<sup>th</sup> and the 63<sup>th</sup> ESA Parabolic Flight Campaign.

A thorough thermo-hydraulic characterization is performed on ground, varying important parameters such as the heat power input, the inclination angle, the ambient temperature and the heating elements position. It is found that a strategic arrangement of multiple heaters may be used in order to enhance the flow motion and consequently the thermal performance.

In micro-gravity, parabolic flight tests point out a PHP working mode. The sudden absence of buoyancy force activates an oscillating slug/plug flow regime, typical of the PHP operation, allowing the device to work in any orientation.

Although the present work demonstrates the feasibility of the TS/PHP concept, and that a strategic position of the heating elements promotes the two-phase flow motion, further tests in prolonged micro-gravity conditions (i.e. onboard a sub-orbital flight or, even better, the International Space) can point out the effective heat transfer performance in weightlessness conditions.

**KEY WORDS:** Pulsating Heat Pipe, Thermosyphon, hyper-gravity, micro-gravity.



---

## Summary

---

**F**or the very first time a novel hybrid two-phase passive heat

transfer device that act as a Multi-Evaporator Loop Thermosyphon on ground (Earth gravity level) and as a Pulsating Heat Pipe only in micro-gravity is designed, assembled and tested both on ground and in hyper/micro-gravity conditions .The main objectives of the thesis are:

- 1) To demonstrate its feasibility both on ground and in weightlessness;

- 2) To demonstrate that peculiar heating arrangement can promote the fluid flow circulation in a preferential direction.

Having this goal in mind, the thesis layout will be the following:

- *Chapter 1. Introduction: Two-Phase passive Heat Transfer Device for ground and Space Applications:* all the different two-phase passive heat transfer device such as Thermosyphons, Heat Pipes and Pulsating Heat Pipes are presented;
- *Chapter 2. PHP and compact loop thermosyphon: working principle and state of the art:* a detailed description on the PHP and compact loop thermosyphon working principle is provided;
- *Chapter 3. Design of the Test Cell:* a detailed description of the experimental apparatus is proposed;
- *Chapter 4. Results on Ground:* the results collected during the ground test campaigns performed, varying important parameters such as the inclination, the heat power input, the ambient temperature and the distribution of the heat power input at the evaporator zone are reported.
- *Chapter 5. Experiments in micro-gravity and design of the rack:* an excursus on the experimental facilities to test experiments in micro-gravity and a detailed description of the rack design is pointed out.
- *Chapter 6. Results obtained during the 61th ESA parabolic flight campaigns:* the results of the experimental analysis performed in reduced-gravity conditions during the 61th ESA Parabolic Flight Campaign are reported;

- *Chapter 7. Results obtained during the 63th ESA Parabolic Flight Campaign:* a report of the results of the experimental analysis performed in reduced-gravity conditions during the 63th ESA Parabolic Flight Campaign;
- *Chapter 8. Conclusions and future works:* the principal results of the entire work will be summarized and possible improvements will be proposed.

*Dopo tre anni passati così velocemente, eccomi arrivato qui alla fine del mio Dottorato di Ricerca. Tre anni bellissimi, difficilissimi ma pieni di soddisfazioni, che mi hanno sicuramente maturato sia umanamente che professionalmente. E' stato un percorso molto ripido, come quando si sale verso una cima impegnativa e piena di precipizi.. ma una volta arrivati su, ecco come tutto appare immenso, chiaro e ben delineato: che spettacolo!*

*Non ce l'avrei mai fatta senza tutte quelle persone che mi sono state vicine, che mi hanno stimolato e che mi hanno fatto sentire un membro importante all'interno di questo gruppo di ricerca "aerospaziale". Un grazie enorme lo devo senz'altro dire a Mauro, che con la sua pazienza e con il suo entusiasmo, è stato il migliore maestro che potessi mai avere in questi anni. A Lucio, che con la sua grande esperienza e la sua determinazione mi ha fatto crescere tantissimo in laboratorio, sia come ingegnere che come ricercatore. Al Prof. Marengo, che ha saputo gestire in modo abile anche situazioni molto delicate. A tutti i miei compagni di dottorato, Miriam, Claudio, Ileana, Dario e Fabio. Ai miei tesisti che hanno valorizzato ancora di più il lavoro svolto, in particolare Giulio Vanoli e Andreea. A Davide Fioriti, ottimo amico e grande ricercatore.*

*Un grazie enorme ai miei genitori, che mi hanno sempre valorizzato ed incoraggiato. A Luca e a Francesco, i miei fratelli che sono convinto potranno fare molto di più del sottoscritto.*

*A Marisa, la mia stupenda ragazza, che anche nei momenti più complicati mi bastava un suo sorriso per vedere tutto in modo più positivo. Con il suo volermi sempre bene, con la sua voglia di essermi vicino, nonostante molto spesso ci siano numerosi chilometri a separarci, mi ha reso questo cammino più facile rispetto a quello che fosse in realtà. Non ce la avrei forse mai fatta senza di te, Mari, e per questo voglio dedicarti questo lavoro.*









# Contents

<b>Contents .....</b>	<b>i</b>
<b>1. Introduction: Two-Phase Passive Heat Transfer Device for Ground and Space Applications .....</b>	<b>3</b>
1.1 Two-Phase Heat Transfer Devices .....	8
1.2 Thermosyphon: working principle and performance .....	12
1.2.1 Transport limitations .....	15
1.2.2 Thermosyphon operating with the “bubble lift principle” 16	
1.2.3 The reverse thermosyphon .....	19

1.3	Heat Pipes .....	21
1.3.1	Transport limitations .....	24
1.3.2	Types of Heat Pipes designed for electronic and space applications.....	25
1.4	The Pulsating Heat Pipe.....	31
<b>2.</b>	<b>PHP and compact Loop-Thermosyphon : working principles and state of the art .....</b>	<b>35</b>
2.1	Compact Loop Thermosyphons.....	36
2.1.1	Effect of the Inner Diameter.....	39
2.1.2	Effect of the working fluid .....	42
2.1.3	Effect of the Heat Power Input.....	46
2.1.4	Literature review Loop Thermosyphons with compact dimensions.....	47
2.2	Pulsating Heat Pipe for space applications.....	55
2.2.1	Main features of a PHP.....	56
2.2.2	PHP fundamental processes .....	57
2.2.3	Thermodynamics of a PHP.....	59
2.2.4	PHP in micro-gravity .....	62
2.3	Effects of a reduced gravity field on the capillary limits: the Space PHP concept.....	78
2.4	Stabilization of the two-phase flow motion within the PHP	

2.5	Motivations and thesis layout .....	93
<b>3.</b>	<b>Design of the test cell.....</b>	<b>98</b>
3.1	Choice of the inner diameter dimension .....	100
3.2	The proposed device .....	104
3.2.1	Vacuum tests and filling procedure .....	110
3.3	The heating element systems: symmetrical and non-symmetrical configuration .....	113
3.4	The heating element system: PWM control system to control the five heating elements independently .....	116
<b>4.</b>	<b>Ground tests.....</b>	<b>120</b>
4.1	Effect of the inclination angle, heat power input and position of the heating elements .....	121
4.1.1	Thermal Characterization in Vertical Position .....	123
4.1.2	Critical Heat Flux Analysis and comparison with standard thermosyphons .....	130
4.2	Effect of the inclination .....	135
4.3	Operational and flow regimes.....	140
<b>4.4</b>	<b>Effect of peculiar heating configurations at the evaporator</b>	<b>142</b>
<b>4.5</b>	<b>Effect of the ambient temperature.....</b>	<b>153</b>
<b>5.</b>	<b>Parabolic Flights and Rack Design .....</b>	<b>160</b>
5.1	Parabolic Flight Campaigns .....	161

5.2	Excursus on other possibilities to perform microgravity experiments.....	166
5.3	Structural requirements for the PFC: rack design .....	168
5.4	Test cell requirements.....	171
5.4.1	Test cell protection cage.....	175
5.4.2	Test cell vertical and horizontal support.....	176
5.4.3	Cage to protect the power supply, the DAQ system and the laptop	178
5.5	Electrical system .....	179
<b>6.</b>	<b>Results obtained in hyper and micro-gravity conditions: 61<sup>th</sup> ESA PFC.....</b>	<b>184</b>
6.1	Experimental procedure during the 61th ESA PFC.....	185
6.2	Results in vertical orientation.....	187
6.3	Results in horizontal orientation.....	195
<b>7.</b>	<b>Results obtained in hyper and micro-gravity conditions: 63<sup>th</sup> ESA PFC .....</b>	<b>199</b>
7.1	Experimental apparatus and procedure .....	201
7.2	Experimental results during the 63th PFC.....	203
7.2.1	Results obtained providing 50 W of global heat power input	204
7.2.2	Results obtained providing 70 W of global heat power input	208

7.2.3	Results obtained providing 90 W of global heat power input	210
<b>8.</b>	<b>Conclusions and future developments</b>	<b>215</b>
8.1	Effect of peculiar heating distributions	216
8.1.1	Main results on ground	216
8.1.2	Main results obtained in micro-gravity	220
8.2	Future developments	225
	<b>Acknowledgements</b>	<b>229</b>
	<b>Appendix</b>	<b>232</b>
	<b>List of publications</b>	<b>241</b>
	<b>List of figures</b>	<b>245</b>
	<b>List of tables</b>	<b>255</b>
	<b>Bibliography</b>	<b>259</b>
	<b>Nomenclature</b>	<b>279</b>





PART I

COMPACT TWO-PHASE  
PASSIVE HEAT  
TRANSFER DEVICE:  
THEORY AND  
KNOWLEDGE



---

# Chapter 1

## 1. Introduction: Two-Phase Passive Heat Transfer Device for Ground and Space Applications

As modern computer chips and power electronics become more densely packed and powerful<sup>1</sup>, the need of more efficient cooling systems increases. As a natural consequence of such ever-increasing trend, nowadays the net heat power input per unit area to dissipate from a chip is becoming unbearable for cooling devices that work mainly by sensible heat transfer.

# **1. Introduction: Two-Phase Passive Heat Transfer Devices for Ground and Space Applications**

---

Two-phase flow systems, in which latent heat due to phase change phenomena can improve the overall heat exchange, are becoming useful tools to dissipate the extremely high heat power input per area from electronic components, maintaining the working temperatures below a threshold value. The latent heat associated to the continuous phase change phenomena that occurs in such devices, coupled with the self-sustained two-phase flow motion between the hot and the cold section, is demonstrated to be a efficient heat transfer vector.

Additionally, according to the more optimistic scenario (Representative Concentration Pathway 2.6) expected by the Intergovernmental Panel on Climate Changes [1], an average 50% reduction of greenhouse emissions is required by 2050 with respect to '90 levels: the main goal is to obtain their substantial decline thereafter. Consequently, the energy consumption and the efficiency of several industrial processes are nowadays under the magnifying glass. Recent studies on information technology data centers showed that the rate of increase of their energy consumption is growing faster than several other major industries [2]. In particular, the electric energy required for electronic thermal management contributes to a large amount with respect to the total (up to 50% for data centers) for the increase of power densities of electronics. Indeed, heat dissipation is nowadays achieved through active systems, such as forced convection liquid loops or fans above the heat sinks directly mounted on the boards. In this context, the application of passive two-phase heat transfer devices would be a breakthrough solution: being very efficient heat flux spreaders, two-phase

## **1. Introduction: Two-Phase Passive Heat Transfer Devices for Ground and Space Applications**

---

passive devices are capable of reducing the extremely high heat powers per unit of surface generated by the electronics, to the lower heat fluxes that may be dissipated on larger and more accessible surfaces. This allows to substantially reduce the energy consumption absorbed by the active cooling systems in the case of optimized natural or mixed convection coolers, being such device completely passive.

Therefore, in the last decades the research on compact, reliable, efficient and cheap two-phase heat transfer device never damped out, not only strictly related to ground applications, but also in the area of space, where the great amount of heat load to dissipate or collect by large space radiators is becoming an important issue to solve. Additionally, further requirements have to take into account for the future long-term exploration space missions regarding the thermal control systems, such as long lifetime, constancy of heat transfer performance and the maintenance procedure simplification, reducing the mechanical parts in movement. Two-phase loop heat transfer device can answer to all of these requirements.

Nowadays, most of the electronic components in the International Space Station (ISS) are cooled by Active Control Systems (ATCS) [3]. AN ATCS uses a mechanically pumped fluid in closes loop circuits to perform different functions such as heat collection, heat transportation and heat rejection. Nevertheless, pumps need periodic maintenance, extremely difficult and dangerous to perform by astronauts within the ISS, considering that it is usually used ammonia in such systems as working fluid, extremely toxic for the human body. Two-phase passive heat transfer

## **1. Introduction: Two-Phase Passive Heat Transfer Devices for Ground and Space Applications**

---

devices, being passive, can avoid this problem. Furthermore, since phase change phenomena are involved in such systems, the heat fluxes that they can dissipate can be even higher than ATCS. Sintered heat pipes and loop heat pipes are already successfully implemented both on ground and in a great variety of space missions. Thanks to their capillary structure on the inner surface, the liquid phase is able to return efficiently from the condenser to the evaporator even if the device is not gravity assisted. However, the complex manufacturing procedure to create a proper capillary structure on the surface increase exponentially the production costs with respect to other “wickless” devices. In order to overcome this inconvenience, a relatively novel two-phase heat transfer device was invented by Akachi [3] in the 90s, named by the author Pulsating Heat Pipes (PHP). The PHP is simply a wickless capillary tube, bended in order to form U-turns both at the evaporator and at the condenser zone, firstly evacuated and then partially filled up with a refrigerant fluid. Thanks to the inner *capillary* dimensions of the tube, the liquid and the vapor phase reside inside the serpentine as an alternation of liquid slugs and vapor bubbles. The continue expansions and contractions of the vapor bubbles create an oscillating motion, able to be sustained also in micro-gravity conditions. The result is a passive, wickless and simple heat transfer device able to work both on ground and on space. After Akachi’s invention, the interest on PHPs is spreading day by day in the scientific community: their advantages, such as compactness, flexibility and the versatility to work without a gravity field are too promising to be ignored. PHPs have been

## **1. Introduction: Two-Phase Passive Heat Transfer Devices for Ground and Space Applications**

---

studied in different fields from that moment, such as in thermal management (electronics cooling, polymeric heat exchangers), heat recovery (thermal solar panels, hybrid TPV panels), and cooling of engines and batteries in automotive and aerospace applications. However, if in one hand these devices represent a cheap and flexible solution able to sustain its motion also in micro-gravity conditions, in the other one the global heat power input that they can dissipate is limited by the capillary dimension of the tube. Furthermore, a great number of operational and constructive parameters are involved, such as the inner diameter dimensions, the number of turns, the filling ratio, the working fluid properties, inclination, the effect of the gravity field, condenser and evaporator area extension, inclinations, etc. [4]. The effect of all of these parameters on the thermo-fluid dynamic behavior of the PHP is not yet clearly fully understood and results reported in literature are sometimes contradictory. The PHP technology is still on the research field essentially for these criticisms, and nowadays only sporadic real applications can be found. Furthermore, since the PHP is capillary, the removable global heat power input is limited by the small dimension of the tube. This is a crucial point regarding possible applications of the PHP technology in space missions, where a slug/plug flow motion activation is mandatory to guarantee the two-phase flow motion also without gravity. Nevertheless, the critical diameter, i.e. the threshold below which the two-phase flow is capillary, depends not only by the thermo-fluid dynamic properties of the selected fluid, but also by the gravity field. In fact, the body forces are negligible in micro-gravity and

# **1. Introduction: Two-Phase Passive Heat Transfer Devices for Ground and Space Applications**

---

the threshold diameter to obtain a slug/plug flow configuration increases. As a consequence, it is theoretically possible to increase the inner diameter dimensions, allowing a slug/plug flow activation only in micro-gravity conditions, permitting to the device to dissipate higher global heat power inputs.

## **1.1 Two-Phase Heat Transfer Devices**

The present chapter provides an excursus on the two-phase passive heat transfer technology, from the readily available Heat Pipes (HP) or Thermosyphons (TS) to the relatively new Pulsating Heat Pipe (PHP), patented in its most common assessment by Akachi [3] [5] in the early '90, with the aim to focus on the attractiveness of such devices.



# 1. Introduction: Two-Phase Passive Heat Transfer Devices for Ground and Space Applications

---

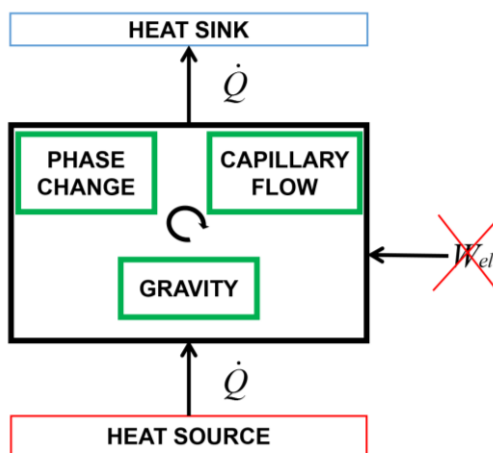


Figure 1.1 General schematic view of the capillary driven heat transfer device (Mameli, 2012) [7].

In general, two-phase heat transfer devices have the main objective to extract efficiently heat from a heat source and release it to a heat sink, with a two-phase flow motion that can be sustained, sometimes also without the assistance of gravity, thanks to the coupled action of phase transitions capillarity. In order to fulfill this main objective, the interplay between phase-change, gravity and capillarity is exploited for enhancing the heat transfer. Figure 1.1 shows a schematic view of the capillary driven two-phase heat transfer devices. The heat power input in the heat source generates phase-change phenomena: the liquid phase that resides in the heat source region evaporates, while the vapor phase that resides in the heat sink condensate. The phase-change phenomena generate a continuous and self-sustained two-phase flow motion, able to exchange heat in a very efficient

## **1. Introduction: Two-Phase Passive Heat Transfer Devices for Ground and Space Applications**

---

way. Such devices are called “passive”, in the sense that there is no need of pumps: it is the heat power input the effective “pumping force” of the two-phase flow motion. In other words, such devices are fully thermally driven, the two-phase flow motion and the heat exchange are intrinsically related between them. Therefore, there is no need of an electrical input. The gravity head between the heated and the cooled zone, as well as the implementation of a proper capillary structure, can promote the two-phase flow motion. Most of the times the three phenomena (capillarity, gravity and phase change phenomena) are acting together, but there are devices in which at least one of them do not participate:

- Thermosyphons: the capillary effects are negligible. In order to decrease the costs of the production, these devices do not present a capillary structure. Consequently, a Thermosyphon needs to be gravity assisted in order to work properly.
- Sintered Heat Pipes: in the most of the cases the gravity effects are negligible with respect to the capillary forces.

The higher value of the heat transfer coefficients related to the phase change phenomena with respect to the forced or natural single phase convection, allows the two-phase heat transfer devices to be a suitable candidate in the electronic cooling, both on ground and on space (Figure 1.2).

# 1. Introduction: Two-Phase Passive Heat Transfer Devices for Ground and Space Applications

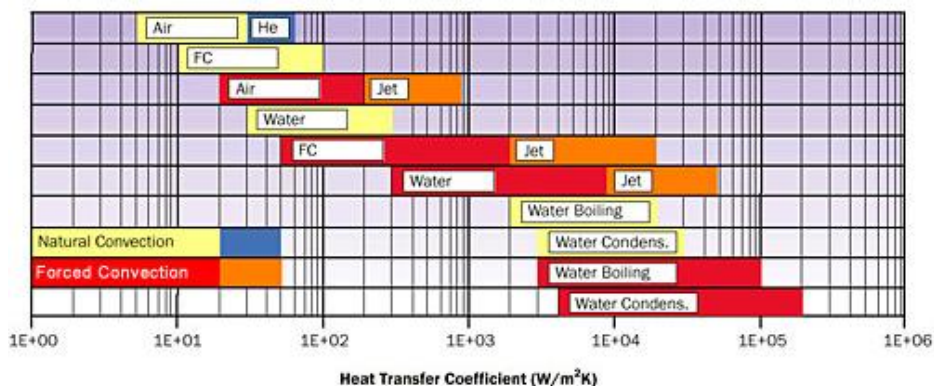


Figure 1.2. Order of magnitude of heat transfer coefficient ( $\text{W}/\text{m}^2\text{K}$ ) depending on cooling technology [8].

The extremely high value of the heat transfer coefficient related to phase change phenomena, permit to such devices to dissipate up to  $200\text{--}250 \text{ W}/\text{cm}^2$  of radial heat flux, with low thermal resistance value (up to  $0.01 \text{ K}/\text{W}$  in some cases).

Indeed, the very high heat transfer coefficient, permits to decrease the amount of refrigerant fluid inside the device, allowing to decrease the dimensions and the weight. These advantages make the two-phase passive heat transfer device to be suitable candidate in the electronic cooling, both on ground and for space applications.

Different two-phase heat transfer devices can be distinguished depending on the geometry, the possibility to work without a gravity field and the working principle:

- Thermosyphon (TS): the most simple two-phase heat transfer device;

# **1. Introduction: Two-Phase Passive Heat Transfer Devices for Ground and Space Applications**

---

- Heat Pipe (HP): capillary forces are present within HP, since a wick structure is positioned in the inner part of the tube. A great number of HP are analyzed in the last decades, varying the wick structure and designing different geometries ;
- The Pulsating Heat Pipe (PHP), the new frontier of the two-phase passive heat transfer device able to work also in micro-gravity conditions, with a simple and “wickless” geometry.

These three big families are presented in this chapter in detail.

## **1.2 Thermosyphon: working principle and performance**

The thermosyphon (TS) is the most simple and ancient two-phase heat transfer device, well known since the end of the XIX<sup>th</sup> century. The word “siphon” is of Greek origin: it means “pump”, while “thermos” means “heat”. Therefore, Thermosyphon literally means “pump of heat”, even though in this case it does not refer to the well known machine based on the inverse thermodynamic cycle [8]. The typical TS consists of a single envelope where the heat-receiving (evaporator) zone is usually filled with the liquid phase and it is located below the heat rejecting (condenser) zone [6]. As the evaporator zone is heated up the liquid starts boiling and vapor rises and condenses on the walls in the heat-rejecting zone. The liquid film flows down the walls to the evaporator zone counter-current the vapor.

## 1. Introduction: Two-Phase Passive Heat Transfer Devices for Ground and Space Applications

---

A schematic representation of a TS is shown in Figure 1.3.

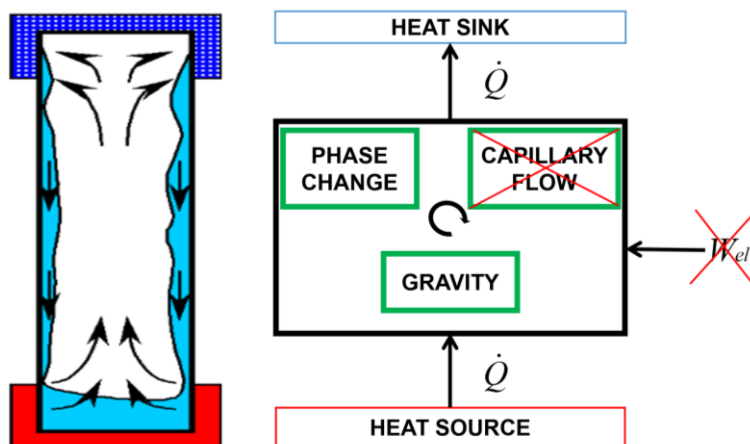


Figure 1.3. Schematic representation of a TS and its working principle.

TSs are the cheapest two-phase heat transfer device, since they are just a tube firstly evacuated and then partially filled up with a refrigerant fluid. Nevertheless, since there is no a capillary structure, the condensate liquid can return from the cold to the hot section only thanks to the gravity field. In other words, the TS needs gravity to work properly: in horizontal orientation or in micro-gravity conditions, the condensate liquid phase is not able to return at the evaporator section and the device will work as a purely conductive medium.

In order to work properly, the ID dimension of a thermosyphon needs to be larger than the so called “*critical diameter value*”, i.e. the threshold value beyond which a transition between a slug/plug flow to a stratified

# 1. Introduction: Two-Phase Passive Heat Transfer Devices for Ground and Space Applications

---

flow is achieved. Only if the liquid and the vapor phase are stratified, gravity pushes back the liquid phase from the condenser to the evaporator through the inner surface of the tube.

In other words, the ID dimension has to be larger enough to allow the body forces to overcome the surface tension forces.

The Bond Number (Eq. 1.1), being the ratio between the body force with respect to the surface tension force, can be an useful a-dimensional number to quantify the critical diameter value at least in static conditions:

:

$$Bo = \frac{(\rho_l - \rho_v) g (ID)^2}{\sigma} \quad (\text{Eq. 1.1})$$

The Bond Number is an useful equation to predict the so called capillary length ( $l_c$ ). In fact,  $l_c$  comes out from the balance of buoyancy and surface tension forces (Eq. 1.2):

$$l_c = \sqrt{\frac{\sigma}{g(\rho_l - \rho_v)}} \quad (\text{Eq. 1.2})$$

If the inner diameter (ID) is less than  $2l_c$ , the liquid and the vapor phase will appear, at least in static conditions, as an alternation of “liquid slugs” and “vapor bubbles” within the tube [11]. In fact, in such conditions the ID is lower than the “*critical diameter value*”, and the device will act as a PHP.

If the inner diameter (ID) is higher than  $19l_c$  [7] the two-phase flow is completely stratified and the device works as a real TS.

# 1. Introduction: Two-Phase Passive Heat Transfer Devices for Ground and Space Applications

---

## 1.2.1 Transport limitations

When the two-phase flow motion is blocked for some reasons, the device is not able anymore to exchange heat from the hot to the cooled section. Different limits can be achieved during its working mode, depending on the operating temperature and the power:

- *Boiling limit (or heat flux limit)*: Boiling limit occurs when the heat fluxes provided to the evaporator section are too high to allow the return of the liquid phase in the heated region. A sudden increase of the temperature at the evaporator occurs, making a failure of the device.
- *Flooding limit*: The flooding limit refers to the case of high shear forces developed as the vapor passes in the counter-flow direction over the liquid saturated, where the liquid may be entrained by the vapor and returned to the condenser. This results in insufficient liquid flow that returns to the evaporator. It usually happens close to the evaporator, where the liquid thickness is the largest
- *Viscous limit*: at the lowest heat power input or at the lowest operating temperature, the pressure of the vapor must be at minimum higher than the pressure drop required to drive the vapor flow along the device. If this situation is not achieved, vapor cannot be driven along the device;
- *Sonic limit*: at low vapor densities, the corresponding mass flow rate in the TS may results in very high vapor velocities, making favorable the occurrence of choked flow in the vapor passage

## **1. Introduction: Two-Phase Passive Heat Transfer Devices for Ground and Space Applications**

---

- *Condenser limit*: if there are some limitations related to the dissipation in the condenser area, such as low heat transfer coefficient related to natural convection or to a non-proper design of the heat sink components, the heat is not able to be dissipated efficiently.

### **1.2.2 Thermosyphon operating with the “bubble lift principle”**

One of the possibility to delay the flooding limit is to create a loop in which both the two-phases can circulate in a preferential direction. This could be achieved with a looped geometry. If the ID dimension is lower than  $19 l_c$ , but still higher than the critical diameter, thanks to the relatively small cross section with respect to the standard TS, the expanding vapor phase is able to push batches of fluid (both liquid and vapor) towards the condenser section [10]. Such devices are called Loop Thermosyphon operating with the “bubble lift principle”, and they fills the gap between TS and the PHPs where the inner diameter dimension is small enough to make the surface tension forces comparable with respect to the body force, as shown in Figure 1.5.



# 1. Introduction: Two-Phase Passive Heat Transfer Devices for Ground and Space Applications

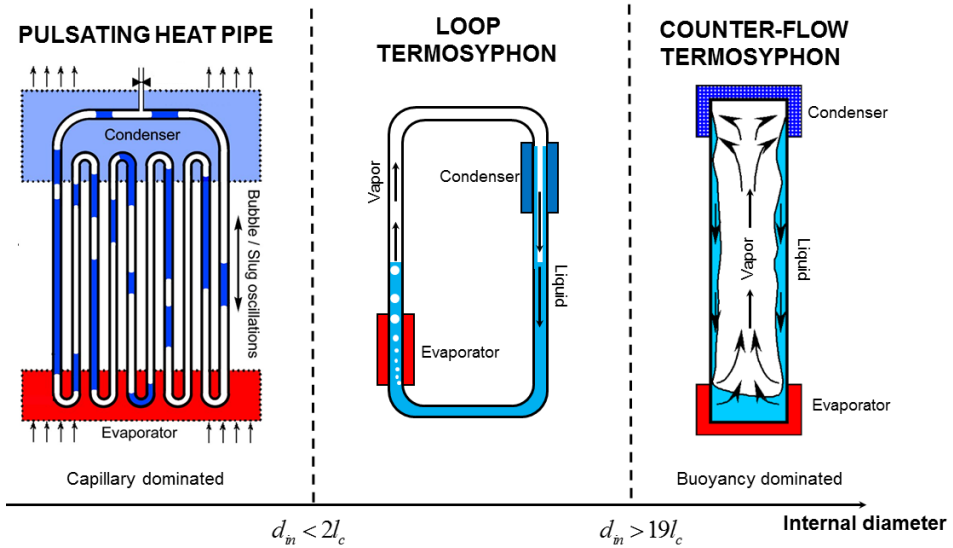


Figure 1.4 Wickless Heat Pipes working principles in the light of the confinement criteria [48].

When the heat power input is sufficient, in the cooled zone, vapor condenses and the tube is completely filled by the liquid phase that is driven back to the evaporator by gravity (Figure 1.5). This particular fluid flow motion is better known as “bubble lift” principle. The looped TPTS based on the “bubble lift” concept, exploits the higher heat transfer performance linked to the convective flow boiling process in order to overcome the limits due to the pool boiling critical heat flux. In the field of electronic cooling, the loop thermosyphons are largely investigated because of their geometrical flexibility in the design of the evaporator and the condenser

# 1. Introduction: Two-Phase Passive Heat Transfer Devices for Ground and Space Applications

---

zone with respect to a single straight channel typical of a normal thermosiphon.

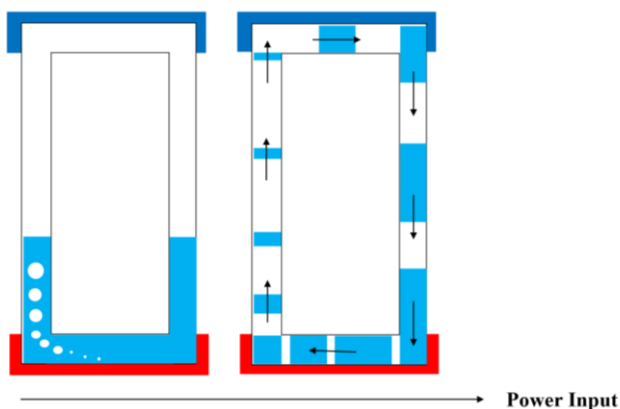


Figure 1.5. Closed Loop Thermosiphon with small cross section operating with the “bubble lift principle”.

Indeed, Closed Loop Thermosiphon operating with the bubble lift principle, being simply a tube firstly evacuated and then partially filled up with a refrigerant fluid, is simple to design and to manufacture.

However, it is worthwhile to stress that, positioning the TS operating with the “bubble lift principle” both horizontally, in micro-gravity conditions or in “anti-gravity conditions”, i.e. when the condenser section is below the evaporator one, the device is not able to work. In other words, the device needs gravity assistance to work properly. These devices with small dimensions will be extensively discussed in the Chapter 2.1, since a

## **1. Introduction: Two-Phase Passive Heat Transfer Devices for Ground and Space Applications**

---

novel kind of Multi-Evaporator Closed Loop Thermosyphon operating with the bubble lift principle will be presented in this thesis work.

### **1.2.3 The reverse thermosyphon**

Reverse thermosiphons (RTS) were developed in the last decades with the main objective to work under “anti-gravity conditions”. This is mandatory in some real cases, for instance in solar thermal energy applications, where usually the heat power input is received from the highest section of the loop. One of the possibility for a two-phase flow passive device to work also without gravity assistance is to create a wick structure by means of a porous medium on the inner surface, in order to create a capillary force able to recall the liquid phase in the evaporator section. This type of devices are usually called Heat Pipe (HP), and they will be discussed extensively in the section 1.3. Nevertheless, the development of a wick structure, that makes such passive device able to work also without gravity requires a specific knowhow and it is the most difficult part to be designed in a HP. It is mainly for this reason that in the last decades the scientific community is studying other “wickless” technology such as RTS or Pulsating Heat Pipes (PHP) able to guarantee a two-phase flow motion also in anti-gravity conditions or in weightlessness. As extensively discussed by Filippeschi [11], it is possible to find in literature over 50 RTS different designs, however generally speaking they have essentially the same basic governing principles.

# 1. Introduction: Two-Phase Passive Heat Transfer Devices for Ground and Space Applications

---

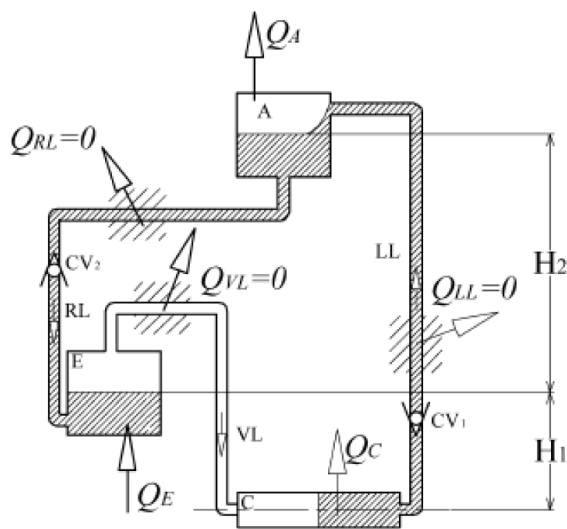


Figure 1.6. The reverse thermosiphon (Filippeschi, 2006).

As shown in Figure 1.6, a RTS is essentially constituted by three main parts, the evaporator E, the condenser C, positioned below E, and an accumulator A. Three channels connect A, E, C in order to form a loop: the vapor line (VL line) between C and E; the liquid line (LL) that interconnects A and C; the return line (RL) between E and A. The loop is finally equipped with two check valves: CV1 in the liquid line; CV2 positioned in the return line. This loop does not work continuously but periodically with consecutive cycles. A single cycle of periodic heat and mass transfer is divided into two main parts:

- a *transfer time*, where vapor is transferred from the evaporator to the accumulator through the condenser;

## **1. Introduction: Two-Phase Passive Heat Transfer Devices for Ground and Space Applications**

---

- *a return time*, where the liquid collected in the accumulator flows back to the evaporator.

When the heat power is provided to the evaporator, the vapor pressure locally tends to increase. Therefore, the vapor phase is pushed in the condenser. As soon as this quantity of vapor leaves the evaporator, a portion of liquid phase is recalled from the accumulator to the condenser. These operations are reached consecutively, permitting to the RTS to work also in anti-gravity mode. Even if the RTS represents nowadays a well know technology able to work also in anti-gravity conditions, it is worthwhile to note that the system is more complex than a TS or a HP. Furthermore, two electro-valve are mandatory to control the cycle: the closing/opening time of the valves depend on the input level, which means that an electronic control system is necessary.

### **1.3 Heat Pipes**

In the last decades, the interest on Heat Pipes (HP) is increasing exponentially for two main reasons. The first one is the development and advances of new heat pipes, such as loop heat pipes (LHPs), micro and miniature heat pipes (MHP), and pulsating heat pipes (PHPs). The second one is that such technology is suitable for many commercial applications. For example, several million HPs are manufactured each month for cooling applications in CPU and laptop computers [12]. HP are usually manufactured as a tubular metal structure closed at both ends. A heat flux, entering the evaporator, for instance from a hot component, vaporizes any

## **1. Introduction: Two-Phase Passive Heat Transfer Devices for Ground and Space Applications**

---

available coolant liquid, thereby absorbing large quantities of heat. The vapor formed in the hot section travels through the adiabatic transport section to the condenser, thanks to the pressure difference. In the cooled zone the vapor condenses as the temperature is lower, releasing its latent heat. The heat can be extracted from the heat pipe by a heat sink. The main difference with respect to above mentioned TS is that in an HP, the return of the fluid from the cooled to the heated section return is assisted by a *capillary or wick structure*. The wick structure is located in the HP inner surface. The capillary forces, acting on the wick structure, permits to the liquid phase to fill it up like a sponge. The liquid phase can return easier from the condenser to the evaporator thanks to the capillary pressure caused by the difference in curvature of the liquid menisci (Figure 1.7 a). In the evaporator section, where the liquid recedes into the pores of the wick, the liquid-vapor interface is highly curved; to the contrary, during the condensation process, the menisci in the condenser section is nearly flat.

# 1. Introduction: Two-Phase Passive Heat Transfer Devices for Ground and Space Applications

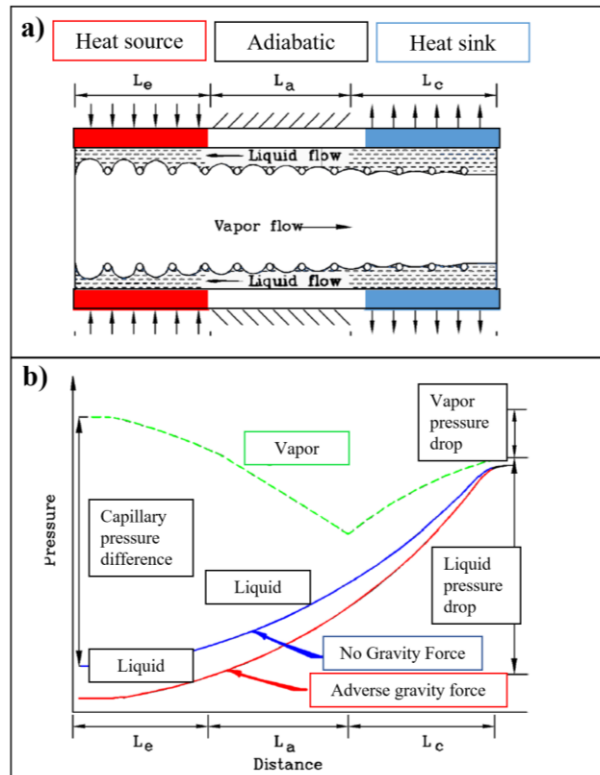


Figure 1.7 a) Heat Pipe schematization, where it is highlighted the liquid-vapor interface variation; b) pressure variations for the liquid and the vapor phase from the heat sink to the heat source.

The difference between the capillary radii in the evaporator and condenser ends of the wick structure results in a net pressure difference in the liquid-saturated wick (Figure 1.7 b), driving the liquid from the condenser through the wick structure to the evaporator region, thus allowing the overall process to be continuous. Sometimes, the capillary forces provided by the wick

# **1. Introduction: Two-Phase Passive Heat Transfer Devices for Ground and Space Applications**

---

structure makes the device able to work also in anti-gravity conditions, i.e. in THM, sustaining the two-phase flow motion also along five meter of path [13].

## **1.3.1 Transport limitations**

As thermosyphons, also HPs can work only inside an operating temperature and heat power range. Different limits can be achieved during HPs working mode, depending by the operating temperature and the power:

- *The capillary limit:* the capillary limit is achieved when the driving capillary pressure is insufficient to provide adequate liquid flow from the condenser to the evaporator. Dry-out conditions are suddenly achieved at the evaporator. Generally speaking, the capillary limit is the primary maximum heat transport limitation of a heat pipe.
- *Boiling limit:* as a thermosyphon, if the heat fluxes or the operating temperature are too high, the refreshed liquid phase that comes from the condenser cannot reach the evaporator, thus bringing the device to a sudden dry-out condition
- *Entrainment limit:* The entrainment limit is the reciprocal of flooding limit for a thermosyphon. Nevertheless, in this case, since there is a wick structure, physically it refers to the case of high shear forces developed as the vapor passes in the counter-flow direction over the liquid saturated wick.

Generally speaking, the most commonly encountered limitation to the performance of a HP is the so called “capillary limit”. Capillary limit occurs when the capillary forces of the wick structure is not able to return the liquid phase to the evaporator to keep it saturated. Therefore, the



## 1. Introduction: Two-Phase Passive Heat Transfer Devices for Ground and Space Applications

---

temperature at the evaporator experiences a sudden increase. The sonic limits, the viscous limits and the condenser limits are physically the same with respect to the limits listed above for a TS (Chapter 1.2.1). A qualitative plot showing the dependency of these limits with respect the operating temperature and the heat flux, is reported in Figure 1.8:

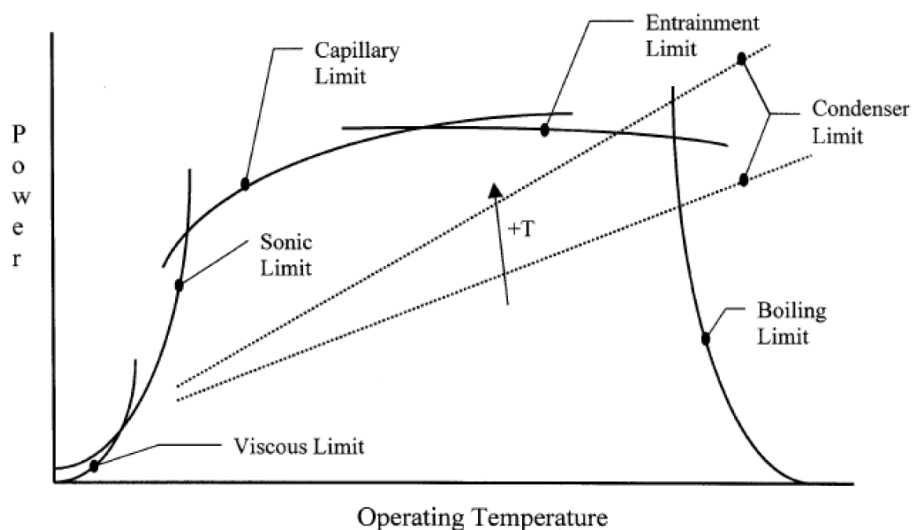


Figure 1.8. Qualitative heat pipe performance map [14].

### 1.3.2 Types of Heat Pipes designed for electronic and space applications

The performance of the HP is strictly dependent on the wick structure. Depending on the wick structure, an HP can be classified in Sintered Powder Heat Pipe, Screen/Wire Mesh Heat Pipe and Axial Groove Heat Pipe as show in Figure 1.9:

# 1. Introduction: Two-Phase Passive Heat Transfer Devices for Ground and Space Applications

---

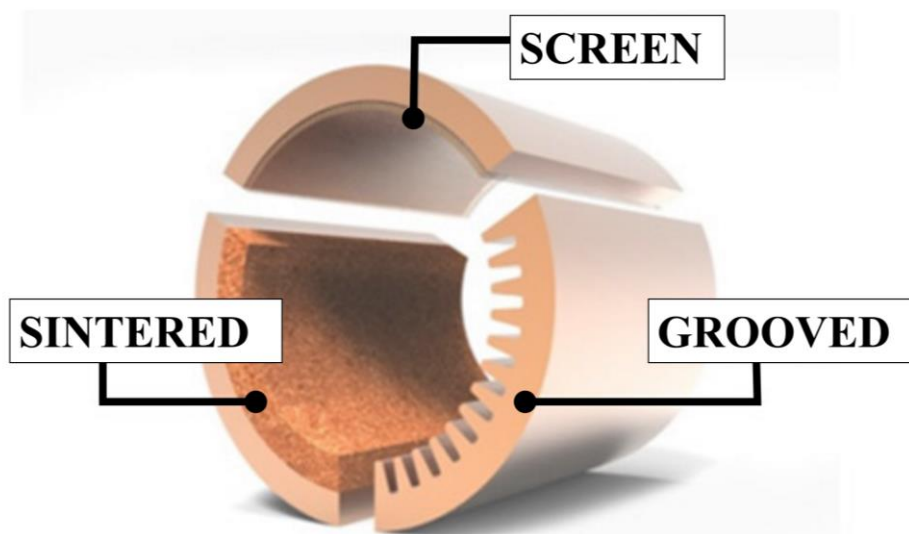


Figure 1.9 Wick structures usually found in a Heat Pipe.

Table 1-1 provides a comparison between screen, sintered and grooved heat pipes, depending on the manufacturing procedure, typical heat fluxes dissipated, the inclination range in which such HPs works properly and the possible applications:

Table 1-1 General classification of HPs depending on the wick structure.

<b>WICK STRUCTURE</b>			
	<b>Sintered Powder</b>	<b>Screen/Wire Mesh</b>	<b>Axial Groove</b>

## 1. Introduction: Two-Phase Passive Heat Transfer Devices for Ground and Space Applications

---

<b>Manufacturing procedure</b>	Powder particles are diffused together and to the tube wall to form a sintered wick structure.	Screen mesh wicks are expanded against the tube wall to form the capillary wick structure	Tubes manufactured usually with axial or circumferential grooves in the wall.
<b>Typical Heat Fluxes</b>	Usually up to 50 W/cm <sup>2</sup> . With special shape of the wick up to 250 W/cm <sub>2</sub>	10-15 W/cm <sup>2</sup>	5-10 W/cm <sup>2</sup>
<b>Inclination</b>	Any orientation	-5° up to 90° (Bottom Heated mode)	0°-90° (from horizontal to Bottom Heated mode)
<b>Application</b>	Electronic cooling, Aerospace	Electronic cooling	Electronic cooling

The most common geometrical shape of an HP is a wick tube sealed at both ends. However, other different geometries can be found, depending essentially on the application:

- *Annular Heat Pipes*: The annular heat pipe is very similar with respect to the conventional HPs. The main difference is that the cross section of the vapor space is annular instead of circular [15] [16].

## **1. Introduction: Two-Phase Passive Heat Transfer Devices for Ground and Space Applications**

---

- *Vapor Chamber*: The so-called vapor chamber is a flat-plate heat pipe in a rectangular or disk shape. A vapor chamber can work also without a gravity field or in anti-gravity conditions, i.e. in THM. A wick structure is needed in the evaporator section in order to spread uniformly the liquid on the surface, preventing local dry-out. Vapor chamber can be successfully applied in electronic cooling applications with heat fluxes also above  $50 \text{ W/cm}^2$  and when the geometrical shape is essentially bi-dimensional, such as desktops and servers.
- *Rotating Heat Pipe*: The rotating heat pipe is usually in the shape of a circular cylinder with or without an axial taper which rotates along its own axis of symmetry or revolves off-axis. The main difference with respect to a conventional HP is linked to the rotation of the tapers: the rotation, providing an additional centrifugal force, allows the liquid phase to return easier at the evaporator section. Some real applications have been used in the automotive industry, when they can be used to cool down the rotating parts of electric motors. They also have been utilized to cool down metal-cutting tools, such as drill bits and end mills.
- *Gas-Loaded Heat Pipe*: the main difference with respect to the conventional HP is that is present also a non-condensing gas. The non-condensing gas reaches the condenser section during operation,

## **1. Introduction: Two-Phase Passive Heat Transfer Devices for Ground and Space Applications**

---

carried by the motion of the vapor phase. Where the non-condensing gas is present in the condenser section, in that zone condensation cannot be achieved by the vapor phase. As a consequence, in that zone the heat cannot be released, hindering the heat exchange, increasing locally the temperature and the pressure, that compresses the uncondensable gases. This in turn increases the condenser area available to transfer heat. This expansion and contraction of a non-condensing gas has the main advantage to keep almost constant the temperature at the evaporator section also when the applied heat load changes in time.

- *Loop Heat Pipe*: The Loop Heat Pipe (LHP) was invented in Russia in 1971 by Maydanik [17]. As shown in Figure 1.10, a LHP consists of a capillary pump (evaporator), a compensation chamber, a condenser, and liquid and vapor lines. The wick is only in the evaporator, where the capillary forces are strong thanks to a sintered powder structure, and in the compensation chamber. The compensation chamber is a very important component of a LHP, and has the main goal to accommodate the excess of liquid during normal operation. The evaporator and the compensation chamber are connected with a wick structure with larger pores, in order to continuously supply the liquid to the evaporator section. Both the liquid and the vapor lines are made of small wickless tubes, that can make the device flexible and bendable. LHPs are very attractive for

# 1. Introduction: Two-Phase Passive Heat Transfer Devices for Ground and Space Applications

---

space applications because they have high heat transfer capability (heat load up to 7 kW and heat flux up to 70 W/cm<sup>2</sup>), the capability to transport energy over long distances, up to 23 m [-], without restriction on the routing of the liquid and vapor lines and the ability to operate at different gravity levels, from 0 to 9 g.

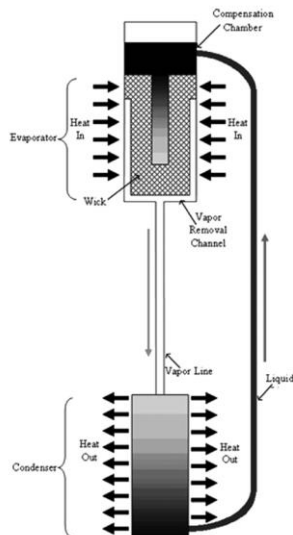


Figure 1.10. Loop Heat Pipe [12].

- *Micro and Miniature Heat Pipes*: The micro heat pipe concept for the cooling of electronic devices was invented by Cotter in 1984 [18]. A micro heat pipe, as the name suggested, is an extremely compact HP with typical diameter ranging from 0.5 to 5 mm [19]. Even if geometrically could be suitable for micro-electronic cooling applications, the small dimensions create problems related to their manufacturing and during the filling procedure.

# 1. Introduction: Two-Phase Passive Heat Transfer Devices for Ground and Space Applications

---

## 1.4 The Pulsating Heat Pipe

The Pulsating Heat Pipe (PHP) represents the last frontier of the two-phase “wickless” and passive heat transfer device. The PHP is essentially a capillary tube, bended in order to create some U-turns both at the evaporator and at the condenser section. Thanks to the capillary dimension of the ID, the liquid and the vapor phase resides inside the serpentine as an alternation of “*liquid slugs*” and “*vapor bubbles*” (Figure 1.11).

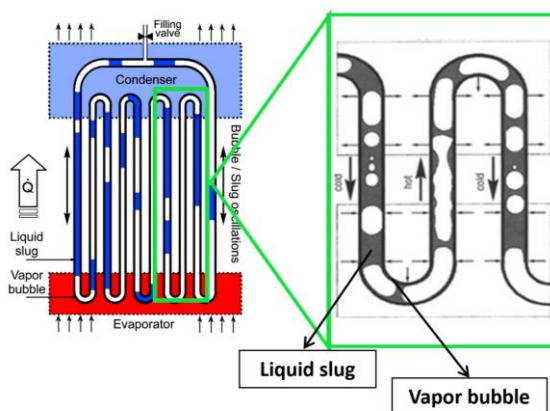


Figure 1.11: Basic scheme of a closed loop PHP; on the right, zoom of the internal flow patterns.

The heat power input provided to the evaporator section expands the vapor bubbles in this zone. The expansion pushes the adjacent two-phase flow in the condenser section, releasing heat efficiently (Figure 1.12).

# 1. Introduction: Two-Phase Passive Heat Transfer Devices for Ground and Space Applications

---

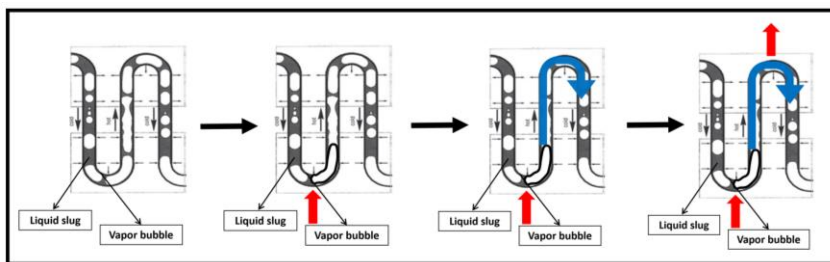


Figure 1.12. Expansion of a vapor bubble in the evaporator section and subsequent push of the adjacent two-phase flow in the condenser section.

To the contrary, vapor bubbles condensate in the cooled region, recalling other fluid. Of course, if a PHP is positioned in BHM, the gravity force allows the liquid phase to easily return in the heated region, promoting the two-phase flow motion and shifting the dry-out conditions towards higher heat power inputs. However, the continue expansions and contractions of the vapor bubbles permit to the PHP to work also without gravity assistance, making such simple device interesting for space applications. Being simply a capillary tube, the production costs are lower than a wick HP. The geometry of a PHP is flexible and can be adapted to the shape of the real application, making this device extremely customizable.

Nevertheless, the two-phase flow motion is intrinsically chaotic within the PHP: the continue phase-change phenomena both in the heated and in the cooled section create a pulsating and unpredictable two-phase flow motion, making the device difficult to study numerically. Many parameters



## **1. Introduction: Two-Phase Passive Heat Transfer Devices for Ground and Space Applications**

---

affect the operation of this complex two-phase heat transfer device, such as:

- *Filling Ratio (FR)*: the volume of liquid with respect to the global volume in the PHP. It is usually referred as a percentage of the global volume;
- *Number of turns*: the numbers of turns at the evaporator zone;
- *Inclination angle*: the inclination angle between the PHP and the vector of the gravity field;
- *Working fluid*: the fluid utilized to partially filled up the PHP;
- *Heat power input*: The heat power provided to the device;
- *Channel diameter*: The inner diameter dimensions;
- *The size and capacity of the evaporator and the condenser*.

Furthermore, the global heat power input that such device is able to dissipate is limited by the capillary dimensions of the tube. It is worthwhile to stress that it is merely the capillary dimension of the tube that creates a slug/plug flow in the PHP, enabling such device to work also in micro-gravity conditions. Consequently, one of the most important parameter to identify during the design of a PHP is the ID dimension, as will be extensively discussed in the Chapter 2.

Furthermore, the continuous phase change phenomena, bubbles interactions along the circuit, the vigorous pressure fluctuations establish a chaotic and unpredictable two-phase flow motion, which is hard to stabilize

## **1. Introduction: Two-Phase Passive Heat Transfer Devices for Ground and Space Applications**

---

in a preferential direction. A more thorough description of the PHP working principles and parameters is provided in chapter 2.

# Chapter 2

## 2. PHP and compact Loop- Thermosyphon : working principles and state of the art

PHPs and Compact Loop Thermosyphons operating with the bubble-lift principle can be a suitable candidate to cool down electronic components both for ground and space conditions.

## **2. PHP and compact Loop-Thermosyphon: working principle and state of the art**

---

Their advantages, such as compact dimensions, low production costs due to any kind of wick structures in the design, the possibility to exchange efficiently heat thanks to the very high latent and sensible heat coefficients, perfectly match with the electronic cooling technological requirements.

This chapter will provide a detailed chronicle on the Compact Loop Thermosyphons and PHPs, pointing out in detail their working principle and parameters.

### **2.1 Compact Loop Thermosyphons**

Creating a closed loop able to establish a circulation in a preferential direction is suitable to delay or avoid completely the flooding limit that hinders the two-phase flow motion in a traditional single envelope thermosyphon. In such loop, the fluid can circulate in a preferential direction by the coupled effect of vapor pressure and gravitational force as thoroughly described by Franco and Filippeschi [10]. In this review, the authors point out that, even if Loop Thermosyphons (LTS) operating with a global power less than 1 kW and with an ID of few millimeters were amply investigated in literature, the results obtained are sometimes contradictory. This is due essentially to the very different geometries tested, the thermo-physical differences between the working fluid choice, the FR and the heat power input levels.

## 2. PHP and compact Loop-Thermosyphon: working principle and state of the art

---

If the device is designed with an ID less than  $19 l_c$ , but however higher than the capillary limits, it acts as a Thermosyphon operating with the so called “bubble lift principle” [7].

In such device, the spontaneous circulation of liquid in a closed system is a result of the natural upward motion of hot fluid (both liquid and vapor) and downward movement of colder fluid thanks to gravity (Figure 2.1).

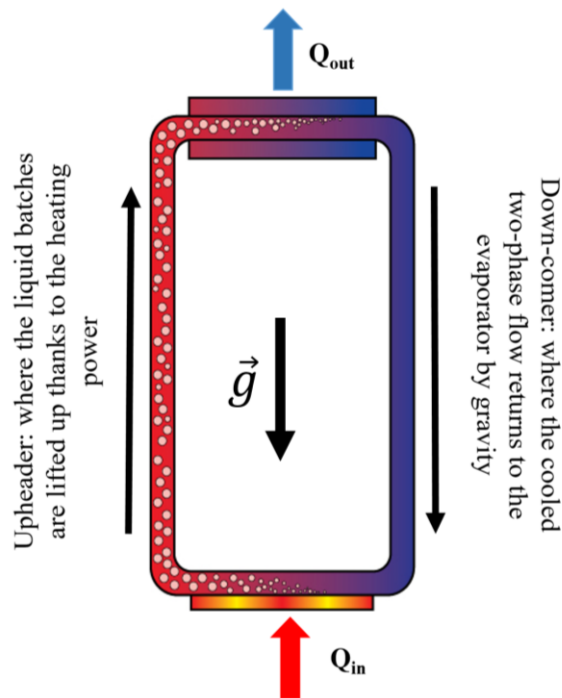


Figure 2.1 LTS working principle [-].

The LTS consists usually of an evaporator and a condenser section connected by two tubes, the up-headers and the down-comers. In the

## **2. PHP and compact Loop-Thermosyphon: working principle and state of the art**

---

evaporator, where the fluid is heated up, the liquid boils and thanks to the restricted dimensions of the tube, the bubbles formed push liquid batches in the condenser section. In the cooled zone, heat is released externally, and thanks to gravity the fluid is able to reach again the evaporator section. As a consequence, the system relies on gravity for the liquid return to the evaporator.

Usually, the devices operates at low pressure (from 0.1 bar up to 10 bar, depending on the selected fluid, its saturation pressure and the operating temperature), and temperatures comprise into the range of 20 °C up to 120 °C (depending on the applications).

The main advantage with respect to the classical single loop thermosyphon is to separate the pathways of the replenishment liquid from that of the vapor escaping from the evaporator section.

In this way, a meaningful increase of heat transport with respect to the two phase closed thermosyphons is achieved, since the classical operative limitations like as the flooding or as the entrainment limitations are overcome. These effects are more remarkable as the size of the device decreases.

This process can be affected by a great number of parameters:

- The inner diameter dimension;
- The heat input;
- The selected working fluid;
- The distance between the evaporator and the condenser section;
- The inclination;

## **2. PHP and compact Loop-Thermosyphon: working principle and state of the art**

---

- The position of the heating and the cooling section.

If, in one hand, LTSs have been extensively studied in the case of high heat power inputs, i.e. nuclear plants [23] or solar collectors [23], only few studies are related in the case of small dimensions and low power but with high heat fluxes to dissipate, like electronic cooling systems. Small LTSs, with an ID comparable with the bubble departure diameter, show different problems connected to the boiling which occurs in confined spaces, and also the fluid dynamic behavior appears different with respect to conventional TS. This is due to the weakness of the buoyancy forces, to the effect of the operative pressure and the low liquid head and finally to the high influence of the pressure drops and the fittings.

### **2.1.1 Effect of the Inner Diameter**

The distinction between small diameter channels, minichannels and microchannels is not yet clearly established in literature. In fact, Kandlikar, in a detailed review about flow boiling in channels [20], imposed as a 3 mm the limit between mini and conventional channels. Nevertheless, the flow pattern not only depends on the ID dimension, but also to the properties of the selected fluid, such as its surface tension force and the difference of density between the liquid and the vapor phase, inertial phenomena and, last but not least, the gravity acceleration value. Therefore, since different parameters are involved, it is very hard to believe in an absolute threshold value beyond which the fluid will appear slug/plug in the tube. In any examined case, it is clear that the ID dimension has a

## 2. PHP and compact Loop-Thermosyphon: working principle and state of the art

---

significant influence on the overall thermo-fluid dynamic behavior of such devices. In static conditions, the formation of vapor plugs inside a channel is attributed essentially to the balance of gravity and the surface tension forces. As a consequence, the Bond number, that establishes a-dimensionally the relation between the body force and the surface tension forces, could be a suitable indicator between the two-phase flow pattern and the pipe diameter, as already pointed out (See chapter 1.2):

$$Bo = \frac{g(\rho_l - \rho_v)d^2}{\sigma} \text{ (Eq. 2.1)}$$

The Bond number could give an indication of the confinement of the bubbles and of the different behavior observed experimentally.

For this reason, it is more reasonable to take it into account in order to establish the limit of the mini-scale, as suggested by Brauner and Maron [21].

Utilizing the Bond number, it is possible to define the so-called capillary length,  $l$ , defined as:

$$l = \sqrt{\frac{\sigma}{g(\rho_l - \rho_v)}} \text{ (Eq. 2.2)}$$



## 2. PHP and compact Loop-Thermsoyphon: working principle and state of the art

---

As the tube diameter decreases, the surface tension forces become predominant, and it is possible to define, at least in static conditions, the minimum tube diameter below which capillary flow is achieved:

$$d_{crit,min} = 2 \sqrt{\frac{\sigma}{g(\rho_l - \rho_v)}} \quad (Eq. 2.3)$$

This is already demonstrated by Kew and Cornwell [22] by means of an experimental analysis in vertical up-flow and of heat transfer in confined spaces under a variety of conditions.

Indeed, if the  $Bo < 4$ , in static conditions, surface tension force will overcome the body force: the two-phase appears as an alternation of liquid slugs and vapor bubbles, typical of a PHP.

If the  $Bo > 4$ , the liquid and the vapor phase will appear separated within the tube, and the liquid batches can be lifted up by the combined action of the vapor bubble formation and the restricted dimension of the ID (the so called “bubble lift principle”). This “pumping action” is possible until a maximum value of the tube diameter  $d_{crit,max}$  (Eq. 2.4) that can be estimated as a multiple of the capillary length, as suggested by Chisolm [7]:

$$d_{crit,max} = 19 \sqrt{\frac{\sigma}{g(\rho_l - \rho_v)}} = 19l_c \quad (Eq. 2.4)$$

## 2. PHP and compact Loop-Thermosyphon: working principle and state of the art

---

For diameters higher than this value, generally no two-phase flow should be observed in the rising pipes.

Franco and Filippeschi in 2010 [23] proposed a general classification of the operating regimes of LTS based on the inner diameter dimensions:

- $d < d_{crit,min}$ : the capillary forces dominates the body forces. In this case, the liquid and the vapor phase resides inside the tube as an alternation of liquid slugs and vapor bubbles respectively;
- $d_{crit,min} < d < d_{crit,max}$ : LTS operating with the bubble lift principle;
- $d > d_{crit,max}$ : only evaporation can be observed (pool boiling in the riser).

### 2.1.2 Effect of the working fluid

The working fluid selected has a primary influence on the LTS thermo-fluid dynamic behavior and its design. The extremely high difference between density, surface tension, viscosity of the fluids usually selected influence heavily not only the heat exchange performance of the device, but also the capillary length (Table 2-1) and thus, the ID selection.

Furthermore, depending by the application, a proper selection of the fluid is not only restricted to its thermo-fluid dynamic properties, but other different parameters of merit such as its toxicity and the related environmental impact needs to be considered.

## 2. PHP and compact Loop-Thermosyphon: working principle and state of the art

Table 2-1 Thermophysical properties of the various fluids at atmospheric pressure

Parameter	Water	FC-72	R134a	R141b	R113	R11	Isobutane	Methanol
$T_{\text{sat}}$ [°C]	100	56.6	-26.1	32	47.6	23.8	-12	64.4
$\rho_l$ [kg/m <sup>3</sup> ]	958.4	1594	1376.8	1227.5	1564	1473	594.1	748.4
$\rho_v$ [kg/m <sup>3</sup> ]	0.59	13.13	5.25	4.79	7.33	5.78	2.8	1.22
$h_{lv}$ [kJ/kg]	2257.9	95.02	216.98	223.09	144.45	181.49	365.32	221
$\sigma$ [N/m]	0.0589	0.00841	0.015441	0.01752	0.01474	0.01793	0.014469	0.019
$\mu$ [mPa*s]	0.279	0.436	0.3788	0.3795	0.665	0.405	0.2284	0.19

## 2. PHP and compact Loop-Thermosyphon: working principle and state of the art

---

<b>d<sub>cr</sub> [mm]</b>	2.5	0.72	1.07	1.2	0.98	1.1	1.58	1.6
----------------------------	-----	------	------	-----	------	-----	------	-----

## 2. PHP and compact Loop-Thermosyphon: working principle and state of the art

---

Indeed, substituting in the Eq. 2.3 and Eq. 2.4 the thermophysical properties of the different fluids at 25 °C, the  $d_{crit,max}$  and  $d_{crit,min}$  are different between each others, as shown in Table 2-2. As a consequence, the design of the device, in particular the ID selection, is strictly dependent on the working fluid.

Table 2-2 Characteristic values of limit diameters for the fluids usually found in literature utilizing a temperature of 25 °C.

Fluid	$D_{crit,min}$ [mm]	$D_{crit,max}$ [mm]
Water	5	47.6
FC-72	1.4	13.8
R141b	2.4	22.8
R113	2.0	19
R11	2.2	20.9
Isobutane	3.2	30.0
Methanol	3.2	30.5
R134a	2.1	20.4

## 2. PHP and compact Loop-Thermosyphon: working principle and state of the art

---

### 2.1.3 Effect of the Heat Power Input

Numerous attempt in literature tried to analyze the effect of the heat power input on the thermo-fluid dynamic behavior of compact LTS. Even if results are sometimes contradictory, generally, two different operating modes can be obtained, as shown in the qualitative plot in Figure 2.2:

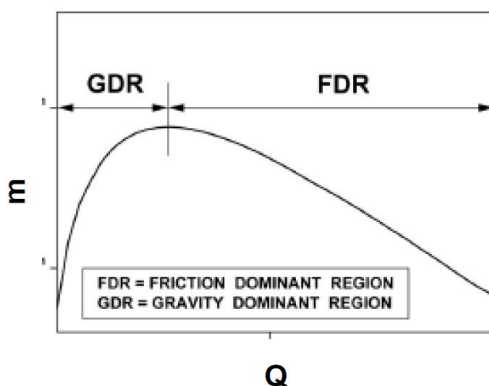


Figure 2.2 Operating mode of Closed Loop Two-Phase Thermosyphons [24].

At the lowest level of heat power inputs, the effect of the buoyancy forces is dominant. It is called the Gravity Dominant Regime (GDR) and for a small change in the void fraction and therefore density and buoyancy force. As a result, the gravity dominant regime is characterized by an increase in the mass flow rate with heat flux.

Nevertheless, by furtherly increasing the heat power input over a certain value (dependent on the combination of the working fluid, the ID, the

## **2. PHP and compact Loop-Thermosyphon: working principle and state of the art**

---

geometry of the device) the mass flow rate starts to decrease as the heat power input increases. This regime, called friction dominant regime (FDR in Figure 2.2) and, as the name suggested, the frictional forces become predominant with respect to the buoyancy forces. The continue conversion between the high density liquid phase and the vapor phase due to the increase of the heat power input requires that the mixture velocity must increase resulting in the increase of frictional losses and thus a decrease in flow rate. For this high power levels, a transition between bubbly flow to an annular flow is usually reached. In such case, the bubble lift principle is not acting anymore and the big amount of vapor that rises from the up-header decreases the mass flow rate, being its density much lower than the liquid phase. In literature the maximum value of mass flow rate not always has been observed.

### **2.1.4 Literature review Loop Thermosyphons with compact dimensions**

In this section, the most important experimental results obtained on the Closed Loop Two Phase Thermosyphons appeared in the last fifteen years are quoted and commented in Table 2-3. The chart may represent a useful handbook for anyone who wants to approach the LTS technologies operating with the bubble lift principle through its crude scientific historical background.

## 2. PHP and compact Loop-Thermosyphon: working principle and state of the art

---

Table 2-3 Experimental results in CLTPT experimental devices from 1999.

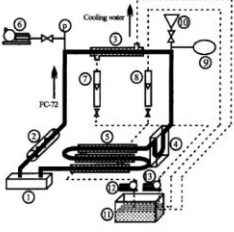
Author's name	Geometry	Working Fluid	ID	Application	Parameters	Main results
Kyung and Lee [25]	Natural single Loop Thermosyphon with 16.6 mm ID and a shell-and-coil type condenser	R113	2.5 mm	Nuclear reactor plane	Heat power (0-750 W)	The mass flow rate, measured by an orifice meter, depend by the inlet subcooling.
Rossi and Polasek [26]	Natural single Loop Thermosyphon		N.A.	High-density electronic packaging		
Chu et al. [27]	Evaporator connected to an air-cooled finned-tube heat exchanger by means of one up-header and one down-come	Water	15.9-25.4 mm	Electronic equipment cooling	Heat Power (500-1000 W)	The best FR is the minimum one tested, even if an unstable and periodical pulsing behavior is observed.
Na et al. [28]	Natural single loop thermosyphon cooled down by	R11	8 mm	Cooling multichip	FR;	Experiments were performed to



## 2. PHP and compact Loop-Thermosyphon: working principle and state of the art

	a water cold plate. Tubes not insulated to better simulate real operations.			modules MCMs	Condenser size	understand the effect of the condenser size and the FR on the overall thermal performance.
Pal et al. [29]	Two-phase compact thermosyphon	Water and PF5060	N.A.	Cooling a Pentium 4 processor in HP Vectra VL800.	Heat Power (20-90 W); Working Fluid	The working fluid greatly influences the overall thermal performance.
Mukhejee and Mudawar [30]	Two Phase Loop with two vertical, parallel, interconnected tube with a forced air heat dissipating device.	FC-72 and water	6.35 mm	Electronic cooling	Heat Power (0-280 W); Working Fluid; Distance between evaporator and condenser section.	Decreasing the gap below 3.56 mm produced a substantial rise in CHF for FC-72.

## 2. PHP and compact Loop-Thermosyphon: working principle and state of the art

<p>Honda et al. [31]</p>		<p>FC-72</p>	<p>5-7 mm</p>	<p>Electronic cooling</p>	<p>Heat Power (50-250 W); Distance between Evaporator and condenser section (250-450 mm)</p>	<p>The distance between the evaporator and the condenser affects the overall thermal performance of the device. For each distance tested, the average flow rate of FC-72 was correlated well as a function of the static pressure difference between the two vertical tubes.</p>
<p>Khodabandeh [32], [33]</p>	<p>Loop thermosyphon with evaporator sections made from small blocks of copper with 7, 5, 4, 3 and 2 vertical channels with different ID dimensions</p>	<p>Isobutane</p>	<p>1.1, 1.5, 1.9, 2.5 and 3.5 mm</p>	<p>Cooling of three parallel high heat flux electronic component</p>	<p>Heat power (0-100 W); Evaporator section</p>	
<p>Huo et al. [34]</p>	<p>Two-phase flow device based on forced circulation with transparent sections.</p>	<p>R134a</p>	<p>4.26 mm</p>	<p>Electronic cooling</p>		<p>Nucleate boiling is dominant when vapor quality is less than 40-</p>

## 2. PHP and compact Loop-Thermosyphon: working principle and state of the art

							50%. A flow pattern map is developed at a pressure of 10 bars.
Kim et al. [35]	Two-Phase single Loop thermosyphon with 1 or 2 evaporators	FC-72	10.8 mm	Electronic cooling	Input power (0-1200 W), Filling ratio		A maximum allowable heat transport rate was identified at 650 W.
Tsai et al. [36]	Loop Thermosyphon consisting of a condensation section and an evaporation section	Methanol	4-6mm		Heat power (0-160 W); Cooling water (20 °C, 30 °C, 40 °C and 50 °C); FR (5%, 10%, 20%, 30%, 40% and 50%)		Among the various results, the optimal FR is suggested to be quite low, 10%
Tuma [37]	Loop Thermosyphon applied directly to a bare die CMOS device. Condenser is liquid cooled.	HFE7000			Evaporator length (7.5, 10, 20, 37 mm) Input power		A competitive thermal resistance of 0.1 K/W was measured at 250 W.

## 2. PHP and compact Loop-Thermosyphon: working principle and state of the art

Garrity et al. [38], [39]	Two-Phase Loop Thermosyphon	HFE-7100	9.5 mm	Fuel Cell Thermal Management	Heat Power (0-390 W); Condenser elevations (from 0.8 m up to 1.33 m);	The largest flow rate occurs when the condenser elevation was the highest.
Franco [40]	Two-Phase devices operating under natural circulation condition like Two-Phase Loops and Bubble PumpsR	Water, R11, R113, R141b, FC-72	5 mm-20mm		Heat Power (0- 1000W); Diameter of the rising tubes (5mm-20 mm); Evaporator-Condenser distance (up to 1500 mm); Working fluid	The mass flow rate is measured with an indirect method. The highest value of mass flow rate were observed for the larger IDs.
Filippeschi [41]	Loop Thermosyphon with flexible pipes	Water, FC-72	4 mm		Immersion depth; Heat power;	A dependence of the CHF on the immersion depth has

## 2. PHP and compact Loop-Thermosyphon: working principle and state of the art

					Diameter of the vesse which contains the pool (72, 64, 52, 42, 34 mm)	been observed for little diameters.
Khodabandeh and Furberg [42]	Two-phase loop thermosyphon loop with interchangeable evaporator channels and transparent sections.	R134a	7.7 mm		Heat Power (0-70 W)	The minimum input power which promotes the start-up in these loops is directly observed
Samanci and Berber [43]	Two equal thermosyphons integrated to a solar collector system, with an eat exchange area of 0.4 m <sup>2</sup>	Water; R-134a	11.7 mm	Solar heater collector systems	Comparison between a single-phase thermosyphon filled up with water and a two-phase thermosyphon	The two-phase thermosyphon, tested under the same conditions, is 42.8% more efficient than the single-phase thermosyphon

## 2. PHP and compact Loop-Thermosyphon: working principle and state of the art

					filled up with R134a	
Mameli et al. [44]	A novel kind of Multi-Evaporator Closed Loop Thermosyphon, with an innovative serpentine geometry	FC-72	3 mm	Electronic cooling applications	Heat Power (0-260 W); Inclination; Heating element positions	The non-symmetric heating position of the heating elements promote a circulation in a preferential direction; the peculiar geometry makes such device able to cool down multiple heat sources

## **2. PHP and compact Loop-Thermosyphon: working principle and state of the art**

---

Although the experimental data in literature try to draw the guidelines to design a LTS with small dimensions, the experimental work appear non-systematic. Some papers study the effect of the FR, over the effects of the heat power inputs on the mass flow rate, but no attempt to give general predictions of their behavior has been made. The working fluids and the tested conditions increase the dispersion of the data. Several authors are interested to the instability of the device, while other to the effect of the FR. However, generally speaking, the LTS geometry is every time the same: the evaporator and the condenser section are linked between an up-header and a down-comer to achieve a two-phase flow circulation during operation. Only the last work presented in the Table 2-3 done by Mameli and Mangini [45] proposes a different design, with an innovative serpentine geometry that makes such device suitable to cool down multiple heating sources. This device, designed and tested in different conditions, will be presented in detail in the Chapter 3, pointing out the more relevant results on ground in the Chapter 4, since it is properly the device designed and investigated in this thesis work.

### **2.2 Pulsating Heat Pipe for space applications**

Pulsating Heat Pipes (PHP), invented by Akachi in 1990 [3], represents one of the most interesting field of investigation and are projected to meet all present and possibly future specific requirements from electronics cooling to heat recovery. The complexity of the internal thermo-fluid

## **2. PHP and compact Loop-Thermosyphon: working principle and state of the art**

---

dynamic phenomena justifies the need for a complete new research outlook with respect to HP or TS. Nevertheless, since the device is simple to design and to build, it is fully thermally driven, does not present “wick” structure (even if recently some PHP prototypes with a sintered metal wick are proposed by Zuo et al. [46], [47]) and it can work in microgravity, the prospects are too interesting to be ignored.

### **2.2.1 Main features of a PHP**

A typical (PHP) is a capillary meandering tube bent in order to have U-turns both at the evaporator and at the condenser zone. The device is firstly vacuumed and then partially filled with a refrigerant fluid. The PHP can be designed as an open loop, or as a closed loop. It is generally agreed in the PHP scientific community that a closed-loop design increases the overall thermal performance, since the fluid can also circulate along the serpentine [48], [49]. For this reason, only the Closed Loop PHP (CLPHP) will be taken into account in this section.

Thanks to the capillary dimensions of the tube, the liquid and the vapor phase reside inside the device as an alternation of liquid slugs and vapor bubbles. When heat is provided to the evaporator section, the thin film between the liquid and the vapor phase evaporates. The vapor phase in this zone, increasing its temperature and pressure, expands and pushes the fluid from the evaporator to the condenser section, where the adsorbed heat can be released to a cold sink. In a CLPHP, the two-phase flow can both pulsate or circulate.



## **2. PHP and compact Loop-Thermosyphon: working principle and state of the art**

---

The remarkable features that distinguish a PHP with respect to other two-phase passive heat transfer devices such as HP or TS are listed here below to avoid any kind of confusions:

- No wick structure;
- Slug/plug flow motion thanks to the capillary dimensions of the tube, that makes the device able to work also without a gravity field;
- The capillary force overcomes the gravity force, thus establishing an alternation of liquid slugs and vapor bubbles along the serpentine;
- No storage volumes in the system;
- There is at least one heat section that receives called evaporator zone;
- There is at least one heat dissipating section, called condenser zone;
- There is usually an adiabatic section between the evaporator and the condenser section;
- Heat is exchanged in sensible and latent way, thanks to the self-oscillating motion;
- There is no need of pumps: the device is completely passive, in the sense that is properly the heat exchange that established the two-phase flow motion.

### **2.2.2 PHP fundamental processes**

Figure 2.4 suggests the various forces, heat and mass transfer processes on a typical liquid-vapor plug system as formed in the PHP.

## 2. PHP and compact Loop-Thermosyphon: working principle and state of the art

---

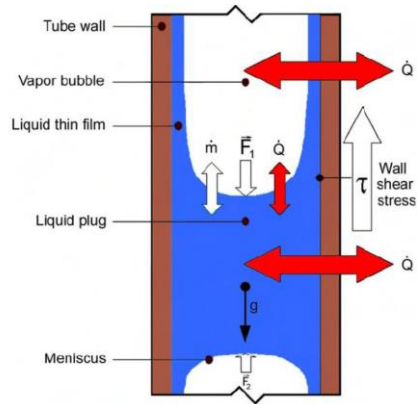


Figure 2.3 Fundamental transport processes in a PHP, Khandekar and Groll 2008 [50].

In a PHP the two-phase flow may be always characterized as a capillary flow. However, if the heat power input increases, it is usually observable a transition between a slug/plug flow to a semi-annular and finally to an annular flow. The liquid slugs having menisci on its edge are formed in the serpentine thanks to the surface tension force and the inner capillary dimensions of the tube. In the evaporator section, two different phenomena will occur, depending on the thermal characteristics that the liquid slug has when it enters in the heated zone. If the liquid slug reaches the evaporator in a sub-cooled condition, sensible heating plays the main role; if the liquid slug is already in saturated condition, the heating process is simultaneously followed by evaporation mass transfer to the adjoining vapor bubbles or breaking up of the liquid plug itself with creation of new

## **2. PHP and compact Loop-Thermosoyphon: working principle and state of the art**

---

bubbles. Indeed, there is a local increase of temperature and pressure. A vapor bubble that travels in the heated zone evaporates. As a consequence, mass transfer from the surrounding liquid film and the adjoining liquid plugs occurs, increasing the instantaneous local saturation pressure and temperature and providing the pumping work to the system.

### **2.2.3 Thermodynamics of a PHP**

The pressure fluctuations in the system are the responsible of the slug/plug flow motion.

The two-phase flow motion primarily depends on the maintenance of the non-equilibrium conditions in the system.

The thermal power provided in the heated zone evaporates bubbles that grow continuously and try to move to point A to point B at a higher pressure/temperature and a larger quality (Figure 2.4). The bubble expansion coupled with the local high pressure push the liquid column toward the low temperature end (condenser). At the same time, the condensation at the other cooled end will further enhance the pressure difference between the two ends, and point A is forced to move to point C at a lower pressure/temperature and a smaller quality.

## 2. PHP and compact Loop-Thermosyphon: working principle and state of the art

---

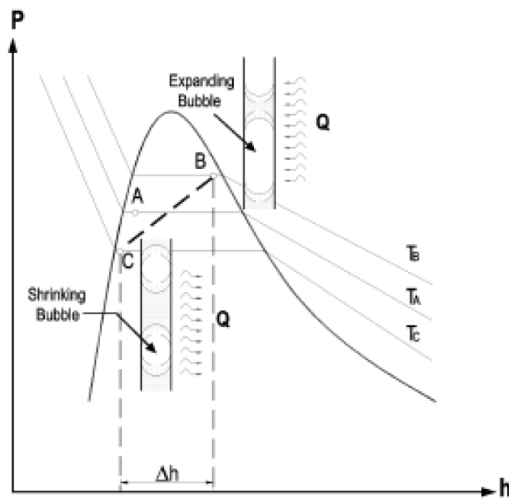


Figure 2.4 Pressure-Enthalpy diagram of a working fluid control volume in non equilibrium conditions [51].

Indeed, non-equilibrium state is formed between the driving thermal potentials and the system. Since the tubes are inter-connected between them, the motion of the liquid slugs and vapor bubbles at one section of the tube towards the condenser also leads to the motion of slugs and bubbles in the other section towards the evaporator in the next section. This works as a restoring force. The result is a self-sustained thermally driven oscillating flow in a PHP. The combined action of the driving force and restoring force leads to oscillation of the vapor bubbles and liquid slugs in the axial direction.

Additional perturbations present in real systems augment pressure fluctuations in the system. One of the main differences with respect to

## 2. PHP and compact Loop-Thermosoyphon: working principle and state of the art

---

conventional heat pipes is that in a PHP no steady-state pressure equilibrium can be achieved during operations. The PHP is an “unstable device” in the sense that are the continue pressure instabilities in the system the principal responsible of the twophase flow motion.

Through these continue oscillations of vapor bubbles and liquid slugs, heat which is supplied by the heat source at the evaporator is carried to the condenser and is removed by a heat sink.

Simplifying the problem and taking into account only one liquid slug (Figure 2.3), three main forces will act on a liquid slug:

- The difference of pressure between the adjacent vapor bubbles;
- The gravity force;
- The shear stress forces.

Its motion can be described using a simplified momentum equation:

$$\frac{dm_{l,i}v_{l,i}}{dt} = (p_{vi} - p_{v(i+1)})A - \pi DL_i\tau + \tilde{g}m_{l,i} \text{ (Eq. 2.8)}$$

Where:

- $m_{l,i}$  is the mass of the liquid slug;
- $v_{l,i}$  is the velocity of the liquid slug;
- $p_{vi} - p_{v(i+1)}$  is the different of pressure between the adjacent vapor bubbles;
- $A$  is the cross section of the tube;
- $\tau$  is the shear stress between the liquid slug and the wall;
- $D$  is the inner diameter;

## 2. PHP and compact Loop-Thermosyphon: working principle and state of the art

---

- $L_{li}$  is the liquid slug length;
- $\tilde{g}$  is the gravity acceleration.

Looking at the Eq. 2.8, if the difference of pressure given by the adjacent vapor bubbles is higher than the frictional force between the slug and the wall, the liquid slug is able to move also when the gravity acceleration approaches  $0 \text{ m/s}^2$ . As a consequence, the peculiar slug/plug flow guaranteed by the capillary dimensions of the tube, guarantees motion in micro-gravity conditions, making the device suitable for space applications.

### 2.2.4 PHP in micro-gravity

Being somehow a recent technology, very few studies were devoted to methodologically test PHPs in micro-gravity conditions. A list of the main theoretical, numerical and experimental work that tried the understanding of PHPs in micro-gravity field by means of Parabolic Flights and Sounding Rocket Campaigns is listed in Table 2-4:

## 2. PHP and compact Loop-Thermsoyphon: working principle and state of the art

Table 2-4: Main numerical, theoretical and experimental works of PHPs in micro-gravity

Principal Investigator	Year	Experimental or Numerical?	Adopted Facility	PHP Layout	Conclusions
Delil [52]	1999	Theoretical	-	-	Scaling of two-phase devices from normal to micro-gravity is complicated. Only distorted scaling offers some possibilities, when not the entire loop but only sections are involved.
Delil [53]	2000	Theoretical	-	-	No differences with respect to the previous work.
Delil [54]	2001	Theoretical	-	-	The author proposed (but did not furtherly build) a test rig for modified gravity experiments.

## 2. PHP and compact Loop-Thermosyphon: working principle and state of the art

---

Kawaji [55]	2003	Experimental	Parabolic Flight	One straight and one bended PHP	All the configurations tested, especially the top heating mode PHPs, show better operating characteristics and improved heat transfer under reduced gravity. Nevertheless, deeply looking to the results, this is evident only when the PHP is tested in anti-gravity mode.
Gu et al. [56]	2004	Experimental	Parabolic Flight	One straight and one bended PHP	All the configurations tested for both the heat pipes show better operating characteristics and improved heat transfer under reduced gravity than under normal or hyper-gravity. However, deeply looking to the results, this is evident only when the PHP is tested in anti-gravity mode.



## 2. PHP and compact Loop-Thermosyphon: working principle and state of the art

Gu et al. [57]	2005	Experimental	Parabolic Flight	Transparent Bottom Heated Mode PHP + One straight and one bended PHP	Steady pulsating flows could be achieved under reduced gravity, while hyper-gravity weakens the pulsating motion. Best performance of the tested devices under micro-gravity. However, deeply looking to the results, this is evident only when the PHP is tested in anti-gravity mode.
de Paiva et al. [58]	2010	Experimental	Sounding rocket	PHP	The test rig has been built and tested in normal gravity. Sounding rocket has been postponed, and no results are furtherly presented.
de Paiva et al. [59]	2013	Experimental	Sounding Rocket	PHP	For the very first time a PHP was tested aboard of a sounding rocket. Even if this work represents the first successful

## 2. PHP and compact Loop-Thermosyphon: working principle and state of the art

					attempt to test a PHP in prolonged micro-gravity conditions, pseudo-steady state conditions are not reached during the 6 minutes of weightlessness.
Maeda et al. [60]	2011	Experimental	Satellite	3D PHP with check valves	The prototype has been build and tested in normal gravity. Experiments on satellite are scheduled.
Mameli et al. [61]	2012	Numerical	-	PHP	Reduced gravity worsens the performance of the device in BHM. A horizontal PHP behaves as a PHP at 0g.
Ayel et al. [62]	2013	Experimental	Parabolic Flight	Transparent Flat Plate PHP	Dry out occurs during micro-gravity; an improvement of the thermal performance during hyper-gravity is assisted.

## 2. PHP and compact Loop-Thermosyphon: working principle and state of the art

					Results suffered from leakage between parallel channels.
Mameli et al. [63]	2014	Experimental	Parabolic Flight	PHP	Horizontal PHP performance is not affected by the gravity field variation occurring during the parabolic trajectories. In the bottom heated mode, the PHP never showed a better heat transfer under reduced gravity. Further ground tests point out analogies between the PHP behavior obtained on ground testing it horizontally and in micro-gravity conditions.
Taft et al. [64]	2015	Experimental	Parabolic Flight	FPHP	For conditions in which the proposed FPHP is terrestrially orientation-independent, it is also likely to be gravity-

## 2. PHP and compact Loop-Thermsoyphon: working principle and state of the art

					independent, and for conditions in which the device is not terrestrially orientation-independent, it is likely to perform better in microgravity than in a terrestrial environment.
Ayel et al. [65]	2015	Experimental	Parabolic Flight	Flat Plate PHP	The device in vertical position is influenced by variations in the applied gravity field. Microgravity increases the temperature at the evaporator, worsening the two-phase flow motion, even if the PHP continues working. No important effects are detected in horizontal position.

## 2. PHP and compact Loop-Thermosyphon: working principle and state of the art

Mangini et al. [66]	2015	Experimental	Parabolic Flight	Hybrid Closed Loop Thermosypho/PHP	In bottom heated mode, the device works as thermosyphon in normal and hyper-gravity conditions, as PHP in reduced gravity. Even if the ID is higher the capillary one on ground, the sudden absence of buoyancy forces in micro-gravity activated a slug plug flow motion.
Creatini et al. [67]	2015	Experimental	Sounding rocket	Hybrid Closed Loop Thermosyphon/PHP	A novel kind of PHP only for space applications was tested aboard of a Sounding Rocket. Nevertheless, the rocket de-spin malfunctioned, maintain a centrifugal acceleration components for the entire flight.

## 2. PHP and compact Loop-Thermosyphon: working principle and state of the art

---

Ayel et al. [68] <sup>1</sup>	2016	Experimental	Parabolic Flight	Flat Plate Hybrid Closed Loop Thermosyphon/PHP	A transparent flat plate PHP with ID higher than the capillary limit is tested in hyper/micro gravity conditions by means of Parabolic flights in vertical orientation. During normal and hyper-gravity phase the flow appears stratified; in micro-gravity the fluid distributed naturally in a slug/plug flow pattern. Dry out periods are recognizable in micro-gravity.
Mangini et al. [69]	2016	Experimental	Parabolic Flight	Hybrid Closed Loop Thermosyphon/PHP	The same device proposed by Mangini et al. [66] is another time tested in microgravity conditions. A novel electronic

---

<sup>1</sup> This work is based on the same idea proposed in the Chapter 3. However, since it is more recent than this thesis, it is not taken into account in the review.

## 2. PHP and compact Loop-Thermosyphon: working principle and state of the art

---

					power control system is developed, allowing the device to be tested non-uniformly at the evaporator. Peculiar heating distributions promote the self-sustained two-phase flow motion in micro-gravity, avoiding stop-over periods.
Manzoni et al. [70]	2016	Experimental/Numerical	Parabolic flights	PHP	An advanced hybrid lumped parameter code for the PHP simulation is developed able to simulate transient gravity field variation. Numerical results are compared with the PHP thermal behaviour during the variation of the gravity field obtained for a similar device in a previous parabolic flight campaign, showing good agreement.

## 2. PHP and compact Loop-Thermosyphon: working principle and state of the art

---

The first experimental test performed in micro-gravity conditions was done by Kawaji and Gu. It is explained in detail in three different papers [55], [56], [57]. Two different aluminum prototypes, one straight and one bended, of a flat plate PHP were tested on board of a Falcon 20 aircraft exposing the test rig to  $\pm 0.02$  g in micro-gravity and 2.5g in hyper-gravity. Both the prototypes had rectangular cross section channels with 1 mm of hydraulic diameter, charged with R-114. The devices were heated up by means of electrical heaters, while the cooling section made use of air fans. Figure 2.5 shows the three different configurations tested are reported: two vertical in Top Heated Mode (A and B) and one vertical gravity assisted (C)<sup>2</sup>.

---

<sup>2</sup> Top Heated mode, also named "Antigravity mode", means vertical top heated mode, gravity assisted means vertical bottom heated mode.



## 2. PHP and compact Loop-Thermosyphon: working principle and state of the art

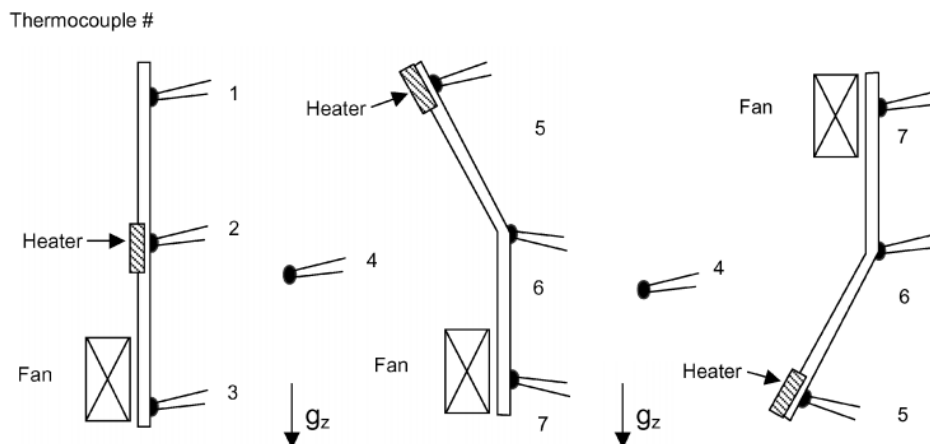


Figure 2.5 PHP configurations tested by Gu et al. [57] [56].

They concluded that under normal and hyper-gravity conditions, the orientation affected the PHP performance: the bottom heating case (C) leads to smaller temperature difference between the evaporator and the condenser, followed by the middle heating (A) and, finally, the top heating cases (B). In addition, in such conditions the BHM prevents unstable operations and temperature fluctuations because gravity helped the liquid motion. In micro-gravity, instead, the authors stated that all the tested configurations showed better operating and heat transport performance than when under normal or hyper-gravity conditions. However, deeply looking to the results reported by the authors, this is evident only for the THM (Antigravity mode), while the gravity assisted one does not show a sensible temperature reduction during the parabolas.

## **2. PHP and compact Loop-Thermosyphon: working principle and state of the art**

---

Maeda et al. [60] proposed and tested on ground a PHP with check valves to be mounted in a satellite. Even if tests on ground showed good results in terms of global heat power input dissipated by the device (up to 100 W in horizontal orientation), no further works that point out the working principle of such device in micro-gravity are published in literature.

Few years later, a new parabolic flight was performed by Ayel et al. [62] making use of the ESA Novespace A300 Zero-G testing a transparent flat plate PHP in gravity assisted configuration. The flat-plate tested, with a transparent glass wall glued on a milled copper block allowed an overall fluid flow visualization. The flat plate PHP, with a hydraulic diameter of 2 mm, has been charged with water, heated up by means of electrical heaters and cooled using an external liquid circuit. However, results are not conclusive since leakage between parallel channels affected the device operation. Nevertheless, the authors observed that micro-gravity was generally accompanied by dry-out phenomena at the evaporator section: heating up the device in BHM, the sudden absence of gravity during the parabolic trajectory, makes more difficult the return of the refreshed fluid from the top (condenser) to the bottom (evaporator). Nevertheless, both in hyper-gravity and in normal gravity, the gravity acceleration helped the liquid to reflow in the hot zone rewetting the channel and, thus, bettering the thermal performance of the device. Improved similar apparatus has been tested again in 2015 [65] yielding to much successful results.

## **2. PHP and compact Loop-Thermosyphon: working principle and state of the art**

---

Mameli et al. conducted ground and micro-gravity experiments (58<sup>th</sup> ESA PF campaign) [75], showing that the PHP thermal response in weightlessness in BHM is very similar to a tilting maneuver from BHM to the horizontal operation on ground. Confirming a previous numerical analysis performed in 2012 by the same author [7]. In fact, a CLPHP with 16 U-turns at the evaporators is tested both on ground and in hyper-micro gravity conditions during the 58<sup>th</sup> ESA Parabolic Flight Campaign. The device had an ID of 1mm, and it is filled up with FC-72 (FR=50%), providing different heat input levels from 40 W up to 100 W. The authors showed the thermo-fluid dynamic response of a PHP in micro-gravity is similar to that one of a PHP tested on ground horizontally: since in both of the cases the gravity field does not help the return of the fluid flow from the condenser to the evaporator, the PHP decreases abruptly its performance in such conditions. Additionally, during parabolic flights, the authors observe that when the device is positioned in BHM, the temperatures in micro-gravity tends to show an ever-increasing trend, synonymous of dry-out conditions, that are not achieved on ground or in hyper-gravity providing the same global heat power inputs, as visible in Figure 2.6. These results have been furtherly compared by Manzoni et al. [70] with a novel Lumped Parameter Method able to predict the thermo-fluid dynamic behavior of a similar device during the variation of the gravity field. The numerical results show a very good agreement with the experimental ones.

## 2. PHP and compact Loop-Thermosyphon: working principle and state of the art

---

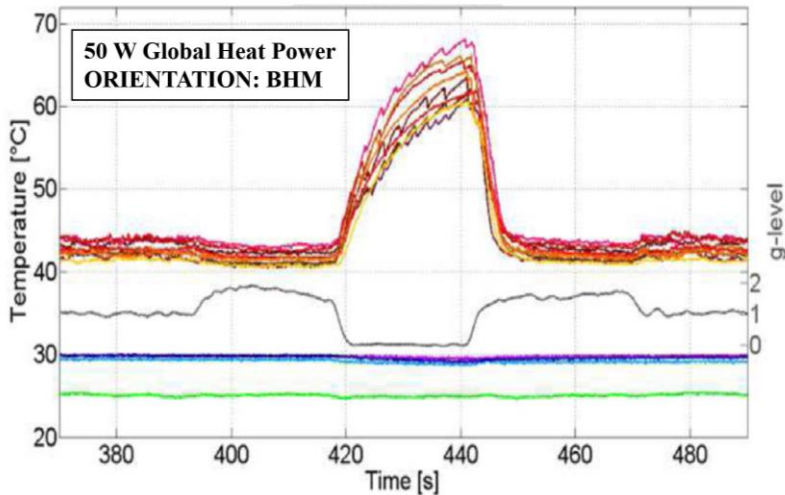


Figure 2.6 Flight tests in BHM [63], testing the device with 50 W. Temperatures at the evaporator are highlighted in red-yellow colors; temperatures at the condenser in blue colors. The ambient temperature is in green. The gravity field is pointed out by means of a black line.

By the critical analysis of the PHP thermal behavior in micro-gravity, even if it is demonstrated that PHPs could be a promising solution to dissipate heat also without the assistance of gravity, the thermal response in microgravity conditions suggests that the device performance may worsen due to the occurrence of local dry-out conditions at relatively low heating power levels.

As a consequence, it is necessary to find a way to expand the working range of such devices towards higher value of heat power inputs in micro-gravity.

## **2. PHP and compact Loop-Thermosyphon: working principle and state of the art**

---

Assuming that in micro-gravity, the critical heat fluxes are lower with respect to the case where gravity assists the flow motion, a straightforward solution could be the increase of the inner diameter (ID). . Being the capillary limit inversely proportional to the gravity field, as amply discussed in the Section 2.3, it is theoretically possible to increase the PHP hydraulic diameter without precluding the formation of a slug/plug flow. Nevertheless, it is mandatory to maintain the ID below the critical limit value, in such a way to have a slug/plug flow motion.

In parallel, it should be to stabilize the two-phase flow motion in a preferential direction, thus improving the overall thermal performance of such devices. This is valid not only for PHPs, but in general for all the two-phase passive heat transfer devices operating both on ground and in micro-gravity. As already pointed out in numerous works in literature, the best PHP performance are reachable when the two-phase flow circulates within the device [48], [71], [72], [73], [74], [75]. Nevertheless, because of the continue expansions and contractions of vapor bubble within the serpentine, the stabilization in a preferential direction of this pulsating flow is still a unsolved issue,. The Section 2.4 will provide an overview of the different efforts in literature that tried to stabilize the two phase flow motion in the PHP, pointing out the main results obtained until now.

### 2.3 Effects of a reduced gravity field on the capillary limits: the Space PHP concept

Both Gu et al. [57] and Mameli et al. [76] illustrated the possibility to design a PHP only for space applications with a diameter bigger than the capillary one on ground. Theoretically, the absence of the Buoyancy forces when the gravity field is absent allows to increase the inner diameter dimensions without precluding a slug/plug flow formation and motion. This could be extremely beneficial also for the heat exchange: since the mass of the thermal fluid per unit length is proportional to the square of the inner diameter, increasing the inner diameter dimension is of course beneficial in terms of total heat exchange.

Theoretically, when gravity tends to  $0 \text{ m/s}^2$ , the critical diameter tends to infinite at least for static conditions. However, it is necessary to take into account also the effect of the inertial and viscous forces.

Since the first adiabatic two-phase flow experimental test in micro-gravity conditions performed in 1975 by Hepner et al. [77], researchers quickly realized the importance of reduced gravity field on interfacial behavior. In particular, Choi et al. [78] compared air–water flow patterns along a 10-mm diameter tube in micro-gravity and hyper-gravity by means of Parabolic Flights aboard an MU-300 aircraft, and in terrestrial gravity level. They pointed out not only the importance of the gravity level on a two-phase flow, but also the relevant role of flow velocities in influencing the flow pattern. As shown in Figure 2.7, low flow velocities allow surface

## 2. PHP and compact Loop-Thermosyphon: working principle and state of the art

tension forces to play a dominant role in micro-gravity, yielding bubbly flow, whereas in normal and hyper-gravity environments produce stratified flow for the same velocities. On the other hand, increasing the velocity causes flow inertia to dwarf any surface tension or gravity effects, yielding similar flow patterns for all gravity levels.

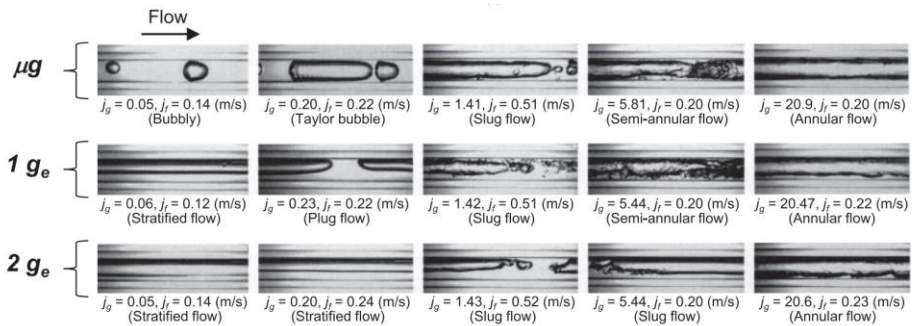


Figure 2.7 Air–water flow patters along a 10 mm diameter tube in micro-gravity (first line) terrestrial gravity (second line), and hyper-gravity (third line) adapted from Choi et al. [78] varying the gas velocity ( $J_g$ ) and the fluid velocity ( $J_f$ ).

Later on Scammel et al. [79] investigated experimentally the thermo-fluid dynamic behavior of a single elongated vapor bubble rising in a vertical, upward, co-current flow under different gravity accelerations by means of Parabolic Flights. Tests were conducted using a flow boiling rig that allows to visualize the two-phase flow motion. The fluid used was HFE 7100 and it pass through a transparent circular tube with an ID of 6 mm.

## 2. PHP and compact Loop-Thermosyphon: working principle and state of the art

---

The  $d_{cr,Bo}$  for HFE-7100 both on ground ( $9.81 \text{ m/s}^2$ ) and in micro-gravity ( $0,01 \text{ m/s}^2$ ) is reported in Table 2-5:

Table 2-5 Critical Diameters for HFE-7100 on ground and in micro-gravity calculated by the Bond Number at  $20 \text{ }^\circ\text{C}$

HFE-7100	$D_{cr,Bo}$
On ground ( $9,81 \text{ m/s}^2$ )	2 mm
In micro-gravity ( $0,01 \text{ m/s}^2$ )	132 mm

As a consequence, since the ID selected during experiments is higher than the  $d_{cr,Bo}$  on ground but lower than that one in micro-gravity, the two-phase flow motion should become capillary only after the advent of micro-gravity.

Visual analysis of the bubbles illustrated the effect of the gravity field. In micro-gravity, bubbles exhibited small drift velocities and shapes characteristic of capillary bubbles at low gravity levels (Figure 2.8 a, b): rounded tail profile whose radius of curvature increases with drift velocity, with a drift velocity ( $U_d$ ) of  $20 \text{ mm/s}$ , small amplitude interfacial waves were observed (Figure 2.8a).



## 2. PHP and compact Loop-Thermosoyphon: working principle and state of the art

---

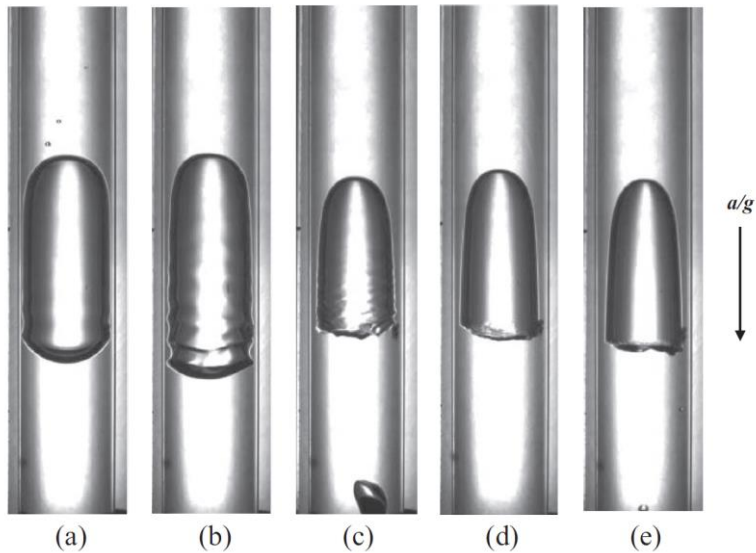


Figure 2.8 Images of representative bubbles at varying accelerations and drift velocities: (a)  $a/g = 0.01$ ,  $U_d = 20$  mm/s,  $Bo = 0.48$ ,  $L = 17$  mm; (b)  $a/g = 0.01$ ,  $U_d = 41$  mm/s,  $Bo = 0.48$ ,  $L = 18$  mm; (c)  $a/g = 0.34$ ,  $U_d = 94$  mm/s,  $Bo = 16.6$ ,  $L = 13$  mm; (d)  $a/g = 1$ ,  $U_d = 106$  mm/s,  $Bo = 48.7$ ,  $L = 13$  mm; (e)  $a/g = 1.8$ ,  $U_d = 214$  mm/s,  $Bo = 87.7$ ,  $L = 13$  mm [79].

Increasing the drift velocity to 41 mm/s (Figure 2.8b), the waves became more frequent, larger in amplitude, and oscillated in the streamwise direction, pointing out an instability of the menisci and thus the importance of inertial effects on a slug/plug flow in micro-gravity. At 1g (Figure 2.8 d) and hyper-gravity (Figure 2.8 e) conditions produced Taylor bubbles moving at higher drift velocities.

## 2. PHP and compact Loop-Thermosyphon: working principle and state of the art

---

Even these experimental works point out the possibility to create a slug/plug flow in micro-gravity with an ID value higher than the critical one on ground, had also stressed that the inertial effects play a significant role in micro-gravity. When the fluid velocity is high, the liquid/vapor interface is unstable and the slug-plug condition is only possible for smaller diameters with respect to the capillary limit. For these reasons, it should be more appropriate takes into account a *dynamic thresholds* to define the limit for space applications, evaluated by means of Weber (Eq. 2.9) and Garimella criteria (Eq. 2.10) proposed by Mameli et al. [63], even if further experimental validations are necessary:

$$d_{We} = \frac{4\sigma}{\rho_l U_l^2} \quad (Eq. 2.9)$$

$$d_{Ga} = \sqrt{\frac{160\mu_l}{\rho_l U_l \sqrt{\sigma/(\rho_l - \rho_v)g}}} \quad (Eq 2.10)$$

Therefore, it is clear from Eq. 2.10 that in micro-gravity conditions the capillary limit tends to increase.

Therefore, it is theoretically possible to design a PHP that is merely a PHP only in micro-gravity choosing properly the inner diameter dimensions. An additional table that points out the confinement diameters for FC-72 at 20 °C is reported, since this fluid will be used in this thesis to explore the effect of micro-gravity on the capillary limit (Table 2-6):

Table 2-6 Confinement diameters for FC-72 at 20 °C accordingly to static and dynamic criteria for FC-72

FC-72	D <sub>cr</sub> [mm] (static)	D <sub>cr</sub> [mm] (dynamic)
Earth g=9,81 m/s <sup>2</sup>	1.68	0.75
Micro-gravity= 0.01 m/s <sup>2</sup>	52.88	4.23

On ground, the device designed with an ID slightly higher than the D<sub>cr,Ga</sub> will act as a thermosyphon, since with a gravity acceleration of 9.81 m/s<sup>2</sup> the fluid flow will be stratified. Additionally, if the ID is between d<sub>crit,min</sub> <d<d<sub>crit,max</sub> pointed out respectively in Eq. 2.3 and Eq. 2.4, the thermosyphon will operate with the Bubble Lift Principle, as amply discussed in the Paragraph 2.1.1.

## **2.4 Stabilization of the two-phase flow motion within the PHP**

It is well known in the PHP community that the stabilization of the two-phase flow in a preferential direction increases the thermal performance.

## 2. PHP and compact Loop-Thermosyphon: working principle and state of the art

For instance, Kandekhar et al. [80] observed a sudden decrease of temperatures at the evaporator when a circulation in a preferential direction is established in a transparent PHP, as pointed out in Figure 2.9:

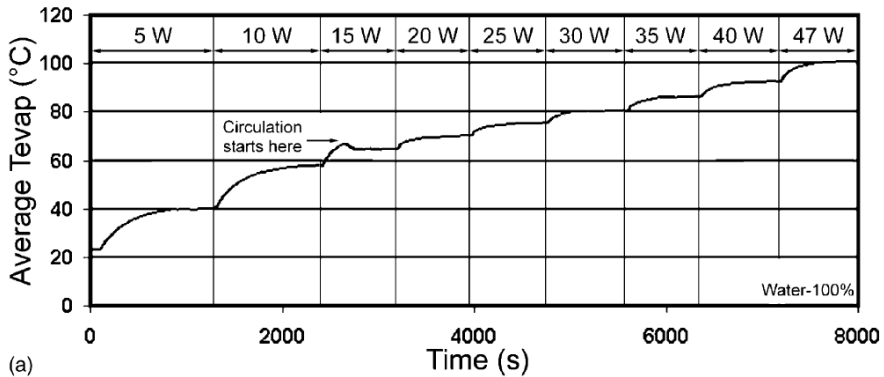


Figure 2.9 Sudden decrease of temperatures at the evaporator when circulation is established [80].

A lot of attempts in literature attempted to stabilize the two-phase flow motion in a preferential direction, thus improving the thermal performance towards wider range of heat power inputs, presenting different technical solutions.

Ridditech et al. [81] studied the heat-transfer characteristics of a closed-loop oscillating heat-pipe with check valves (CLPHP/CV). The idea was to enhance the fluid flow circulation by means of an additional hydraulic unbalancing force given by check valves. A Check valve is a floating type valve that consists of a stainless ball and brass tube, in which ball stopper

## 2. PHP and compact Loop-Thermosyphon: working principle and state of the art

---

and conical valves seat are at the ends, respectively (Figure 2.10). The ball can move freely between the ball stopper and the valves seat. The check valve should establish a two-phase flow motion in a preferential direction, making possible the passage of liquid slugs only in one direction.

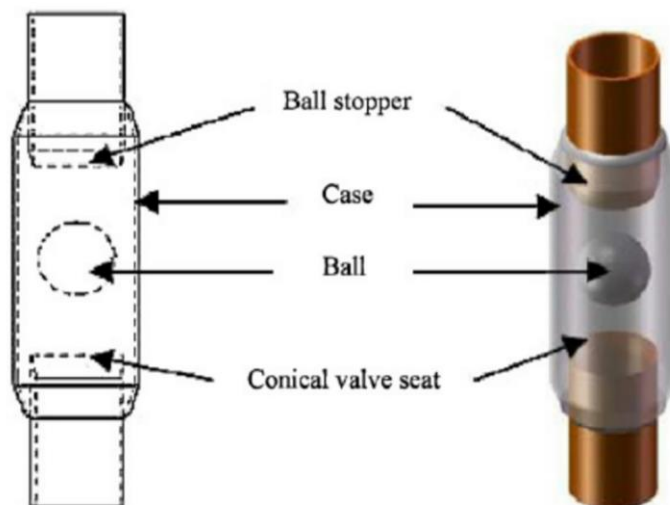


Figure 2.10 Scheme of a Check Valve [82].

Nevertheless, it is difficult and expensive to install these valves in the PHP, where it is worthwhile to stress that the design simplicity and compactness have been considered two of the strongest points of such emergent technology. Additionally, results reported in literature do not clearly highlight the improvement on the thermal performance of the CLPHP/CV. Meena and Rittidech [83] provides a comparison between a

## 2. PHP and compact Loop-Thermosyphon: working principle and state of the art

CLPHP and a CLPH/CV to prove how much check valves can influence the thermo-fluid dynamic behavior. Both of the devices were made of copper tubes with an ID 2.03 mm inside diameter, bended in order to have 40 turns at the evaporator. The unique difference between the two PHPs is the installations of check valves in the CLHP/CV. The working fluid was filled in the tube at the filling ratio of 50%, using different working fluids (water, ethanol and R134A). The tests were performed with three different temperature levels at the evaporator (60 °C, 70 °C and 80 °C). The main results are reported in Figure 2.11:

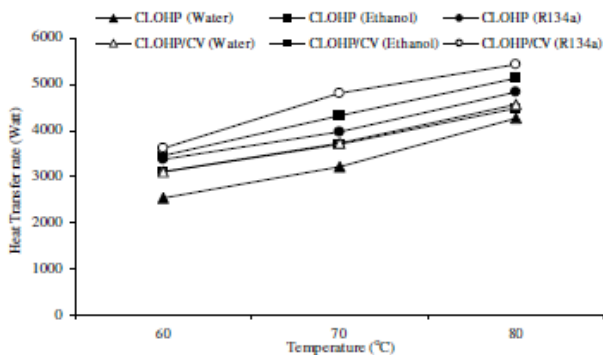


Figure 2.11 Heat Transfer rate for all the working fluids and the evaporator temperature tested using a CLOHP and a CLOHP/CV [83].

The results showed only a slight increase of the heat transfer rate and no information about the standard deviation are reported in the work.

Another attempt was done by Rittidech et al. [84] to better understand the effectiveness of Check Valves on the PHP performance. They studied

## **2. PHP and compact Loop-Thermosoyphon: working principle and state of the art**

---

different closed loop oscillating heat pipe with different number of check valves (2, 5 and 8). The maximum heat flux was obtained with a minimum number of check valves, for all the working fluid selected (water, Ethanol, R134a). This may occur because an increase in the number of check valves reduced the working fluid pressure between the evaporator and condenser sections, worsening consequently its heat exchange performance. Furthermore, there is no a comparison between the same CLPHP without check valves in this work.

Later on, Pastukhov and Maydanik [90] investigated a copper PHP with 40 turns at the evaporator with check valves. The ID was 1.25 mm, and the device was partially filled up with R-152a, with a FR=40%. It was shown that ball check valves stabilizes the two-phase flow motion in a preferential direction, increasing the value of the limiting heat load with respect to the same PHP without check valves. Nevertheless, its thermal resistance increases and orientation sensitivity decreases.

Another easier idea to promote the two-phase flow circulation in a preferential direction is to vary the ID dimensions between adjacent channels. With the introduction of alternative diameter size within the PHP, additional un-balancing capillary forces may prevail amid adjacent channels, thereby promoting the fluid motion alongside the PHP.

Holley and Faghri [85] studied the effect of the ID variation with a one-dimensional model, where the momentum equation was calculated for the liquid slugs. In the modeling domain the channel is considered as one straight flow path where the diameter increases along the axial tube (Figure

## 2. PHP and compact Loop-Thermosyphon: working principle and state of the art

---

2.12). The model is one-dimensional with some assumptions to simplify the analysis (derivatives of viscosity and density were assumed negligible, vapor exists at saturated conditions and its pressure is assumed uniform, and the number of turns effect neglected). The results pointed out that heat transfer can be enhanced when the diameter of the channel is varied along the channel length, thereby providing increased range of heat load capability and less sensitivity to gravity. A bubble in an expanding tube (gradually increasing in diameter, as shown in Figure 2.12) has a net force acting in the expanding direction because of uneven capillary forces: a non-symmetric flow resistance and capillarity can assist fluid movement. As movement ensues, the lower flow friction in the direction of the expansion further influences the fluid flow.

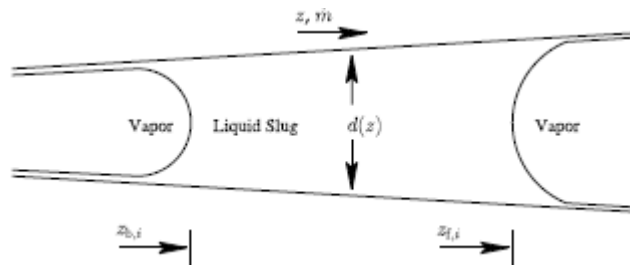


Figure 2.12 Schematic of the liquid slug proposed in the simplified model with a non-constant ID.



## 2. PHP and compact Loop-Thermsoyphon: working principle and state of the art

---

C-M. Chiang et al. [86] developed an analytical model to predict the fluid motion of pulsating heat pipe with non-symmetrical arrayed mini-channel configuration, as it is possible to see in Figure 2.13:

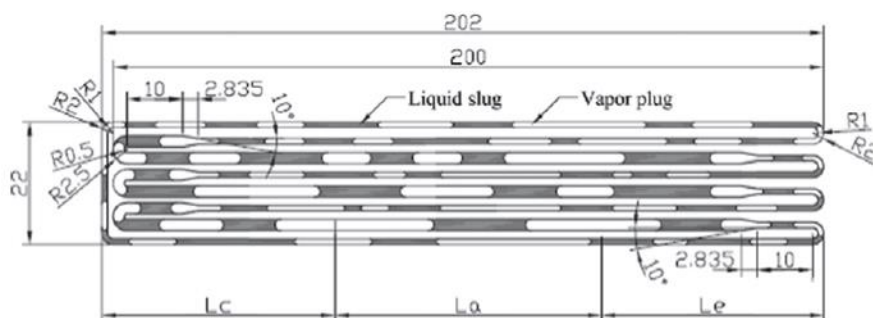


Figure 2.13. Schematic of the PHP configuration used in the numerical simulation done by C.M. Chiang et al. [86].

The calculated results confirmed that the PHP with non-symmetrical arrayed mini channels could attain a better performance with respect to the constant cross flow configuration, also when horizontally placed. The additional un-balancing surface tension established by the variation of the ID is able to amend the loss of gravity contribution, establishing a net two-phase flow also horizontally, i.e. when the device is not gravity assisted.

These numerical results have been validated by Chien et al. [87] in a further experimental work. Two flat plate pulsating heat pipes made by copper capillary tubes were investigated. The first one was milled in order to have 16 parallel square channels (7 number of turns at the evaporator) maintaining the same cross section (2 mm x 2 mm). The other one was

## **2. PHP and compact Loop-Thermosyphon: working principle and state of the art**

---

milled in such a way to have 16 alternative square channels of 2 mm x 2 mm and 1 mm x 2 mm. The thermal resistance of the non-uniform cross-section channel PHP was less dependent by the orientantion. proving experimentally the previous work of C-M. Chiang. However, the smaller cross-sections in the non-uniform PHP, increasing the distributed pressure losses along the circuit, decreases the overall thermal performance of the device in BHM. .

Another similar and more recent work was performed by Jang et al. [88], where different Flat Plate PHP with various a-symmetric channels were tested, varying the depth of the different channels. The depths of channels were 0.4, 0.6, and 0.8 mm. FC-72 was utilized as a working fluid, using a FR=50%. As the a-symmetric ratio increased, active oscillating and circulation motion occurred with increased driving force showing better thermal performance. In high heat input region, high a-symmetric ratio acted as the flow resistance showing lower thermal performance. The thermal performance increased with the increase of the channel depth due to decreased flow resistance. Nevertheless, the original design proposed by these authors is applicable only in a flat panel, which shows less flexibility when the space constraint is conspicuous. Also, it may not directly apply to the conventional corrugated PHP configuration.

Another experimental work done by Tsieng et al. [89] aims to extend the applicability of the previous concept to the commonly PHPs. In this study, two CLPHPs having either uniform or alternating tube diameter were tested. Detailed geometries and dimensions of the tested CLPHPs are

## 2. PHP and compact Loop-Thermsoyphon: working principle and state of the art

---

shown in Figure 2.14. The PHPs were tested both in vertical and horizontal orientation, using different working fluids (methanol, HFE-7100 and water), with a  $FR=60\%$ .

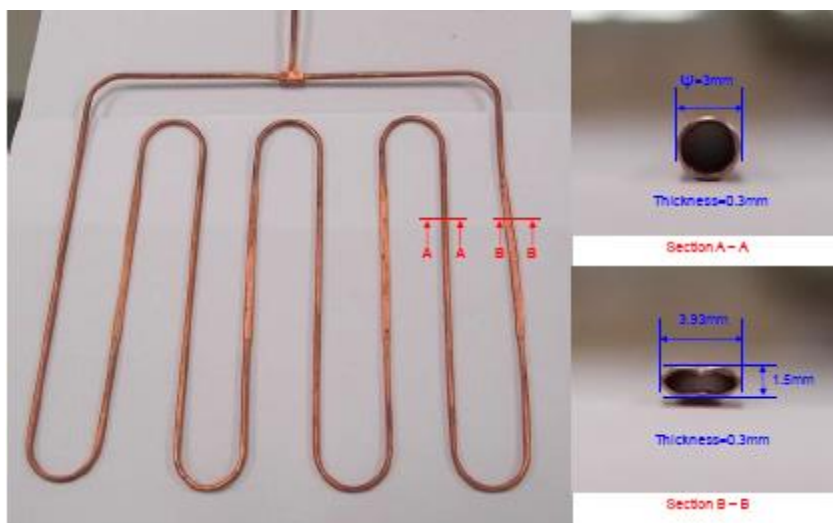


Figure 2.14. The PHP tested with a different inner diameter along the tube [89].

The alternating design reveals considerable oscillation of the surface temperatures at the evaporator and condenser, suggesting a self-sustaining periodic motion of the vapor slug. However, since both of the devices are entirely in copper, there is no the possibility to perform flow visualization analysis. Furthermore, the thermal resistances obtained when the devices are tested in BHM are significantly lower with respect to those obtained horizontally.

## **2. PHP and compact Loop-Thermosyphon: working principle and state of the art**

---

It is worthwhile to stress that both of the solutions reported, i.e. CLPHP/CV and the creation of non-uniform channels increase of course the complexity in the design of the PHPs. Furthermore, the results obtained and analyzed do not reveal an important improvement in terms of thermal performance. The efforts found in literature highlights that is of particular interest to stabilize the two-phase flow motion within this complex passive device, but the actual methods add too much complexity to the system. As a consequence, it is necessary to find other solutions to promote the two-phase flow motion in a preferential direction.

A possible solution to stabilize the two-phase flow motion is to implement a non-symmetric thermal boundary conditions on the fluid, maintaining the actual PHP simple geometry and construction. Using some heated spots distributed conveniently along the PHP tube, a stabilization of the fluid motion could be achieved. For instance, Thompson and Ma [90] characterized the PHP performance under localized heat fluxes. Three local spot heaters were positioned along the PHP's line of symmetry. It was observed an internal fluid activity only in the region close to the heating elements, while the fluid located away from the point of heating remained stagnant.

The thermal performance of the device could be enhanced, without precluding the design simplicity, exploiting and improving this "spotted" heating mode. Positioning the heating elements in strategic locations along the serpentine, i.e. creating a non-symmetric configuration, the circulation in a preferential direction could be achieved. This concept is one of the main ideas investigated by the present work and it will be explained in details in the next sections.

### **2.5 Motivations and thesis layout**

Two-phase passive heat transfer device applied on electronic cooling problems both on ground and in micro-gravity conditions have been largely investigated in the last decades.

Designing a heat exchanger that is simple, passive and able to work also without gravity assistance is not an easy task. HPs has the main advantage to dissipate extremely high heat fluxes and the possibility to work in anti-gravity conditions with an appropriate wick structure. To the contrary, the fabrication costs are very high, and a certain knowhow is needed to design properly the wick.

LHP are other two-phase passive devices able to work without gravity, but are difficult to design and to manufacture, since they need a proper wick structure to work effciently.

The PHPs advantages, such as the production simplicity, low costs, high flexibility and above all the possibility to work in micro-gravity conditions, could make them the possible future candidate in electronic cooling also for space applications. Nevertheless, the pulsating motion involved in such system is chaotic and unpredictable. Furthermore, the global heat power input that they can dissipate is limited by the capillary inner diameter.

This thesis has the main objective to partially avoid these two limitations of a PHP. By means of peculiar heating element positions and heat power configurations at the evaporator, the main goal is to stabilize the two-phase flow motion direction in a preferential direction, increasing

## **2. PHP and compact Loop-Thermosyphon: working principle and state of the art**

---

also the thermal performance of the device without avoiding its intrinsic design simplicity.

Furthermore, since the capillary limit depends on the gravity field, for the first time in literature is tested in micro-gravity conditions a device with an ID slightly higher than the capillary one on ground. The main objective is to demonstrate that the sudden absence of buoyancy forces in micro-gravity will activate a slug/plug flow motion typical of a PHP, allowing the device to work even with a larger diameter in weightlessness. The main goal to achieve is to demonstrate that it is possible to design a device with a larger diameter than the capillary one on ground, with the relevant advantage to dissipate higher value of heat power inputs and able to work also without gravity-assistance. During the research activities performed and highlighted in this thesis, it is designed and tested an “hybrid” device that acts as a compact Multi-Evaporator Closed-Loop Thermosyphon on the Earth and as Pulsating Heat Pipe Only in micro-gravity conditions at the Thermal Physics Laboratories of the University of Bergamo. Then, the device is tested both on Earth gravity and in micro (0.01 g) and hyper gravity (1.8 g) conditions by means of two different Parabolic Flight Campaigns, with the main goal to demonstrate its feasibility both on ground and on space.

PART II

EXPERIMENTAL

ASSESSMENT

## **2. PHP and compact Loop-Thermsoyphon: working principle and state of the art**

---



## **2. PHP and compact Loop-Thermsoyphon: working principle and state of the art**

---

# Chapter 3

## 3. Design of the test cell

The review reported in Chapter 2 has shown that actually there are many works on the influence of the gravity field on the capillary limit but not so many on the influence of the gravity field on two-phase passive heat transfer device. Furthermore, a great number of studies were performed

with the main goal to stabilize the two-phase flow motion inside a PHP in a preferential direction. Nevertheless, the actual solutions, such as the use of check valves along the serpentine or the variation of the cross section geometry increase the complexity in the design and the dimensions of the PHP, hindering its possible applications in electronic cooling, where restricted volumes and surfaces are needed.

The lack of experimental test with respect to micro-gravity and the difficulties related to find a simple way to stabilize the two-phase flow motion within such passive devices lead to a series of interesting questions: *how does micro-gravity affect the capillary limit of a two-phase passive heat transfer device? Could micro-gravity activate a slug/plug flow motion inside a device with an ID higher than the capillary one on ground? Does such device works as a loop thermosyphon operating with the “bubble lift” principle on ground and as a PHP in micro-gravity? Is it possible to stabilize the two-phase flow motion by means of a strategic position of the heating elements both on ground and in micro-gravity preserving at the same time the design simplicity?*

In order to answer to all these issues, experiments must be performed both on ground and in micro-gravity conditions with a proper device.

One possible solution is to perform test during parabolic flight campaigns. During a parabolic manoeuvre, both micro and hyper-gravity conditions can be experienced. Consequently, it is possible to test the device under this peculiar conditions, otherwise impossible to achieve on the Earth.

Additionally, a thorough and complete ground test characterization is mandatory, with the main objective to investigate experimentally if peculiar heating configuration at the evaporator could stabilize the two-phase flow motion in a preferential direction, thus increasing the thermal performance of the device.

In this chapter, the experimental setup is presented in detail, focusing on the selection of the ID dimensions and the peculiar position of the heating elements.

#### **3.1 Choice of the inner diameter dimension**

As amply discussed in the Chapter 2, it is theoretically possible to build a PHP for space application (SPHP) with an ID bigger than the static critical diameter on ground. Since under reduced gravity the body forces are negligible, the threshold diameter to obtain a slug-plug configuration increase. This has an important consequence on the heat exchange: since the mass of the thermal fluid per unit length is proportional to the square of the ID, increasing the inner diameter is also beneficial in terms of global heat exchanged.

Since, as already discussed in Section 2.3, the capillary limit threshold is also due to inertial and viscous effects, the dynamic threshold levels, evaluated by means of Weber and Garimella criteria proposed by Mameli et al. [13] may be more suitable to define the limit for space applications. In order to provide some order of magnitudes, Table 3-1 shows the confinement diameters relatively to static and dynamic criteria both in earth

### 3. Design of the test cell

and reduced gravity environments conditions for FC-72 at 20 °C, since this is the fluid used in this thesis work.

Table 3-1 Capillary limit in static and dynamic conditions on ground and reduced gravity conditions for FC-72.

FC-72 at 20°C	$D_{cr}$ [mm] (static)	$D_{Ga}$ [mm] $U_l=0.1$ m/s
Equations	$d_{cr,bo} \approx 2 \sqrt{\frac{\sigma}{g(\rho_l - \rho_v)}}$	$d_{cr,Ga} \approx \sqrt{\frac{160\mu_l}{\rho_l U_l} \sqrt{\frac{\sigma}{(\rho_l - \rho_v) \cdot g}}}$
Earth gravity level: $g = 9.81$ m/s <sup>2</sup>	1.68 mm	0.8 mm
Mars gravity level: $g = 3.73$ m/s <sup>2</sup>	2.72 mm	1.3 mm
Lunar gravity level: $g = 1.62$ m/s <sup>2</sup>	4.13 mm	1.97 mm
Microgravity: $g = 0.01$ m/s <sup>2</sup>	52.88 mm	4.2 mm

As shown in Table 1, taking also into account viscous and dynamic effects, it is still possible to design a device with an ID higher the capillary limit on ground but able to guarantee theoretically a slug/plug flow motion in micro-gravity. For example, designing a device with an ID of 3 mm, filled up with FC-72, the fluid will appear stratified; on ground it should be expected a stratified flow; in micro-gravity a slug/plug flow, as shown qualitatively in Figure 3.1.

### 3. Design of the test cell

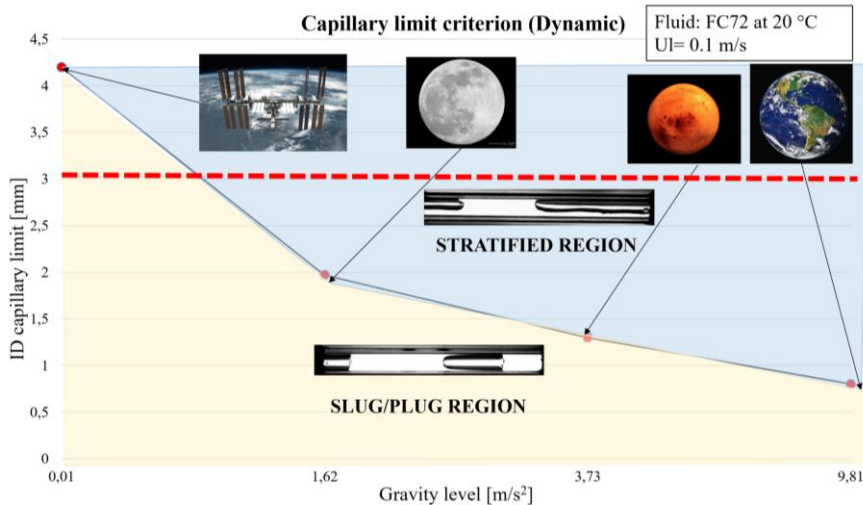


Figure 3.1 Qualitative plot in which is shown the capillary limit varying the gravity level.

Designing a two-phase close loop heat transfer device with an ID of 3 mm and filled up with FC-72, a stratification of the two-phase flow motion should be theoretically achieved on Earth, making the device to work as a Loop Thermosyphon, while a slug/plug flow typical of PHP should be activated in micro-gravity conditions, opening the frontiers to a new family of *Pulsating Heat Pipe only for Space Applications* (SPHP).

In such a way, it should be possible to dissipate higher value of global heat power with respect to the standard PHPs in micro-gravity, maintaining however the simplicity in the design.

### 3. Design of the test cell

Taking into account both the static and the dynamic criterion, the inner diameter range where a device may work as a SPHP can be qualitatively represented in Figure 3.2:

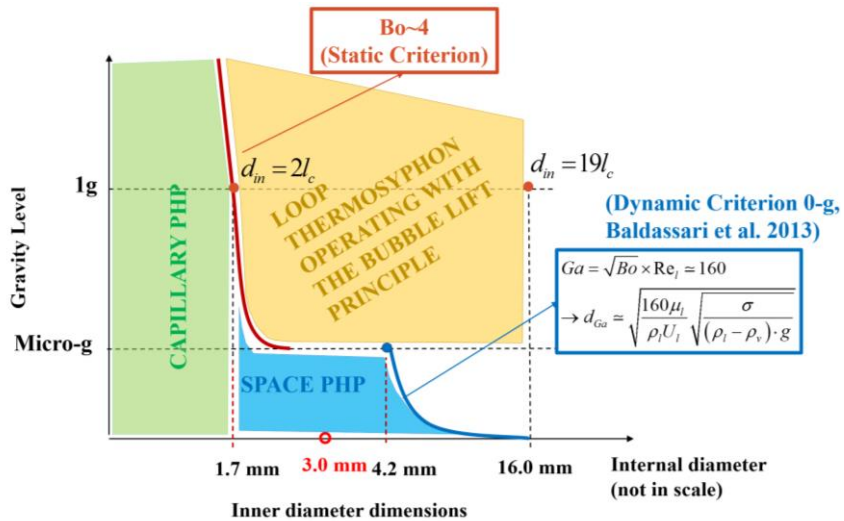


Figure 3.2 Qualitative representation of the two-phase flow passive heat transfer devices varying the ID dimensions and the gravity field.

The first experimental validation of such a hybrid concept are presented in this thesis work.

For these reasons it is designed a device with an an ID of 3 mm and filled up with FC-72. The detailed experimental apparatus is described in the sequent section.

#### 3.2 The proposed device

The proposed cooling device is made of an aluminum tube (I.D./O.D. 3.0 mm/5.0 mm) bent into a planar serpentine with ten parallel channels and five turns at the evaporator (all axial curvature radii are 7.5 mm), as shown in Figure 3.3.

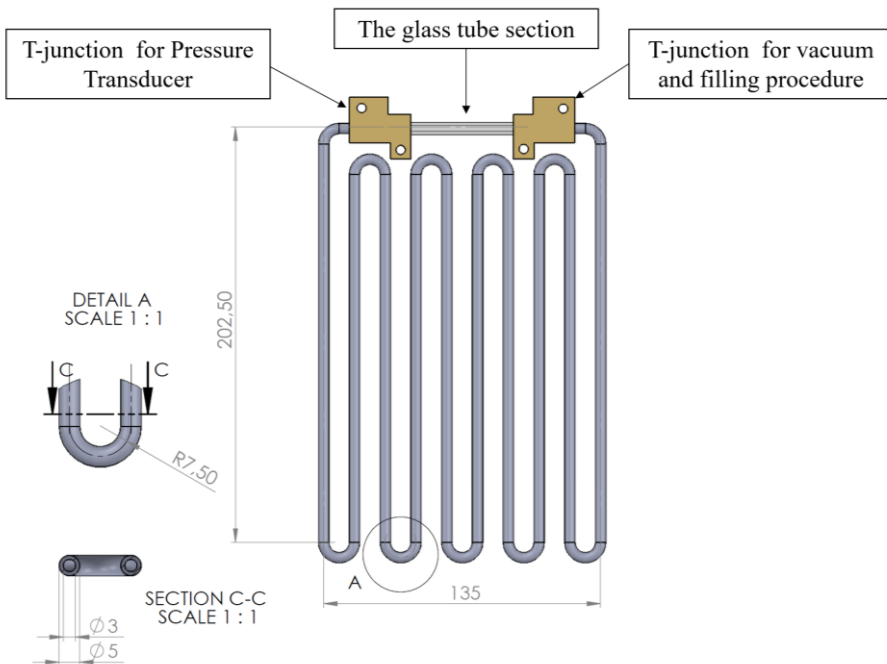


Figure 3.3 Geometry of the device.

The aluminum tube is partially filled with FC-72 as a working fluid, utilizing a FR of  $0.5 \pm 0.02$  corresponding to 8.3 ml. FC-72, also known as perfluorohexane or tetradecafluorohexane, is an electrically non-conductive, non-flammable, inert fluorocarbon-based fluid of the



### 3. Design of the test cell

---

“Fluorinert™” line of commercial coolant liquids sold by 3M. It is colorless and odorless. Its properties are pointed out in Table 3-2:

Table 3-2 FC-72 properties

Molecular composition	C <sub>6</sub> F <sub>14</sub>
Boiling point	56 °C
Melting point	-90 °C
Molar mass	338.042 kg/kmol
Vapor pressure at 25°C	27 kPa
Density	1680 kg/m <sup>3</sup>
Liquid specific heat	1100 J/kgK
Liquid thermal conductivity	0.057 W/mK
Surface tension $\sigma$	0.01 N/m

A 50 mm glass tube closes the loop at the top of the condenser zone, allowing the flow pattern to be observed directly. The glass tube is connected to the aluminum serpentine by means of two “T” junctions that derive two ports at each side: one is devoted to the vacuum and filling procedures, while the second one hosts a pressure transducer (Kulite®, XCQ-093, 1.7 bar A, Table 3-3). A specific low vapor pressure glue (Varian Torr Seal®) seals the aluminum tube, the “T” junctions and the glass tube together.

### 3. Design of the test cell

---

Table 3-3. Pressure transducer Kulite® XCQ-093 specs

Pressure range	0 - 1.7 bar absolute
Operating temperature range	-55 °C to +120°C
Excitation	10 V (maximum 12 V)
Full Scale Output (FSO)	100 mV (Nom.)
Residual Unbalance	± 5 mV (Typ.)
Combined Non-Linearity, Hysteresis and Repeatability	± 0.1% FSO BFSL (Typ.), ± 0.5% FSO (Max.)
Thermal Zero Shift	± 1% FS/100°F (Typ.)
Thermal Sensitivity Shift	± 1% /100°F (Typ.)
Weight	0.4 g

Sixteen “T” type thermocouples (bead diameter 0.2 mm, ± 0.1 K) are located on the thermosyphon external tube wall: ten in the evaporator zone and six in the condenser zone, while an additional thermocouple is utilized to measure the ambient air temperature as illustrated in Figure 3.4.

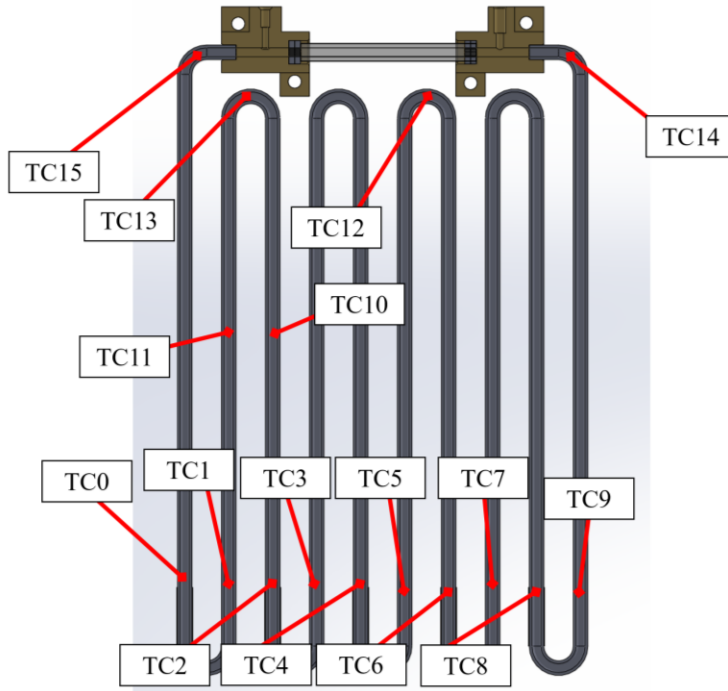


Figure 3.4 Thermocouple locations along the serpentine

The exploded view of the test cell, with its main components, is visible in Figure 3.5.

### 3. Design of the test cell

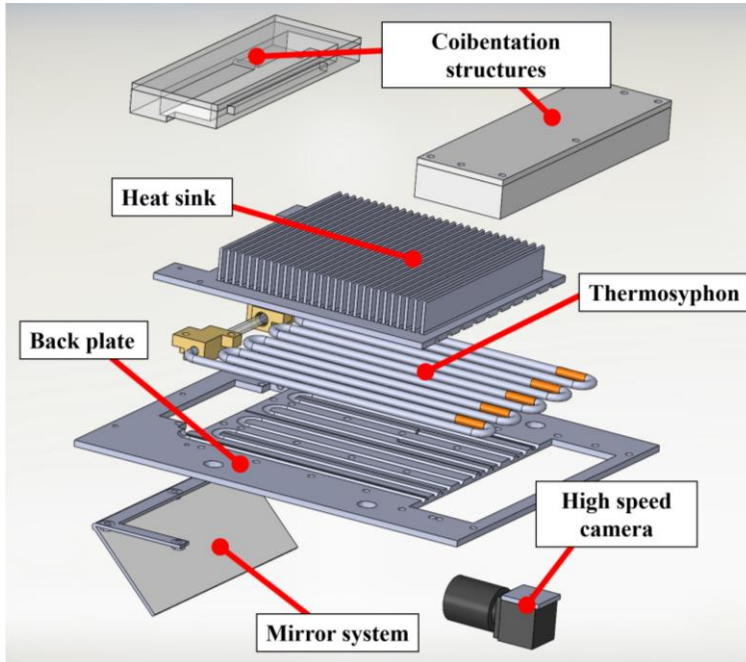


Figure 3.5 Exploded view of the test cell with all its main components.

The device is cooled down by forced air convection, utilizing two fans Sunon<sup>®</sup> PMD1208PMB-A), positioned just above the heat sink (165 mm total length), as shown in Figure 3.6a. The heat sink is milled with a CNC milling machine in order to fix the geometry of the SPHP, improving the heat exchange area (Figure 3.6b). The thermal contact between the heat sink, the aluminum back plate and the SPHP is enhanced by the use of thermal conductive paste (RS<sup>®</sup> Heat Sink Compound).

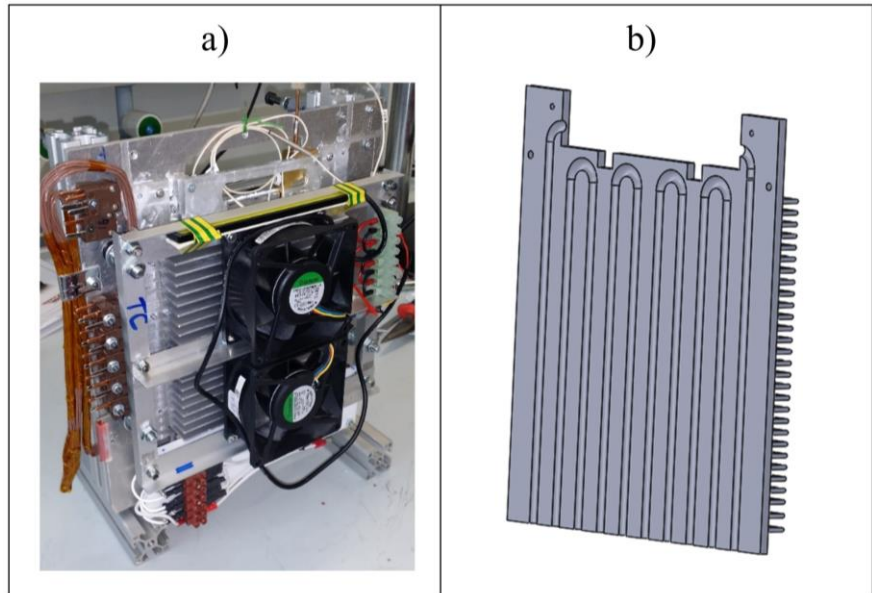


Figure 3.6 a) The two fans mounted above the heat sink; b) CAD view of the milled heat sink.

A compact camera (Ximea<sup>®</sup>, MQ013MG-ON objective: Cosmocar/Pentax<sup>®</sup> C2514-M, Fig 2.8) records the fluid dynamics through the glass tube. Decreasing the field of view solely at the glass tube in the condenser zone, the camera records image in the transparent section up to 400 FPS, acquiring images at a resolution of 1280x162 pixels (meaning a spatial resolution of 25 pixel/mm in the visualized region of interest). The Streampix<sup>®</sup> software package to produce very high (up to 100 MBps) bitrate video, where each frame can be separately saved as an image. In order to reach these high FPS, a LED with 5 W of electrical power input (COB LED<sup>®</sup>) is positioned in front of the glass tube.

#### 3.2.1 Vacuum tests and filling procedure

Completed the mounting procedure of the SPHP and glued the T-junctions, the glass tube and the aluminum tube, a vacuum test is mandatory in order to check if the sealing is leak proof.

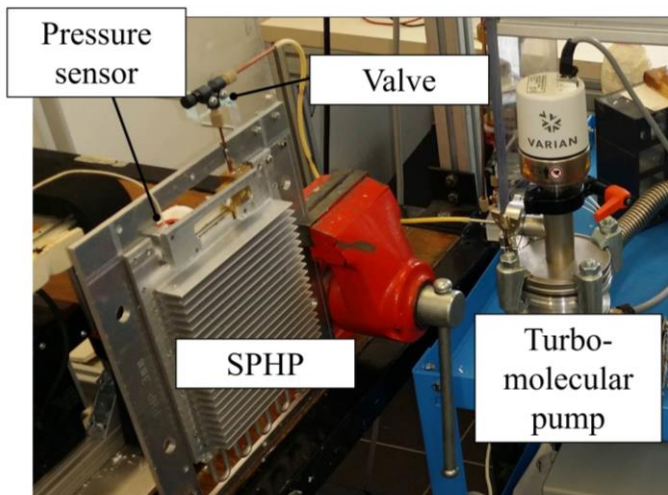


Figure 3.7 Vacuum test of the device

The device is connected to the Ultra High Vacuum System (Varian<sup>®</sup> DS42 and TV81-T) by means of a micro-metering valve (Upchurch Scientific<sup>®</sup> UP-P-447, leak rate  $< 1 \cdot 10^{-7}$  mbar/l/s). The SPHP is vacuumed down to  $6 \cdot 10^{-6}$  mbar (measured by the UHV system at the pump outlet) and the valve is closed. The pressure level inside the PHP is monitored for 24 hours. The pressure recorded by means of the pressure transducer directly glued inside the SPHP did not increase during the 24 hours, pointing out the leak

proof of the device. Checked successfully that the device is leak proof, the device has to be partially filled up properly with a certain amount of FC-72 with a proper filling procedure. The emptying and filling procedure includes the operations whose main objective is to ensure the correct filling of the loop. The circuit was another time vacuumed by means of the vacuum system described before, until an inner pressure of approximately  $1 \times 10^{-6}$  mbar is reached. Then, the micro-metering valve connecting the SPHP to the emptying and filling system was secured. Vacuuming the device up to this ultra-high vacuum level is necessary to ensure a correct working mode of the two-phase passive heat transfer device: the presence of even small quantities of non-condensable gases inside the device in fact contributes to increase the sub-cooling degree of the working fluid [91]. If this happens, the resulting effect will be an increase of the working fluid temperatures and pressure, as well as a deterioration of the thermal performance of the device [92]. Therefore, it is necessary to partially filled up the loop with pure FC-72 firstly properly degassed. In order to achieve this goal, it is realized a filling system (Figure 3.8)

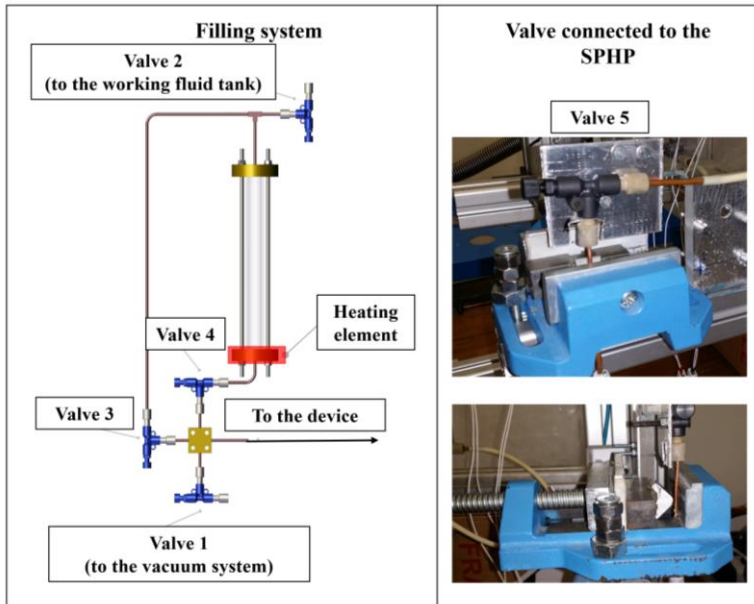


Figure 3.8 The filling system and the valve connected to the system.

The emptying and filling procedure was completed through some actions that involves the opening or closing of the micro-metering valves sketched in Figure 3.8.

The main actions can be summarized as follows:

- The working fluid tank was filled up to 15 ml (valve 2 opened in Figure 3.8). The tank is a graduated cylinder made by a borosilicate glass, with a precision of  $\pm 0.2$  ml;
- The working fluid tank was heated from below through a heat element until the working fluid temperature reached the boiling point;



- The non-condensable gases released during the boiling process and accumulated at the top of the working fluid tank were sucked through the vacuum pump (valve 3 and valve 1 opened in succession);
- The aforementioned step was repeated at least four times in order to ensure the proper degassing of the working fluid [93];
- The connection lines between the working fluid main tank and the SPHP was filled (valve 4 in Figure 3.8 opened);
- The SPHP was filled (valve 0 in Figure 3.8 opened); the working fluid level was recorded in order to ensure the correct filling ratio, helped visually by the variation of the liquid free surface in the graduated transparent tank.
- As soon as the desired volume of liquid filled the loop, the valve directly mounted close to the T-junction was finally closed (Valve 5 in Figure 3.8);
- The device was finally sealed compressing mechanically the tube between the valve and the device and braising it utilizing a tin soldering machine by means of the press.

### **3.3 The heating element systems: symmetrical and non-symmetrical configuration**

In order to demonstrate if the non-symmetric position of the heating elements could stabilize the two-phase flow motion in a preferential

### 3. Design of the test cell

direction is necessary a comparison with a “baseline case”, in which the device is heated up “symmetrically” with respect to the gravity field. For this reason, tests on ground are performed both with a symmetric and a non-symmetric position of the heating elements.

In fact, each U-turn at the evaporator zone is covered by an electrical heating wire (Thermocoax<sup>®</sup> Single core 1Nc Ac, 0.5 mm O.D., 50  $\Omega$ /m, each wire is 720 mm long, corresponding to 36  $\Omega$ ). Two different arrangements of the heaters are tested on ground: in the first (Figure 3.9 a), wires are located on each bend symmetrically, while in the second layout (Figure 3.9 b), they are positioned on the branch just above the U-turn, non-symmetrically with respect to the gravity direction.

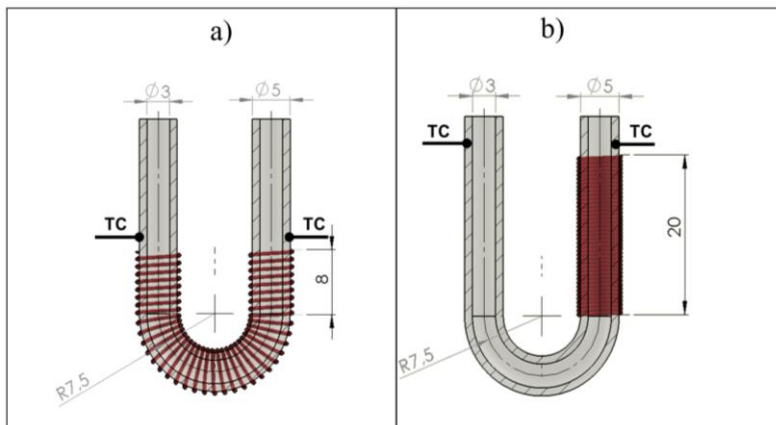


Figure 3.9 Heater and thermocouples arrangements, a) symmetrical, b) non-symmetrical.

### 3. Design of the test cell

Since the evaporator length of the non-symmetrical case (20 mm) is half the symmetrical case (40 mm), the heat flux dissipation capability of the non-symmetrical case is much larger, since. This means that if the same power is provided to the evaporator zone, the wall to fluid heat flux in the non-symmetrical arrangement is twice as much the heat flux provided to the symmetrical case as shown in Table 3-4.

Table 3-4. Heater layouts characteristics

Layout	$l_e$ [mm]	$\dot{Q}$ [W]	$q''$ [W/cm <sup>2</sup> ]
Symmetrical	40	10 - 260	0.53 – 13.75
Non symmetrical	20		1.06 – 27.5

During tests on ground, a power supply (GWInstek® 6006A) is connected to the heaters, providing a heating power input of up to 260 W, corresponding to a wall to fluid heat flux input of 13.75 W/cm<sup>2</sup> for the symmetrical case and 27.5 W/cm<sup>2</sup> for the non-symmetrical one. Steady state conditions can be reached in approximately three minutes due to the low thermal inertia of such heating system.

It is worthwhile to note that each branch at the evaporator zone is equipped with one thermocouple (see Figure 3.4): for the symmetrical case (Figure 3.9a) all of them are located 1 mm just above the heating wire. For the non-symmetrical layout, since the thermocouple array is shifted up by 10 mm, only one thermocouple per curve (TC-1, 3, 5, 7, 9 in Figure 3.4) is

close to the heater but this is still sufficient to characterize the evaporator zone.

In micro-gravity, the device is tested with the non-symmetric heating arrangement. During the 61th ESA Parabolic Flight Campaign, the five heating elements are connected electrically in parallel, allowing all the five heating elements to dissipate the same heat power input.

#### **3.4 The heating element system: PWM control system to control the five heating elements independently**

Before the 63<sup>th</sup> ESA Parabolic flight Campaign, the power control system is modified in such a way to control the five heating elements independently. Therefore, the device can be tested with different non-uniform heating configurations at the evaporator, creating an additional unbalance in the thermal boundary layers that could improve the overall thermal performance on ground and stabilizing the two-phase flow motion in weightlessness. In the text, the heating configurations in which all the heating elements dissipate the same heat power input are called “Homogeneous heating configurations”. To the contrary, the configurations in which the five heating elements dissipate different heat power inputs are called “Non-Uniform Heating configurations”.

The power supply (MW RSP-320) provides an electric power input up to 160 W, corresponding to a wall to fluid radial heat flux up to 17 W/cm<sup>2</sup>, with a maximum error of 4.7%. As shown in figure 2, the power is supplied

### 3. Design of the test cell

to the five heaters using a custom electronic interface between the powerlines and the data acquisition/control system (NI-cRIO-9074®).

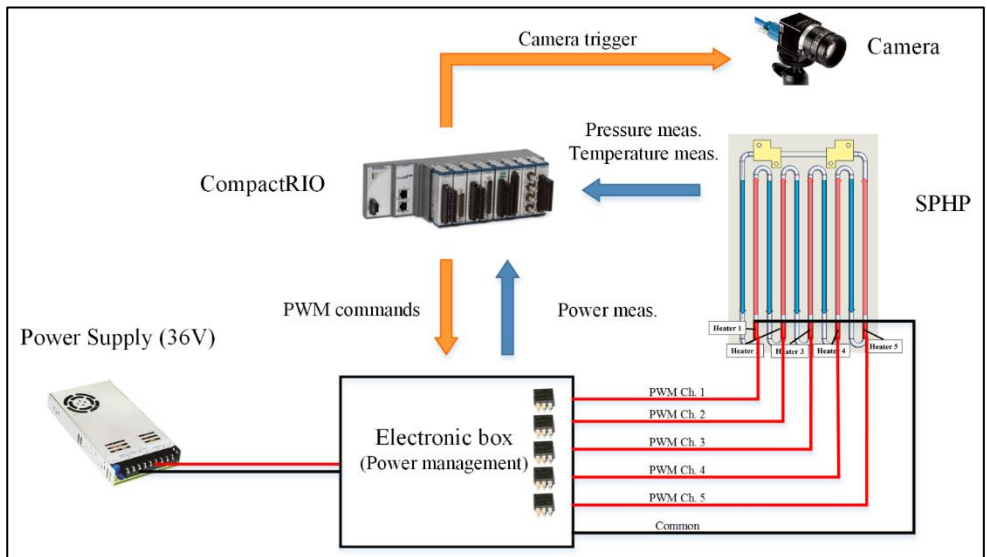


Figure 3.10 Experimental layout.

Each heater is managed by an isolated solid-state relay (PVG612A) controlled by the NI 9472 module. The PWM at 10 Hz is used to supply custom power levels to each channel. The actual mean and RMS voltages are measured through a voltage divider in the electronic box and acquired by the NI-9205 module. The camera is triggered at request by control system, and it is synchronized to the pressure measurement through a custom made code based on the Field Programmable Gate Array (FPGA) capability embedded in the NI-cRIO-9074®.

All the results that come from the ground test characterization and the two Parabolic Flight Campaigns will be pointed out in the next chapter:

- Chapter 4: in which are pointed out the results on ground testing the device with the two different heating arrangements, changing also important parameters such as inclination, the ambient temperature and the heating distribution at the evaporator by means of the PWM control system highlighted in Figure 3.10;
- Chapter 6: in which are pointed out the most important results obtained in hyper and micro-gravity conditions, heating up the device non-symmetrically during the 61th ESA Parabolic Flight Campaign;
- Chapter 7: in which are pointed out the most important results obtained in hyper and micro-gravity conditions, heating up the device non symmetrically and non-uniformly during the 63th ESA Parabolic Flight Campaign by means of the PWM control system highlighted in Figure 3.10.

# PART III

## GROUND TEST CHARACTERIZATION

---

# Chapter 4

## 4. Ground tests

In order to provide an overall characterization of the device on ground, different ground test campaigns were performed.

Specifically, the research team focused on:



## 4. Ground Tests

---

- The effect of the inclination angle and the heat power input [94] [95];
- The effect of the non-symmetrical heating distribution [45];
- The effect of peculiar non-uniform heating distributions [96];
- The effect of the ambient temperature [97].

In this chapter are extensively reported all the results obtained on ground. Initially, the experimental procedure is explained in detail. Then, the most relevant results will be pointed out.

Since on ground the ID is higher than the critical diameter value, there is no a slug/plug formation within the serpentine. Therefore, the device will acts like a Compact Loop Thermosyphon able to dissipate the heat power from multiple heated sections. It is worthwhile to stress that for the very first time in literature a thermosyphon with such geometry is designed and tested. As a consequence, this new kind of **Multi-Evaporator Loop Thermosyphon** will be called in the work with the acronym MELT.

### 4.1 Effect of the inclination angle, heat power input and position of the heating elements

The ground test campaign is carried out in order to compare the two different heater arrangements (see section 3.3) by identifying:

- the temporal evolution of the tube temperatures and local fluid pressure at the condenser zone at different heat flux levels;

## 4. Ground Tests

---

- the thermal performance of the device and operational limits in terms of heat input levels and orientation with respect to the vertical position: 75°, 60°, 45°, 30°, 15°, 2.5°, 0° (Horizontal);
- the operational regimes in terms of fluid motion;

For each inclination, the heat input power is increased in multiples of 10 W steps, with finer detail in the lowest power region in order to detect the start-up heat flux. Then, the power is increased with coarser heat input levels so as to reach the Critical Heat Flux (CHF) and, consequently, the evaporator dry-out condition<sup>3</sup>. After the sudden increase of the evaporator temperatures due to the dry-out condition, the heating power is reduced following the same heating level pattern in order to preserve the integrity of the system.

Each power step is maintained for at least 15 up to 16 minutes so that the system can reach a pseudo-steady state condition. The equivalent thermal resistance can be calculated only when the temperatures do not change in time and it can be evaluated as follows (Eq. 4.1):

$$R_{th} = \Delta \bar{T}_{e-c} / \dot{Q} \quad (\text{Eq. 4.1})$$

Where  $\Delta \bar{T}_{e-c}$  is the difference between the evaporator (TC1, TC3, TC5, TC7, TC9 for all the configurations tested, see Figure 3.4) and the condenser mean temperatures (TC10, TC11, TC12, TC13, TC14, TC15,

---

<sup>3</sup> For dry-out condition is intended when the temperature of at least one channel increases abruptly and suddenly, meaning that the liquid phase is not able to refresh this zone.

## 4. Ground Tests

---

see Figure 3.4), averaged in time during the last minute of the pseudo-steady state, and  $\dot{Q}$  is the effective global heat power input provided to the evaporator zone by the five heaters. Before doing tests, the liquid is distributed equally along the tubes by holding the device horizontally before raising it to the desired inclination.

### 4.1.1 Thermal Characterization in Vertical Position

The temporal evolution of the tube wall temperatures and of the fluid pressure is shown both for the symmetrical case (Figure 4.1 a) and the non-symmetrical case (Figure 4.1 b). The secondary x-axis (upper side) indicates the total heating power as well as the corresponding heat flux levels. Odd number thermocouples (TC1, TC3, TC5, TC7, TC9) are labeled with red/yellow lines while even (TC0, TC2, TC4, TC6, TC8) are represented with pink colors (Figure 4.1 c). The temperatures recorded in the condenser zone are illustrated with blue color lines (TC10, TC11, TC12, TC13, TC14, TC15); the ambient temperature “TC<sub>env</sub>” is shown in green color; finally, the fluid pressure “P” temporal trend is pointed out (secondary y- axis, on the right) in dark grey color. The detection of the different operational regimes is recognizable with such representation:

- the start-up when the temperature oscillation is recognizable only on a single or a few branches;
- the complete activation when the fluid motion is activated through all the channels, and the circulating regime when the fluid circulates in a preferential direction.

## 4. Ground Tests

---

- It is immediately worthwhile to mention that the dry-out limit was not reached in both cases, due to the power supply capability.

## 4. Ground Tests

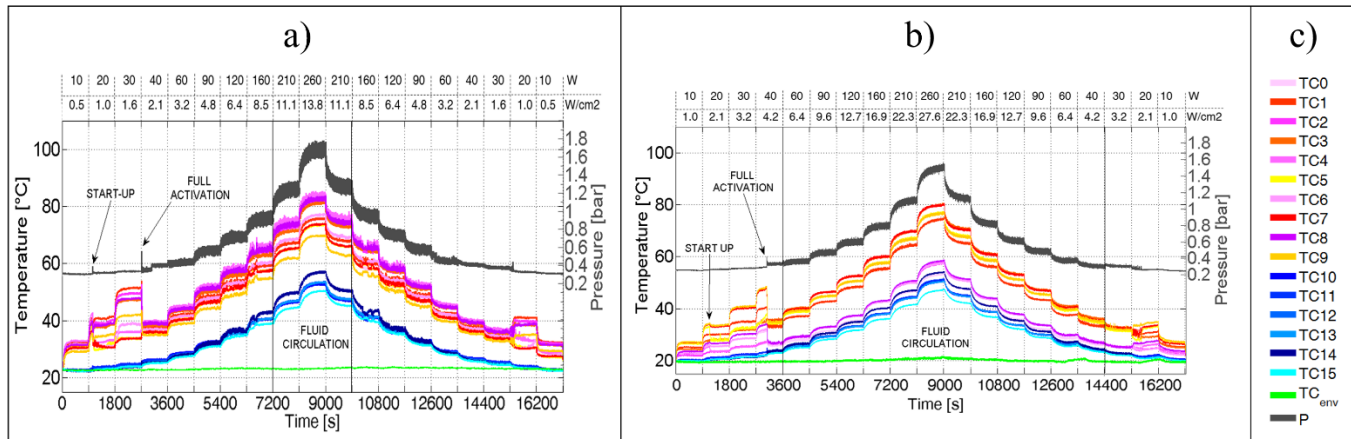


Figure 4.1 Temperature, pressure and power input diagram in vertical position, a) symmetrical heating; b) non-symmetrical heating; c) Legend.

## 4. Ground Tests

---

During the first heat input level, i.e. the lowest heat power levels tested, the fluid is not moving, as evidenced by the smooth pressure signal. Heat is transferred mostly by pure conduction along the tubes. For this reason, even small differences in the thermal contact between the five heating wires and the tube portions can cause a large temperature spread within the evaporator zone. Only a single or a few heated zones reach the superheating level required to activate the phase change process for the lowest heat power inputs: boiling may indeed occur locally in a single evaporator portion, causing the temperature drop only for the two corresponding temperature measurements, resulting only in a partial start-up (Figure 4.2a).

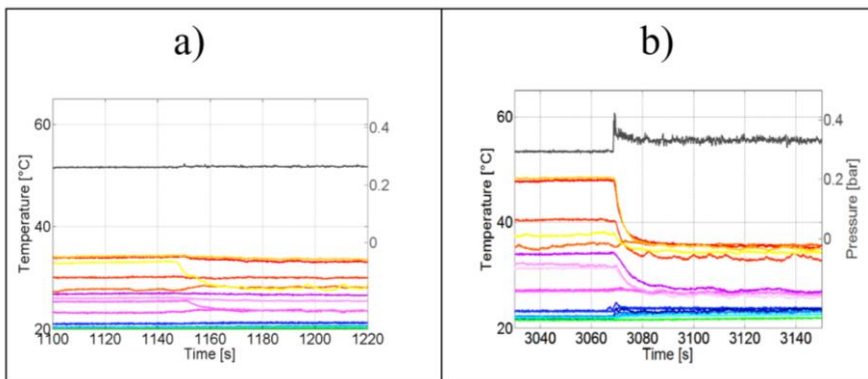


Figure 4.2 Wall temperature and fluid pressure: a) partial startup at 20W; b) Complete activation at 40W.

This partial start-up occurs at 20 W both in the symmetrical and non-symmetrical case. Only when all the heated zones are above the

## 4. Ground Tests

---

superheating temperature level, the full activation occurs and all the temperature trends drop down (Figure 4.2b), while a sudden peak in term of pressure points out the passage of a two-phase flow with an higher temperature in the condenser zone. The full activation occurs at 40 W for both the configurations but, interestingly enough, the non-symmetrical case switches to the circulating mode immediately after. This is pointed out not only by the fluid visualization study (Figure 4.3a and Figure 4.3b), but also from the tube wall temperature trend recorded just before and after the glass tube section (TC14 and TC15) as shown in Figure 4.3c and in Figure 4.3d.

## 4. Ground Tests

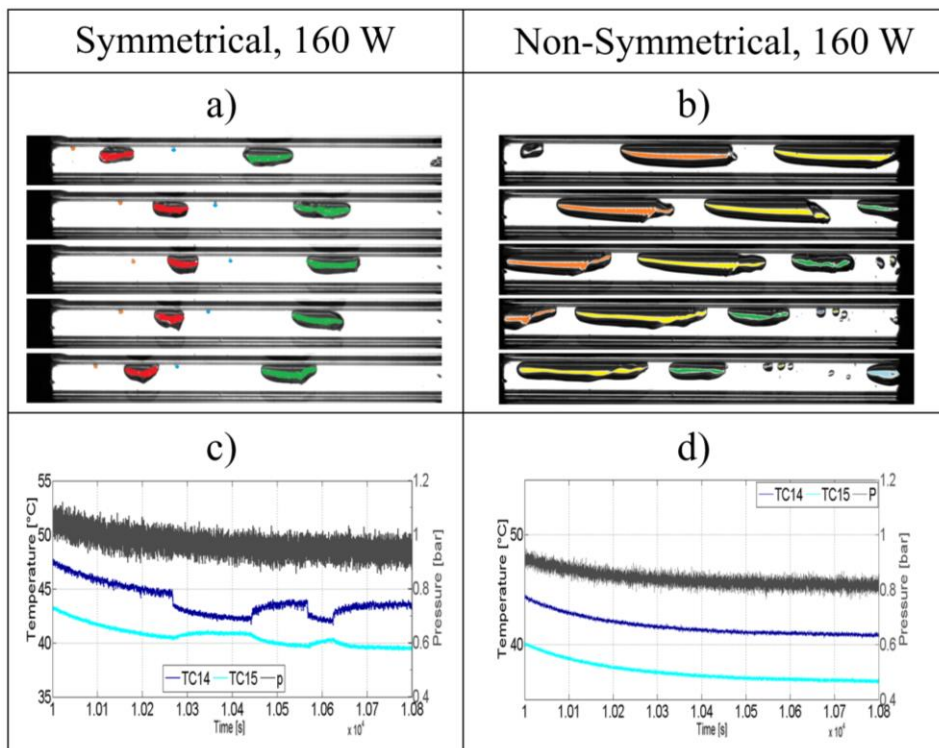


Figure 4.3 Symmetrical, a) visualization of oscillating motion 45 fps; b) Temperature and Pressure measurements at the transparent section ends; Non-Symmetrical, c) visualization of oscillating motion 45 fps; d) Temperature and Pressure measurements at the transparent section ends.

In the symmetrical arrangement, after the complete activation, the fluid inside the transparent section does not move in a preferential direction as shown in Figure 4.3a. The temperature measurements at the extremities of the transparent section (Figure 4.3c) reveal the occurring of frequent flow reversals: TC14, TC15 come close to each other depending on the actual



## 4. Ground Tests

---

flow direction. Only when the heat input level reaches 210 W the fluid starts moving in a preferential direction.

In the non-symmetrical configuration, fluid circulation (Figure 4.3c) is detected immediately after the full activation. From then up to the highest heat power input tested (260 W) the temperature recorded by TC14 is indeed always higher than the one recorded by TC15 (an example of flow circulation at 160W is shown in Figure 4.2d).

Furthermore, the higher pressure oscillations recorded in the symmetrical case (Figure 4.3c), points out high accelerations/decelerations, and flow reversals.

In the non-symmetrical heating arrangement, the combined effect of vapor bubble-lift and gravity helps the fluid rise up from the heated tubing sections and descend into the cooled sections respectively, as shown in Figure 4.4.

In the heated branches (up-headers, highlighted with red arrows in Figure 4.4), the fluid batches are lifted up from the evaporator to the condenser in the form of slugs, by means of the expanding vapor bubbles. The gravity head along the adjacent branches (down-comers, highlighted with blue arrows in Figure 4.4), assisting the return of the fluid from the condenser down to the evaporator zone, generates a stabilization of the fluid motion in a preferential direction. Therefore, the heated section are continuously refreshed by the two-phase flow with a lower temperature that comes directly from the condenser through the down-comers.

## 4. Ground Tests

---

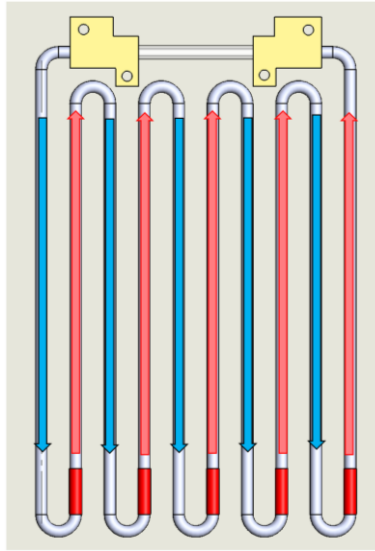


Figure 4.4 Fluid circulation scheme with up-headers (red arrows) and down-comers (blue-arrows).

### 4.1.2 Critical Heat Flux Analysis and comparison with standard thermosyphons

Since for a standard TS and for evaporator length to tube diameter ratios ( $l_e/d_{in} > 5$ ), the boiling limit is the less severe among the operational constraints (i.e. entrainment limit) [98], the general pool boiling CHF for FC-72 can be considered as the ideal maximum heat flux achievable.

Furthermore, the CHF achievable by the MELT is compared with existing correlations developed for CHF values for standard TS. The CHF is calculated for each case by means of the Kutateladze equation [99] considering the thermo-physical properties of FC-72 at 80°C (Eq. 4.2):

## 4. Ground Tests

$$q''_{CHF} = Ku \Delta h_{lv} \rho_v^{0.5} \left[ \sigma g (\rho_l - \rho_v)^{0.25} \right] \quad (\text{Eq. 4.2})$$

Table 4-1. Critical Heat Flux Correlations for FC72

CASE, [References]	Equation	Ku	q'' <sub>CHF</sub> [W/cm <sup>2</sup> ]
Pool boiling on large finite surfaces, [100]	$Ku = \pi/24$	0.131	16.4
Pool boiling in confined channels, [101]	$Ku = 0.1 / \left[ 1 + 0.491 (l_e / d_{in}) Bo^{-0.3} \right]$ Where: $Bo = g (\rho_l - \rho_v) d_{in}^2 / \sigma$	0.043	5.4
Pool boiling in confined channels, [102]	$Ku = 0.131 \left\{ 1 - \exp \left[ - \left( \frac{d_m}{l_e} \right) \left( \frac{\rho_l}{\rho_v} \right)^{0.13} \cos^{0.18} (\varphi - 55^\circ) \right] \right\}^{0.8}$	0.041	5.2

The obtained values listed in Table 4-1 can be compared to the experimental data from other literature Table 4-2. In particular, the Pool boiling CHF obtained by Jung et al. [103] agrees well with the prediction by Zuber [100] and also the Maximum heat flux achieved by the Closed

## 4. Ground Tests

---

Thermosyphon tested by Jouhara and Robinson [104] matches with the one predicted by Katto [101] and also by Piro and Voroncova [102].

In order to appreciate the increase of heat flux capability of the MELT technology with non-symmetric heating distribution with respect to the MELT heated up symmetrically, to TS, to the Pulsating Heat Pipe tested on ground [105], Table 4-2 also contains the technical data of three very similar experimental cases linked to the mentioned technologies.

## 4. Ground Tests

---

**Table 4-2.** Comparison between different technologies.

Reference	Jouhara and Robinson [104]	MELT Symmetric Heating Distribution	MELT Non Symmetric Heating Distribution	Mameli et al. [17]	Jung et al. [103]
Fluid	FC-84	FC-72	FC-72	FC-72	FC-72
FR (Vol.)	0.25	0.50	0.50	0.50	-
Fluid Vol. [ml]	1.8	5.6	5.6	3.1	-
$d_{in}$ [mm]	6.0	3.0	3.0	1.1	-
$l_{tot}$ [m]	0.2	0.2	0.2	0.2	-
$l_e$ [m]	0.05	0.04	0.02	0.015	
N° of heated sections	1	5	5	16	1
$A_e$ [cm <sup>2</sup> ]	9.42	18.84	9.42	8.53	4
$\dot{Q}_{CHF}$ [W]	50	260	260	90	62.8

## 4. Ground Tests

---

$q''_{CHF}$ <sup>4</sup> [W/cm <sup>2</sup> ]	<b>5.31</b>	<b>13.8</b>	<b>27.59</b>	<b>10.55</b>	<b>15.7</b>
$R_{th}$ [K/W]	1.0	0.1	0.1	0.2	-
MELT with non-symmetric heating distribution improvement [%]	520	200	-	261	175

---

<sup>4</sup>  $q''_{CHF}$  is the maximum heat flux achievable with a stable operation before the occurrence of the thermal crisis.

## 4. Ground Tests

---

In order to give an idea of the heat flux capability enhancement due to the circulation of the fluid thanks to the non-symmetric heating distribution with respect to the other cases, the last row of Table 4-2 summarizes the percentage improvement.

In particular, a three times increase with respect to the Pool Boiling limit suggests that the actual working mode of the MELT technology is somehow closer to the flow boiling principles, even though the mass flow rate is rather than constant.

In such ground test characterization, further work are mandatory to provide a suitable correlation for evaluating the CHF. Interestingly the MELT technology is also filling some gaps still present in the PHP when it is heated up non-symmetrically: the circulation obtained by the smart use of gravity assistance, not only contributes to obtain larger heat flux capabilities but also to stabilize the circuit operation, making it more reliable and predictable.

### 4.2 Effect of the inclination

Beyond the characterization in vertical position, further tests at 75°, 60°, 45°, 30°, 15°, 2.5° and the horizontal position (0°) are performed with the main goal to evaluate the effect of the inclination on the thermal hydraulic behavior. The Equivalent Resistance ( $R_{eq}$ ) values for all the combination of heat power input/inclinations tested are reported in Figure 4.5:

## 4. Ground Tests

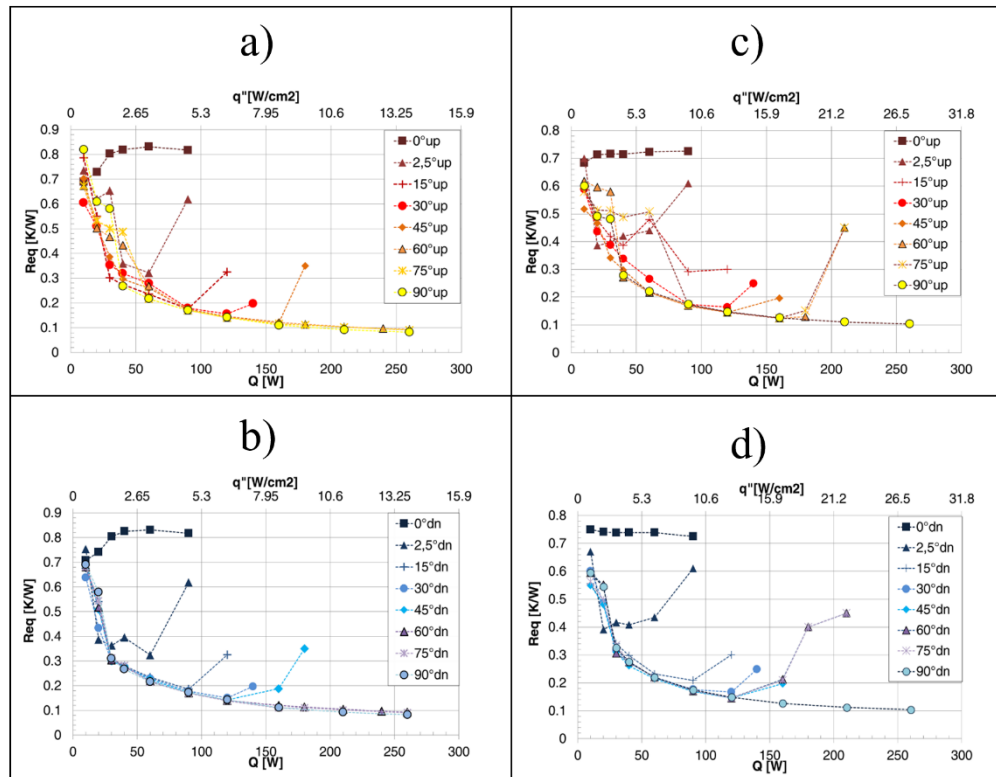


Figure 4.5 Equivalent thermal resistance for the various inclinations. The first power-up: a) symmetrical case, b) non-symmetrical case; the subsequent power-down: c) symmetrical case, d) non-symmetrical case.



## 4. Ground Tests

---

When the device is positioned horizontally, since the phase distribution is completely stratified, the liquid phase resides in the lower half of the pipe while the vapor phase in the upper one. Consequently, there is no any possibility of macroscopic fluid motion for all the tested heat input levels in this orientation, proving that even a small gravitational assistance is required to activate the device on ground.

For all the four tests performed in a horizontal orientation, the equivalent thermal resistance is constant for all the heat power tested and sets to the highest value of 0.8 K/W: the heat transfer is mainly due to conduction within the tube wall and the fluid itself.

Figure 4.5a and 4.5b show respectively the equivalent thermal resistance during the power-up and the power-down phase for the symmetrical case, while Figure 4.5c and 4.5d display the equivalent thermal resistance during the power-up and the power-down phase for the non-symmetrical heating arrangement.

When the device is heated up starting from ambient temperature there is no univocal dependence between the start-up heat input level and the device orientation. In fact, one could expect that for the lower inclinations, start-up may occur at lower heat input levels but, looking at Figure 4.5a and 4.5c, it is evident that the start-up heat input ranges randomly from 20 W to 60 W. This start-up issue not only depends on the heat input level and on the wall to fluid superheat but also on the initial distribution of liquid and vapor phases inside the channels and must be furtherly investigated.

## 4. Ground Tests

---

On the other hand, during the power-down case (Figure 4.5b and 4.5d) the fluid motion remains active down to 30 W for all the inclinations: the liquid phase is pushed back to the condenser more efficiently when the gravity effect is coupled with fluid inertial effects. This is also confirmed for medium-low power inputs, since all the curves collapse into a narrower band with respect to the power-up case. This behavior is technically positive: once the device is fully activated, a subsequent decrease of the heat flux below the first start up level does not compromise the device operation.

The only peculiar trend among all the orientations is detected when the device is just slightly tilted with respect to the horizontal position ( $2.5^\circ$ ); this small gravity head is sufficient to assist the fluid motion and makes the device less sensitive to the aforementioned start-up issues. Most probably, for the lowest inclination tested, the rising bubbles flatten against the upper side of the tubing and, despite the bubble lift effect being drastically reduced, vapor is able to slide upwards and contribute to convective cooling. Nevertheless, at  $2.5^\circ$  the fluid does not circulate inside the serpentine for all the tested heat inputs, resulting in a higher equivalent thermal resistance with respect to the other inclinations.

Increasing the heat power input, to the thermal resistance gradually decreases until the thermal crisis condition is reached, causing temperatures in the affected sections to rise over  $100^\circ\text{C}$ , noticeably penalizing thermal performance. In such conditions, a local dry-out condition occurs meaning that a vapor film prevents heated surface from being rewetted by the liquid.

#### 4. Ground Tests

---

As a consequence, the local temperature rises abruptly in at least one channel of the device, significantly increasing the equivalent thermal resistance. When it happened during tests, the reported thermal resistance values are approximated and are only qualitatively representing a trend, since the heat power was suddenly decreased to prevent the integrity of the device. Differently from the start-up, a direct relationship between the orientation and the dry-out heat input level is detected for both the symmetrical and the non-symmetrical case: increasing the tilting level towards the horizontal results in a lower value on the heat input capability. Therefore, the gravity head assists the evaporator rewetting: the lower the gravity head, the lower the fluid momentum opposing to the vapor expansion in the down comer, the higher the risk of local dry-out.

## 4. Ground Tests

### 4.3 Operational and flow regimes

Table 4-3 Flow pattern maps: a) Symmetrical case; b) Non-symmetrical case.

a)																										
SYMMETRICAL HEATING																										
Power-up phase (Q-up)												Power-down phase (Q-down)														
90°	-	-	-	S	O	O	O	O	O	C	C	C	C	C	O	O	O	O	S	-	-	-	90°			
75°	-	-	-	-	O	O	O	O	C	C	C	C	C	C	O	O	O	O	O	-	-	-	75°			
60°	-	-	-	-	O	O	O	O	C	C	C	C	C	C	O	O	O	O	S	S	-	-	60°			
45°	-	-	O	O	O	O	O	O	D						D	O	O	O	S	S	-	-	45°			
30°	-	-	S	O	O	O	O	O	D						D	O	O	S	-	-	-	-	30°			
15°	-	-	S	S	O	O	O	D							D	O	O	O	O	-	-	-	15°			
2.5°	-	S	S	S	O	D									D	O	O	O	S	-	-	-	2.5°			
0°	-	-	-	-	-	-									-	-	-	-	-	-	-	-	0°			
q''[W/cm2]	0.5	1.0	1.6	2.1	3.2	4.8	6.4	7.4	8.5	9.5	11.1	12.7	13.8	12.7	11.1	9.5	8.5	7.4	6.4	4.8	3.2	2.1	1.6	1.0	0.5	q''[W/cm2]
P[W]	10	20	30	40	60	90	120	140	160	180	210	240	260	240	210	180	160	140	120	90	60	40	30	20	10	P[W]
b)																										
NON SYMMETRICAL HEATING																										
Power-up phase (Q-up)												Power-down phase (Q-down)														
90°	-	-	S	C	C	C	C	C	C	C	C	C	C	C	C	C	C	C	O	S	S	-	-	90°		
75°	-	-	S	S	S	S	C	C	C	D					D	C	C	C	O	S	S	-	-	75°		
60°	-	-	-	C	C	C	C	C	C	D					D	C	C	O	O	S	S	-	-	60°		
45°	-	-	-	O	C	C	C	D							D	C	C	C	O	S	S	-	-	45°		
30°	-	-	-	-	C	C	C	D							D	O	C	C	O	S	-	-	-	30°		
15°	-	S	S	S	S	O	D								D	O	O	S	S	S	-	-	-	15°		
2.5°	-	O	O	O	D	D									D	O	O	O	-	-	-	-	-	2.5°		
0°	-	-	-	-	-	-									-	-	-	-	-	-	-	-	-	-	0°	
q''[W/cm2]	1.0	2.1	3.2	4.2	6.4	9.6	12.7	14.9	16.9	19.1	22.3	27.6	22.3	19.1	16.9	14.9	12.7	9.6	6.4	4.2	3.2	2.1	1.0	q''[W/cm2]		
P[W]	10	20	30	40	60	90	120	140	160	180	210	260	210	180	160	140	120	90	60	40	30	20	10	P[W]		
LEGEND																										
	Test not performed																									
-	No fluid motion nor temperature fluctuations																									
S	Partial start-up																									
O	Oscillation (after full start-up)																									
C	Circulation (after full start-up)																									
D	Dryout																									

## 4. Ground Tests

---

Indeed, special attention to the results should be given in terms of heat flux and flow regime maps.

Several different operational regimes can be observed and distinguished through the transparent tubing section, as shown in Table 4-3:

- the intermittent oscillating flow, recorded during the partial start-up and labelled with “S”;
- the oscillating flow, detected after the full start-up and labelled with “O”;
- the circulating flow, labelled by “C”;
- the dry-out condition, labelled with “D”.

During the power up side, the start-up phase for the symmetrical case (Table 4-3a) is less affected by the inclination both in terms of heat flux and flow pattern with respect to the non-symmetrical case. Furthermore, the fluid flow is always oscillating for the symmetrical case, except for the highest heat fluxes tested, where it is observed a circulation in a preferential direction, maybe due to the little asymmetries typical of an experimental apparatus. The start-up for the non-symmetrical case is more sensitive to inclination even if there is no a clear relation between them, but in such heating configuration, its flow pattern is immediately circulating in most of the cases. The circulating flow is maintained until the dry-out condition is reached and also recovered during the power down phase for a wider heat flux range with respect to the symmetric case.

## 4. Ground Tests

---

Furthermore, the non-symmetrical heating pattern is able to withstand higher heat fluxes before the dry-out occurs with respect to the symmetrical case for every inclination from horizontal to  $45^\circ$ . For instance, at  $45^\circ$  tilting angle, the symmetrical case stops working between 8.5 and 9.5  $\text{W}/\text{cm}^2$ ; the non-symmetrical pattern reaches the dry-out condition between 14.9 and 16.9  $\text{W}/\text{cm}^2$ . The higher heat flux capability of the non-symmetrical case would be most probably confirmed also for the vertical orientation if the power supply could cover a wider range. Interestingly enough, if one considers the power down as more representative of the device performance after the full start up, the symmetrical heating case maintains full operation for all the inclinations between 3.2 and 4.6  $\text{W}/\text{cm}^2$ ; the non-symmetrical case sets its threshold a just bit higher, between 4.2 and 6.4  $\text{W}/\text{cm}^2$ .

It is important to notice that recovering from the dry-out condition is not a trivial issue for such device. In fact, both patterns are able to recover once the heat flux is lowered down, but the crisis phenomenon usually persists at the subsequent heat input levels, and the heat flux must often be decreased by more than one step in order to restore the correct device operation.

### **4.4 Effect of peculiar heating configurations at the evaporator**

The results obtained providing to the device a non-symmetric heating distribution highlights that an unbalance of the thermal boundary layer can

## 4. Ground Tests

---

promotes a circulation in a preferential direction, thus expanding the working range towards higher heat fluxes and delaying dry-out conditions for all the inclinations tested.

The non-symmetrical heating distribution, creating an alternation of up-headers and down-comers, guarantees passively a circulation in a preferential direction. If the five heating elements are controlled independently between them, the device will be also heated non-uniformly at the evaporator, creating an additional unbalance in the thermal boundary layers at the evaporator. The additional unbalance could promote the circulation in a preferential direction, thus furtherly increasing the thermal performance for peculiar hating distributions.

Following this line of concept, it is performed an additional ground test characterization, modifying the power control system in order to control independently all the five heating elements.

The power per each heater is regulated with the PWM technique at 10 Hz operated by the control system. Five independent MOSFET relays PVG612A work as interfaces between the control system and the power side permitting to heat up the device with different heating distributions at the evaporator. The power supply (MW RSP-320 series) provides an electric power input up to 160 W, corresponding to a wall to fluid radial heat flux up to  $17 \text{ W/cm}^2$ , with a maximum error of 4.7%.

The device has been thermally characterized on ground in Bottom Heated Mode with different heating distributions utilizing three different levels of global heat power input: 50 W, 70 W and 90 W. All the heating

## 4. Ground Tests

---

configurations are kept constant for at least 15 minutes, in order to reach pseudo-steady state conditions. The thermal performance of the device is standardly calculated by means of the Equivalent Thermal Resistance ( $R_{eq}$ ). Table 4-4 shows all the configurations tested on ground providing to the device a global heat power input of 50 W.

Table 4-4. Heating configurations tested on ground providing to the device a global heat power input of 50 W.

Configuration Number	HEATER 1 [W]	HEATER 2 [W]	HEATER 3 [W]	HEATER 4 [W]	HEATER 5 [W]	GLOBAL [W]
1	10	10	10	10	10	50
2	9	9	9	9	14	50
3	6	8	10	12	14	50
4	4	7	10	13	16	50
5	2	6	10	14	18	50
6	6	6	6	6	26	50
7	14	8	6	8	14	50
8	12	8	10	8	12	50

The Configuration 1, in which all the heating elements dissipate the same heat power input of 10 W, is called “Homogeneous Configuration” and it represents the baseline case useful to compare results with the other “Non-Uniform Configurations” in terms of  $R_{eq}$ , temporal evolution of the temperatures and the inner pressure. From the Configuration 2 to the



## 4. Ground Tests

---

Configuration 5, the power is ever increased from the heater 1 to the heater 5, maintaining however a global heating power of 50 W. These configurations are selected and tested because the fifth heater pumps the fluid for a longer path (i.e. in the horizontal transparent section that closes the loop in the condenser zone) which dissipates a higher heat power. These kind of heating configurations will be named “Increasing” Configurations. Following this line of concept, another configuration (number 7 in Table 4-4) where the heating power is mostly concentrated only on the fifth heater (26 W that corresponding to the 52% of the global heat power input provided to the device), is called “Local High Value” configuration. Results obtained heating up homogeneously the device points out that the temperature at the lateral branches is lower than the temperature at the central braches, being the transversal thermal conduction lower in this region. Consequently, other two additional configurations (Configurations 8 and 9) are tested so as to decrease the heat power provided to the most central branches and to increase it at the most lateral ones. These kind of configuration are named “V-shape” configurations being the heating trend a “V-shape” split between the five heating element, higher at the edges and lower at the center.

Results point out that providing to the device a global heat power input of 50 W,  $R_{eq}$  decreases up to 8.7% from the Configuration 2 to the Configuration 5 with respect to the uniform heating configuration (Figure 4.6a).

## 4. Ground Tests

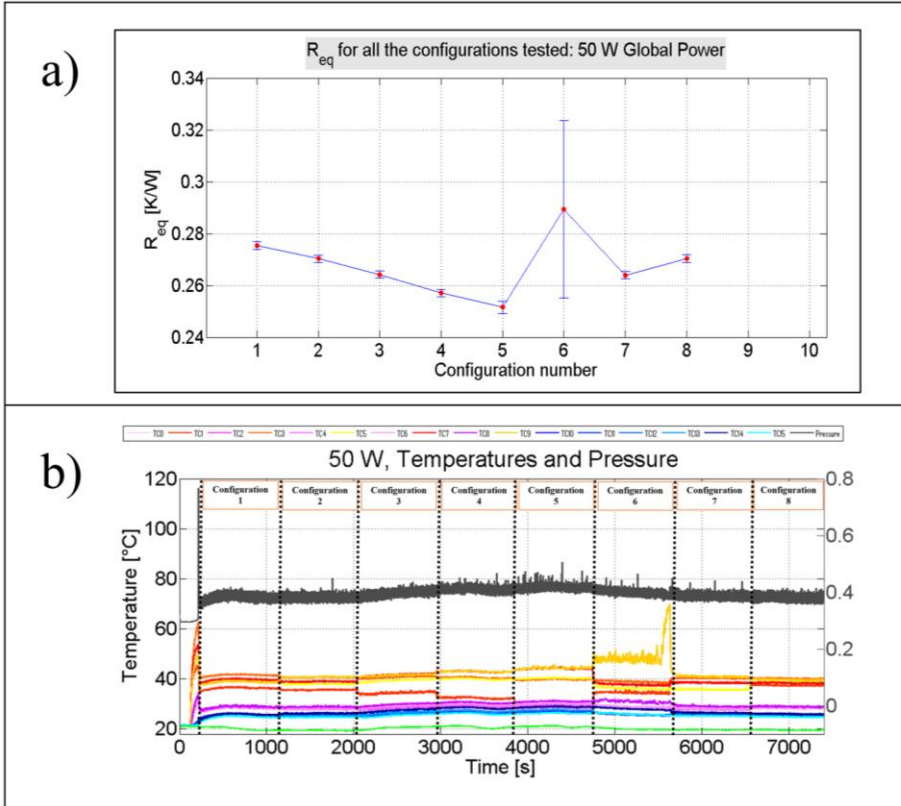


Figure 4.6 a)  $R_{eq}$  values for the configurations tested on ground providing a global power of 50 W; b) Temperatures and Pressure evolutions during test.

This is due to a better circulation of the two-phase flow motion in a preferential direction within the device: increasing the heat power input provided to the heater 5, the continue bubble expansions push the liquid batches more vigorously in the horizontal section of the condenser. Nevertheless, by increasing excessively the amount of power provided to the

## 4. Ground Tests

---

Heater 5 (“Local High Value”, Configuration 6) the thermo-fluid behavior gets unstable: the high RMS value (11,8%) in the  $R_{eq}$  plot points out continue oscillations of the temperatures both at the evaporator and at the condenser zone, as it is possible to see also from Figure 4.6b. By increasing the heat power at both of the lateral up-headers (“V-Shape” configurations), the  $R_{eq}$  decreases by the 4.1% with respect to the homogeneous heating configuration. Since the most lateral channels are subjected to a lower transversal conduction along the condenser plate with respect to the central channels, the temperature is locally lower at the edges of the condenser when the device is heated up homogeneously. Therefore, heating the most lateral channels with an higher value of power has a beneficial effect on the overall performance of the device, as pointed out by the  $R_{eq}$  value obtained with such configuration.

Similar results are obtained providing to the device 70 W of global heat power input and testing a specific “Increasing” heating configuration, where the power is continuously increased from the heater 1 to the heater 5. Results point out that the  $R_{eq}$  value in such non-uniform configuration decreases by 0.1 K/W with respect to the homogeneous case, as pointed out by Figure 4.7 (Homogeneous case) and Figure 4.8 (Increasing case).

### 4. Ground Tests

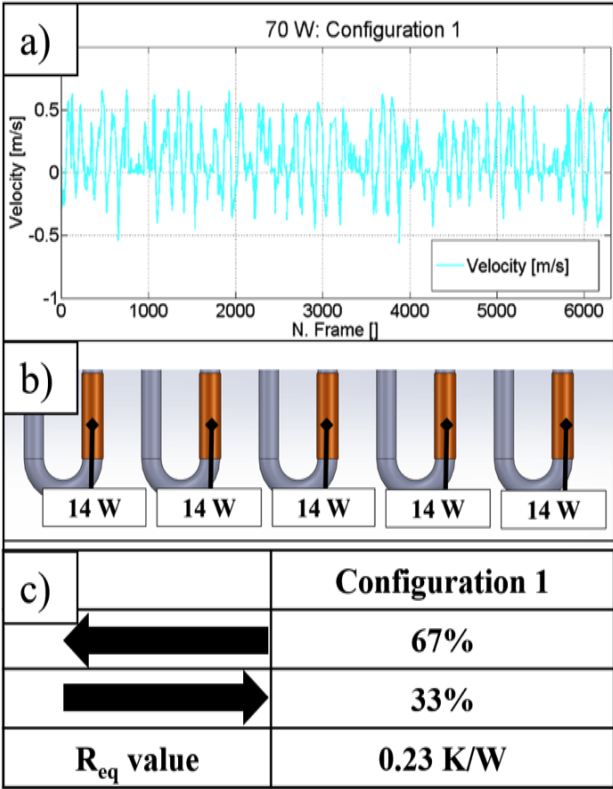


Figure 4.7 a) Bubble velocity when the device is heated up uniformly; b) the heating configuration provided; c) Bubble direction and  $R_{eq}$  value.

## 4. Ground Tests

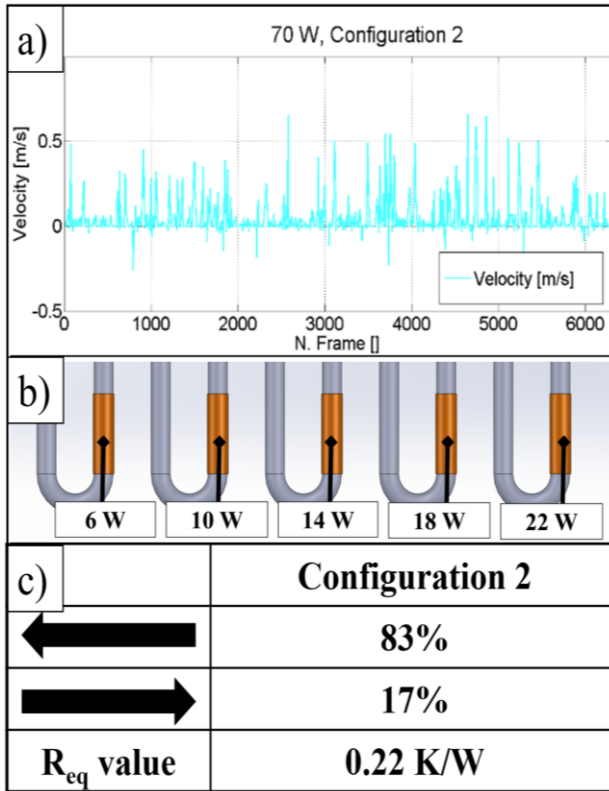


Figure 4.8 a) Bubble velocity when the device is heated up non uniform; b) the heating configuration provided; c) Bubble direction and  $R_{eq}$  value.

Additionally, a sequence of images (30 seconds at 200 fps) is post-processed to find the liquid/vapor interface velocity between each frame recorded both for the “Increasing” and the homogeneous heating configuration. Results show an improvement of the circulation in a preferential direction in case of the peculiar non-uniform heating tested. In such configuration, the bubbles move towards the transparent section for

## 4. Ground Tests

---

the 83% of the time (Figure 4.8 a and c) in the same direction; while when the device is homogeneously heated up, the circulation is observed for the 67% of the time (Figure 4.7 a and c). The circulation in a preferential direction has a positive impact on the overall performance, since the heated sections are continuously cooled down by the two-phase flow coming from the condenser, permitting to improve the overall thermal performance.

Heating up the device with a global power input of 90 W (Figure 4.7 c), the  $R_{eq}$  tends to 0.2 K/W for all the configurations tested: no significant improvements in terms of performance are detectable changing the heating distribution. For such global power, it is sufficient the non-symmetric position of the heaters to stabilize the two-phase flow motion in a preferential direction with such high power. As it is visible from the Figure 4.9, the temperatures both at the evaporator and at the condenser zone are stable for all the heated configurations. As a conclusion, the non-uniform heating distribution has a positive impact on the performance of the MELT especially for the lower global power tested. Increasing the global-power, the only non-symmetric position of the heaters is sufficient to provide a stabilization of the flow motion.

## 4. Ground Tests

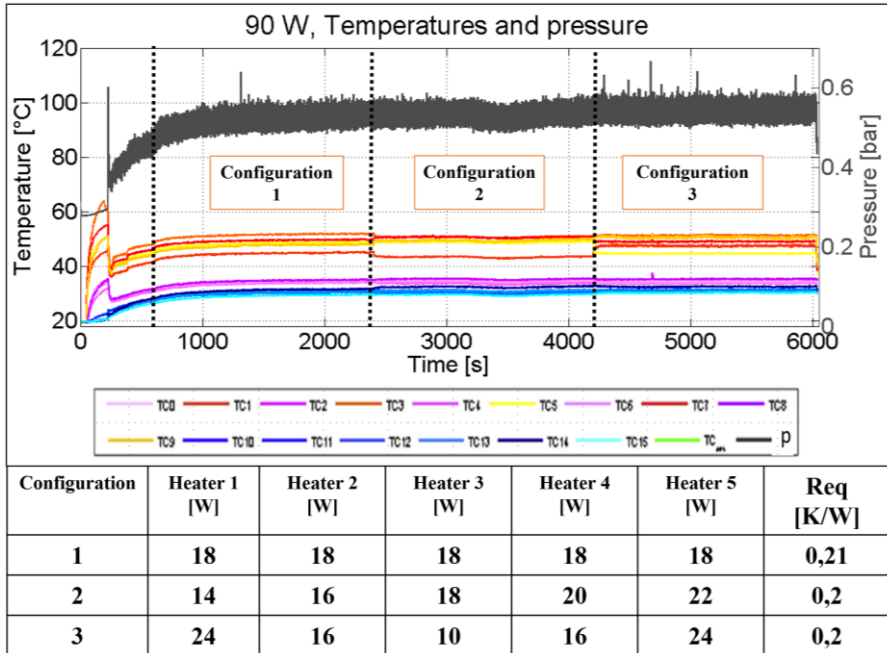


Figure 4.9. Temperatures and pressure for the configurations tested providing 90 W to the device.

Resuming, the peculiar non-uniform heating configuration increases the overall performance especially for the lower global powers tested, as shown in Figure 4.10.

## 4. Ground Tests

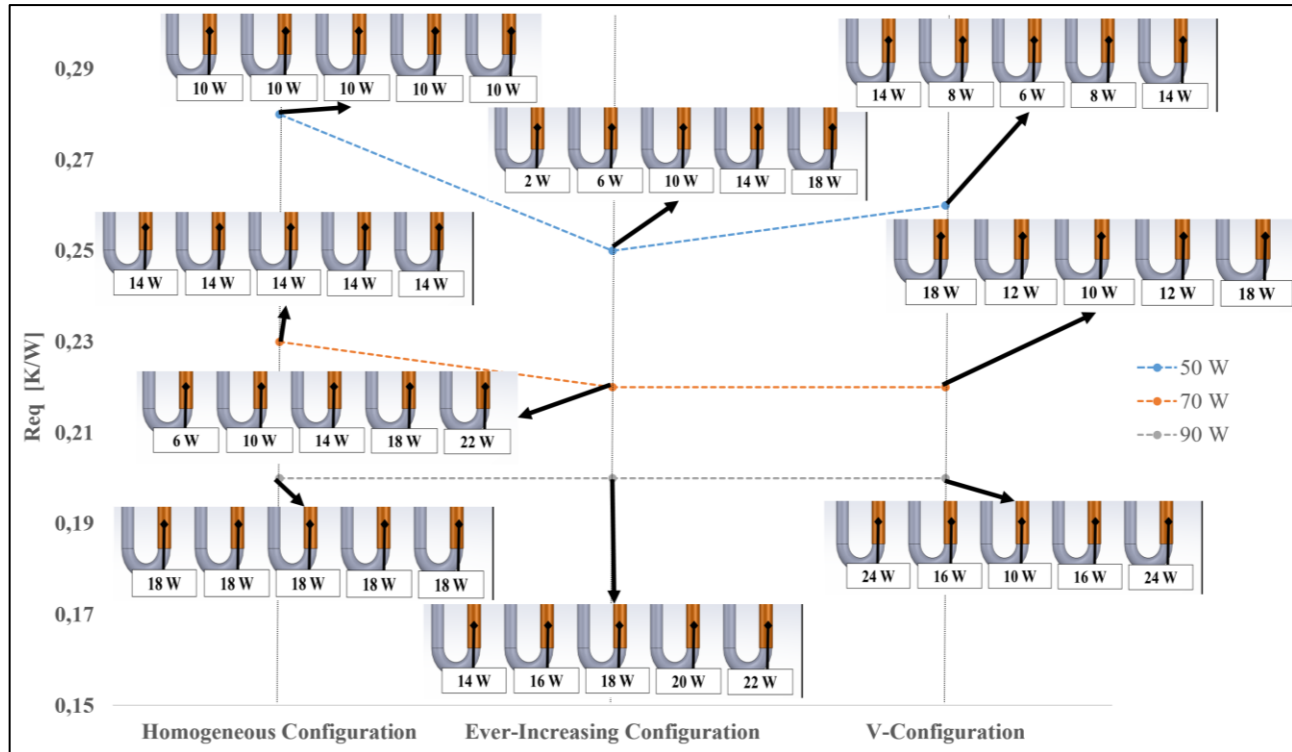


Figure 4.10.  $R_{eq}$  values for the main heating configurations tested providing to the device a global heat power input of 50 W, 70 W, 90 W.



## 4. Ground Tests

---

### 4.5 Effect of the ambient temperature

Two-phase heat transfer devices are becoming fairly ubiquitous and they are currently investigated in different fields such as nuclear plants, energy systems, solar heat recovery, air conditioning, electronic cooling in avionics and in railway traction. As a consequence, they can operate under different environmental conditions that can affect their behavior. Nevertheless, it is difficult to find in literature something related to the effect of the ambient temperature on the thermal performance of such devices. The ambient temperature, changing the thermo-fluid properties of the fluid, the condensation and the evaporation phenomena, could affect the overall performance. Indeed, another ground campaign is performed in collaboration with the Polytechnic of Milan. The MELT is tested at different ambient temperatures, ranging from  $-20\text{ }^{\circ}\text{C}$  up to  $30\text{ }^{\circ}\text{C}$ . The start-up behavior, as well as the thermal performance, are analyzed by means of temperature and pressure measurements and fluid flow visualization. Tests are performed imposing a constant ambient temperature by means of a thermal chamber (Discovery 1200 by Angelatoni Test Technologies<sup>®</sup>) and changing the global heat power input provided by the device.

The ambient temperatures tested are  $-20\text{ }^{\circ}\text{C}$ ,  $-10\text{ }^{\circ}\text{C}$ ,  $0\text{ }^{\circ}\text{C}$ ,  $10\text{ }^{\circ}\text{C}$ ,  $20\text{ }^{\circ}\text{C}$  and  $30\text{ }^{\circ}\text{C}$ . For each ambient temperature tested the heater input power, starting from a global power of  $10\text{ W}$ , is firstly increased by steps of  $10\text{ W}$ , with finer detail in the lower power region to detect when the start-up occurs. Power is furtherly increased with coarser steps up to  $150\text{ W}$ . After

## 4. Ground Tests

---

that, the heating power is reduced following the same heating steps, in order to understand the role of possible inertial effects on the flow motion deactivation. Then, the power is increased again in order to detect possible hysteresis phenomena with respect to the first start-up. All the heating power levels are kept constant for 15 minutes, in order to reach the steady-state conditions. Tests are performed in vertical position, in Bottom Heated mode.

The experimental results show that the ambient temperature clearly affects the device start-up and the internal flow motion.

Results show that the power levels at which the different thermo-fluid behavior occurs depend on the ambient temperature. The images, coupled with the temperature and pressure trends, permit to draw a flow pattern maps for the experimental matrix, establishing a relationship between the two-phase flow motion and the device thermal behavior. For the lowest ambient temperature tested, after the start-up, the device has an unstable behavior for a wide range of power levels. Temperatures do not stabilize and partial activations are detectable.

## 4. Ground Tests

Table 4-5 Flow pattern map for all the configurations. The full activation is highlighted with red lines.

Power-up phase (Q-up)													Power-down phase (Q-down)									
-20°C	-	-	-	-	-	S	S	S	S	O	C	O	O	O	S	S	S	S	-	-	-	
-10°C	-	-	-	-	S	S	S	O	C	C	C	C	C	O	S	S	S	-	-	-		
0°C	-	-	-	-	-	O	O	C	C	C	C	C	C	C	O	S	S	S	S	-	-	
10°C	-	-	-	-	-	O	C	C	C	C	C	C	C	C	C	C	C	S	S	-	-	
20°C	-	-	S	O	C	C	C	C	C	C	C	C	C	C	C	C	C	C	O	-	-	
30°C	-	S	S	S	C	C	C	C	C	C	C	C	C	C	C	C	C	C	O	S	-	
q''[W/cm <sup>2</sup> ]	1.0	2.1	3.2	4.2	5.3	6.4	7.5	8.6	9.7	12.7	16	12.7	9.7	8.6	7.5	6.4	5.3	4.2	3.2	2.1	1	
P[W]	10	20	30	40	50	60	70	80	90	120	150	120	90	80	70	60	50	40	30	20	10	

Second Power-up phase (Q-up 2)									
-	-	S	S	S	S	S	O	O	-20 °C
-	-	-	-	S	S				-10 °C
-	S	S	S	O	C				0 °C
-	-	-	S	C					10 °C
-	-	S	C						20 °C
-	S	O	C						30 °C
2.1	3.2	4.2	5.3	6.4	7.5	8.6	9.7	12.7	q''[W/cm <sup>2</sup> ]
20	30	40	50	60	70	80	90	120	P[W]

LEGEND	
-	Test not performed
-	No fluid motion nor temperature fluctuations
S	Partial start-up
O	Oscillation (after full start-up)
C	Circulation (after full start-up)

The thermal behavior is different also after the full activation.

At -20 °C, the device is affected by frequent short stopovers that do not prevent it from reaching a pseudo steady state (Figure 4.11a). Increasing the ambient temperature at 20 °C and heating up the device with the same power, the temperatures remain stable and the pressure in the condenser zone shows always strong fluctuations (Figure 4.11b), evidence of a vigorous two-phase flow motion. The flow motion recorded in the transparent section is different too: for the lowest ambient temperature, the

## 4. Ground Tests

flow is oscillating at 120 W, while for the 20 °C case a circulation in a preferential direction is observed.

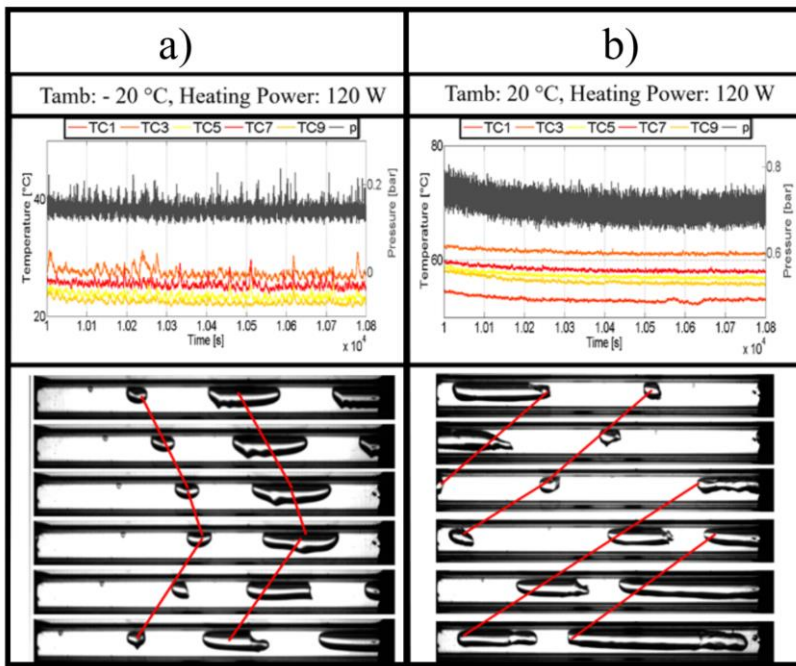


Figure 4.11 . a) Test with  $T_{amb}$  of -20 °C: temperatures and pressure and Flow oscillations at 50 fps; b) Test with  $T_{amb}$  of 20 °C: temperatures and pressure and Flow oscillations at 50 fps.

Noteworthy, all the liquid and vapor properties for FC-72, such as the saturation pressure, density, liquid surface tension, liquid Prandtl, specific heat of the liquid phase changes sharply in the selected temperatures range (Table 4-6).

Such differences may have a direct impact on the overall heat exchange. Further experimental data, coupled with numerical analysis, are therefore

## 4. Ground Tests

---

necessary to better understand the effects of the physical parameters, even if another recent work performed by Betancur and Mangini [106] pointed out similar results also for a PHP filled up with water.

Table 4-6 FC-72 thermo-fluid properties between -20 °C to 30 °C.

Temperature (°C)	Pressure (kPa)	Liquid Density (kg/m <sup>3</sup> )	Vapor Density (kg/m <sup>3</sup> )	Liquid Cp (kJ/kg-K)	Liquid Kin. Viscosity (cm <sup>2</sup> /s)	Liquid Prandtl	Surf. Tension (mN/m)
-20	2,5383	1780,6	0,41045	0,97231	0,0085508	23,156	15,82
-10	4,8176	1760,9	0,75221	0,98803	0,0070558	19,635	14,809
0	8,6037	1741,3	1,3007	1,0041	0,0058892	16,836	13,812
10	14,572	1721,6	2,1389	1,0206	0,0049698	14,59	12,83
20	23,562	1701,6	3,3681	1,0377	0,0042379	12,773	11,863
30	36,584	1681,1	5,108	1,0553	0,0036495	11,289	10,912

PART IV

EXPERIMENTS IN  
HYPER/MICRO-GRAVITY  
CONDITIONS

Chapter **5**

# 5. Parabolic Flights and Rack Design

The details of Parabolic Flight experiments are highlighted in this chapter, firstly pointing out what is a Parabolic Flight Campaign and how experiments are performed in such experimental activity. Later on, it is explained how the experiment is designed in order to follow the severe Technical restrictions imposed by Novespace to test the experiment in micro-gravity.



## 5. ESA Parabolic Flight Campaigns and rack design

### 5.1 Parabolic Flight Campaigns

A parabolic flight campaign (PFC) is an experimental activity where a specially modified Airbus A300, called Zero-G aircraft, is used to obtain hyper and micro-gravity conditions for approximately 20 seconds at a time, by repeatedly performing a parabolic maneuver which involves balancing engine thrust with drag and nullifying lift, so that the resulting force acting on the aircraft is only the gravitational pull. The gravity field achieved during the 20 seconds of micro-gravity condition is approximately 0.01 g. This causes the crew and cargo to travel along the same free-fall trajectory and velocity as the aircraft itself, therefore experiencing an apparent weightlessness within the cabin.

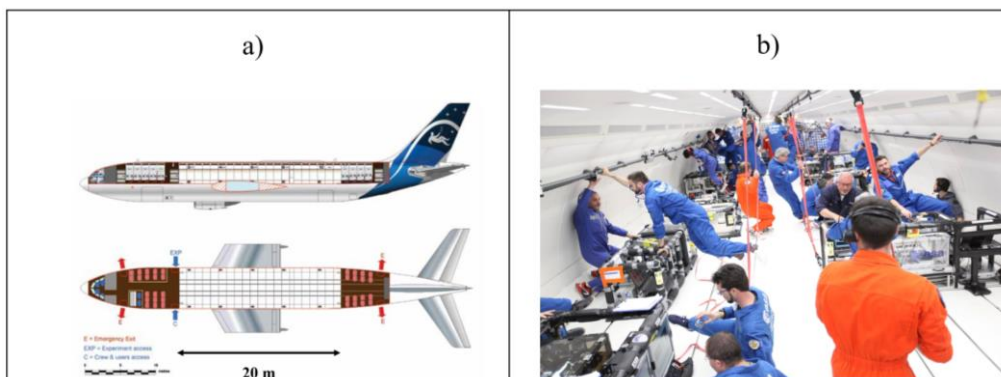


Figure 5.1 a) Airbus A300 “ZERO-G” aircraft internal side and upper views and b) the experimental area during a parabolic flight, with tests rack being mounted and the scientific crew perform tests.

## 5. ESA Parabolic Flight Campaigns and rack design

---

These campaigns are organized by Novespace, a Bordeaux-based company (France). In the Zero-g Airbus, all seats are positioned just in the front and in the back, while they are removed from the central section of the fuselage to make space for a 20 m experimental area (Figure 5.1a and b). In this area, experiments are bolted onto the floor and all surfaces are padded to prevent injury while floating in micro-gravity. During flight, the research teams remain within the experiment area under supervision of the safety crew. The main advantage of the Parabolic Flight is that both the experiment and the experimenter are on board during the flight. The experimenter can modify the different parameters and check directly the status of the experiment during the transition of the gravity field. To the contrary, the period of micro-gravity is limited up to 20/22 seconds as maximum. PHP needs time to reach pseudo-steady state condition after that one parameter, i.e. the gravity field is changed. Only when pseudo-steady state conditions are reached, it is possible to measure its thermal performance. Twenty seconds of micro-gravity are not sufficient in this case to reach a stationary condition, and, even if PFC gives the possibility to test the thermo-fluid dynamic evolution during the gravity transition, no measurement of the thermal performance in micro-gravity can be provided.

Each PFC, which lasts two weeks, is thusly organized:

- First week: starting Monday, research teams arrive at Novespace. Experiments are security-checked and installed in the aircraft;

## **5. ESA Parabolic Flight Campaigns and rack design**

---

- Safety checks are performed by staff each day. Teams must be prepared to comply with requests to modify and improve padding, electrical layout, equipment restraints etc.;
- Monday of the second week: a safety briefing is given to all passengers of the flight and the aircraft is closed. All experiments must have been approved for flight and no further modification is allowed;
- Tuesday → Friday: Three flights are performed, with one day reserved in case of bad weather. Before each flight, medication against flight sickness is administered (1 ml of scopolamine). The aircraft takes off and flies to one of three pre-approved areas where weather and air traffic conditions are acceptable. There, 31 parabolas are performed;
- The aircraft returns to base and each team gives a short briefing on experimental results.

Parabolic flights was first introduced for astronaut training; today they are mainly used for testing of space technology and for short duration scientific experiments mainly because of their short turnaround time, low cost, flexible experiment approach and direct on-board intervention possibilities [107].

## 5. ESA Parabolic Flight Campaigns and rack design

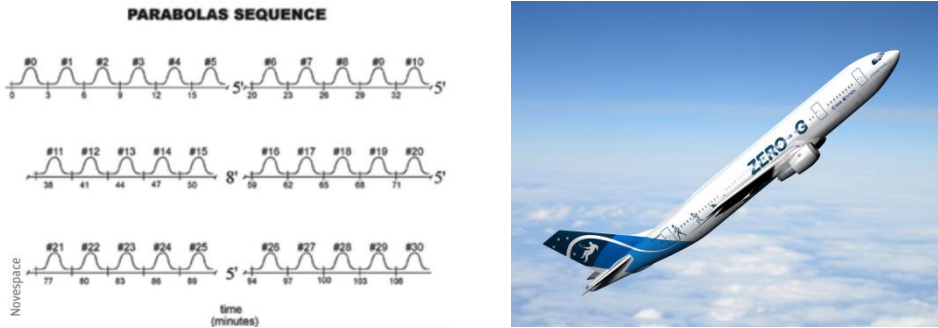


Figure 5.2: On the left, time schedule of the parabolas performed during each parabolic flight; on the right, the Airbus A300 Zero-G during a pull-up phase.

During each campaign, there are typically three flights: a normal mission lasts two or three hours and consists of thirty-one parabolic maneuvers (Figure 5.2). As a consequence, 93 parabolic flight trajectories are performed in a single PFC.

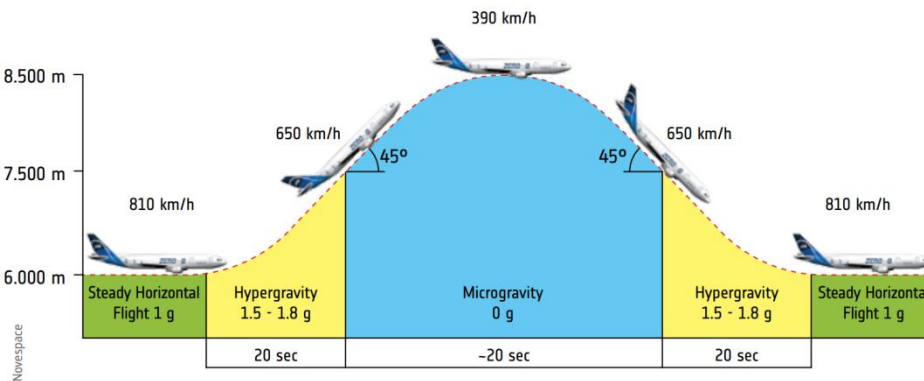


Figure 5.3: Parabolic flight maneuver profile.

## **5. ESA Parabolic Flight Campaigns and rack design**

---

Each maneuver begins with the aircraft flying a steady horizontal attitude. Approximately, the altitude and speed of 6000 m and 810 km/h respectively (Figure 5.3). During this steady phase, the gravity level is approximately 1 g, as a normal flight. At a set point, the pilot gradually pulls up the nose of the aircraft and it starts climbing up to 7500 m. This phase lasts for about 20 s, during which the aircraft experiences acceleration between 1.5 and 1.8 times the Earth gravity level (first hyper-gravity period in the parabola). At an altitude of 7500m, with an angle of around 45/50° to the horizontal depending by the peculiar trajectory and the weather conditions, and with an air speed of 650km/h, the engine thrust is reduced to the minimum required to compensate for the air drag. At this point the aircraft is able to follow a free fall ballistic trajectory (i.e. a parabola) lasting approximately 20s, during which weightlessness is achieved (micro-gravity period). The peak of the parabola is around 8500 m, at which point the speed has dropped to about 390 km/h. A symmetrical 1.8 g pullout phase is then executed on the down side of the parabola to bring the aircraft back to its steady horizontal flight in about 20 s (second hyper-gravity period). There is an interval of approximately two minutes between two subsequent parabolas. Parabolas are executed in sets of five. At the end of each set, a longer time (i.e. 5 or 8 minutes) is elapsed to provide to the experimenters enough time to carry out modifications to their set-up.

## **5. ESA Parabolic Flight Campaigns and rack design**

---

### **5.2 Excursus on other possibilities to perform microgravity experiments**

There are other facilities in which is possible to test the experiment for a long term micro-gravity, such as:

- On board of satellites, in which is possible to test the experiment for prolonged micro-gravity conditions;
- Many minutes (up to five consecutive minutes) of micro-gravity can be reproduced on suborbital rockets.

However, performing experiments on such kind of platforms is expensive, complicated, because of the high number of strictly technical requirements, and, unfortunately, in the case of suborbital rocket experiments, sometimes the launch could be postponed resulting in a loss of time and resources. Obviously, the experimenter is not on board in these cases, and the experiment needs to be designed to work properly also without a direct supervision when it reaches micro-gravity conditions. Furthermore, the experiment has to be designed in order to transmit efficiently data on Earth during flight.

Some attempts of testing two-phase heat transfer devices aboard of suborbital rockets can be found in the last years. For instance, in 2010 de Paiva et al. [58] proposed an experimental analysis of four two-phase technologies (one mini heat pipe, one heat spreader, one copper/acetone PHP and one device based on phase change materials) for the thermal management and heat dissipation of electronics in micro-gravity conditions. The previous ground test characterization showed a thermal

## **5. ESA Parabolic Flight Campaigns and rack design**

---

resistance small enough to make them possible candidates for electronic equipment heat management in normal gravity. Unfortunately, the launch of the testing suborbital rocket which was scheduled for the same year, was postponed. Therefore the results in micro-gravity are missing in the present thesis. In addition, no further publications have been produced after the launch, probably due to technical problems during the sounding rocket launch.

Another attempt was done by Maeda et al. [60] the following year, where it is developed a flat plate oscillating heat pipe with check valves to be placed on a Small Demonstrate Satellite-4 (SDS-4) built by JAXA. The ground test characterization of the device, made of stainless steel and charged with HFC-134a, showed thermal conductivity 250-350 times higher than the wall material alone. Additionally, they prepared the test rig to be place on the satellite and checked if the system was able to operate without problems under a microgravity environment. The launch was scheduled in 2012, but another time no further publications can be found in literature.

In 2015, Creatini et al. [63] designed a novel type of Pulsating Heat Pipe only for space application, following the idea presented in this thesis, and they tried to test it aboard to a sub-orbital rocket. Even if the experiment works successfully and the radar system transmitted efficiently data during the flight, the de-spin system was not opened during the trajectory, keeping the centrifugal acceleration around the axis of the rocket for the entire period of the test.

## **5. ESA Parabolic Flight Campaigns and rack design**

---

### **5.3 Structural requirements for the PFC: rack design**

It is mandatory to design the rack, i.e. the structure that holds the experiment and all the components useful to perform properly the experiments (power supply, laptop, acquisition system) and the experiment (test cell) in order to respect the restrictive ESA Experiment design Guidelines in Parabolic Flight [108]. The experiment is allowed to flight only if all the mechanical, electrical and chemical restrictions listed in the ESA guidelines are fully respected.

Experimenters that intend to flight and to perform experiments have also to pass appropriate medical examinations and present a certification of good health, which includes an ECG. This is because the repeating hyper-gravity and micro-gravity phases can be taxing on the human body; in fact, cardiac activity can increase by up to 70% during hypergravity to continue pumping blood up to the head, leading to increased risk for cardiopathic or otherwise vulnerable subjects. On average, about 10% of passengers suffer acute nausea due to the gravity transitions' stimulation of the inner ear. To reduce this risk, the flight surgeon administers a sub-cutaneous shot of 1 ml of scopolamine to all flight members; this is the same drug which is commonly used in household medications against seasickness or car sickness, but the dose is 10-20 times higher. In addition, passengers are strongly advised to keep their heads still during hyper-gravity, to avoid overstimulating the ear labyrinths. Hyper-gravity is also taxing on the body: during a 1.8 g maneuver, an 80 kg individual will effectively weigh



## 5. ESA Parabolic Flight Campaigns and rack design

over 140 kg, forcing some passengers to lie down during parabola entry and exit to avoid passing out.

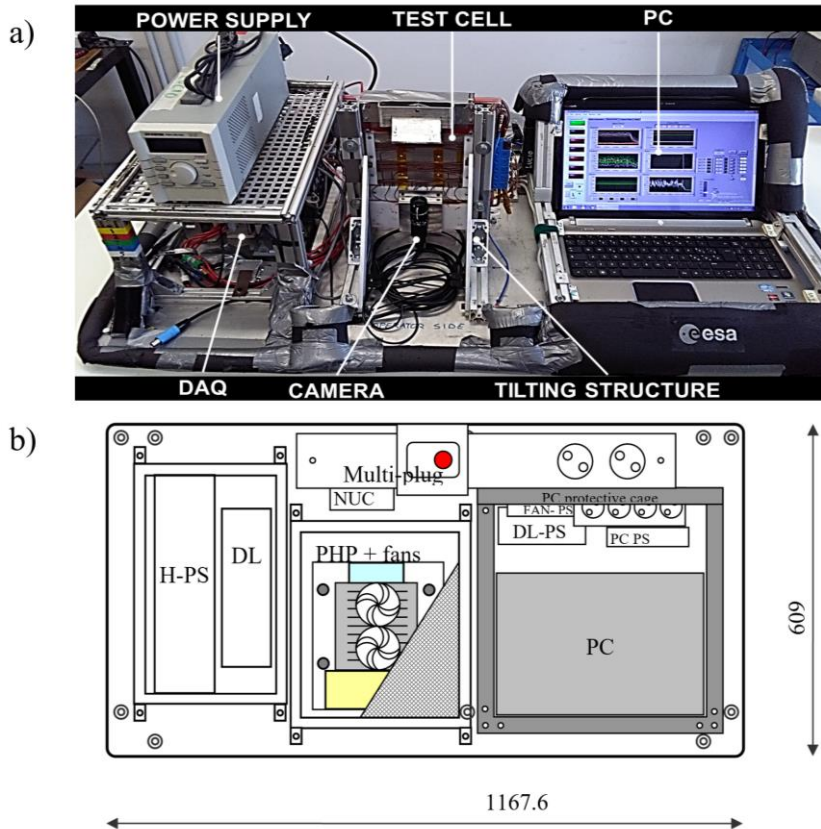


Figure 5.4 a) Test rig and main components and b) its scheme, in which are pointed out: the rack plate with the test cell cage covering the test cell assembly, PS=Heater power supply DL=data logger, notebook PC with its protective cage, PS and multiplug; NUC= compact laptop connected to the high speed camera.

## 5. ESA Parabolic Flight Campaigns and rack design

---

Experimental racks firstly include a primary structure, which is generally composed of an aluminum base plate or frame, which is used to attach the rack to the aircraft floor, and other aluminum profiles which provide mechanical support and protection to the various components of the experiment. Each piece of equipment and subassembly must be attached so that it will remain safely locked in the X, Y and Z directions when subjected to external forces.

A detailed figure of the rack and the main component of the experiment is pointed out in Figure 5.4.

The experimental setup is composed of one single plate racks, consisting of an aluminium plate measuring about 1170x610mm, supporting the various equipments:

- the test cell assembly (the two-phase heat transfer device with the heat sink, the fans and the electric heater). The test cell can be tilted in horizontal and vertical position, allowing to test the device in both direction during flights;
- the power supply for the heaters. During the 61th ESA PFC, the power supply was a GW Instek<sup>®</sup> 3610A; during the 63th ESA PFC, the power supply mounted was a MW RSP-320 series;
- An NI data logger for data acquisition A data acquisition system (NI-cRIO-9074<sup>®</sup>, NI-9264<sup>®</sup>, NI-9214<sup>®</sup>, 2xNI-9205<sup>®</sup>, NI-9217<sup>®</sup>, NI-9472<sup>®</sup>);
- one portable PC with its power supply for instrument control and data storing;

## **5. ESA Parabolic Flight Campaigns and rack design**

---

- one Intel NUC (nano PC) controlled by the PC and used to store data from the USB high-speed camera,
- The general power distribution with a small power supply to the heat sink fans.

The devices are directly fixed to the base plate, and are covered by removable cages that have only protection purposes, but do not have any structural function.

### **5.4 Test cell requirements**

The test cell is designed and assembled in order to respect the ESA rules and guidelines for Parabolic Flights [107].

In the experiments that involve liquids or small particles like this one, it is mandatory to design a second containment (double containment) to decrease as maximum as possible the possibility to release fluids during flight in the cabin. The fluids in fact can be hazardous if released into the cabin during flight, because liquids can cause an electrical fire if they come into contact with an electrical circuit, while small particles can cause choking or damage to the eyes.

As a consequence, it is designed a secondary containment around the primary one with the main function to prevent the propagation of leaking materials and to resist to a sudden loss of pressure in the cabin without bursting, as shown in Figure 5.5. The double containment in the evaporator section has also the other important function to thermally insulate the heated zone. It is made by 5 mm of PTFE, a plastic material able to resist

## 5. ESA Parabolic Flight Campaigns and rack design

---

up to 200 °C, with a thermal conductivity of 0.25 W/mK, as it is possible to see in Figure 5.6. Furthermore, due to the presence of electricity in the evaporator section, the electrically insulated PTFE avoid electric conductions in case of electric failure.

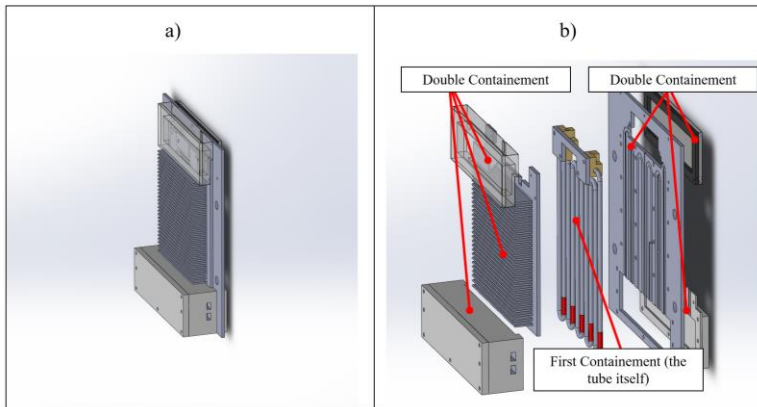


Figure 5.5 a) the test cell and b) its exploded view (highlighted the double containment).

Red silicon avoids possible leakages between the different parts of the evaporator double containment, as shown in Figure 5.6 a.

## 5. ESA Parabolic Flight Campaigns and rack design

---

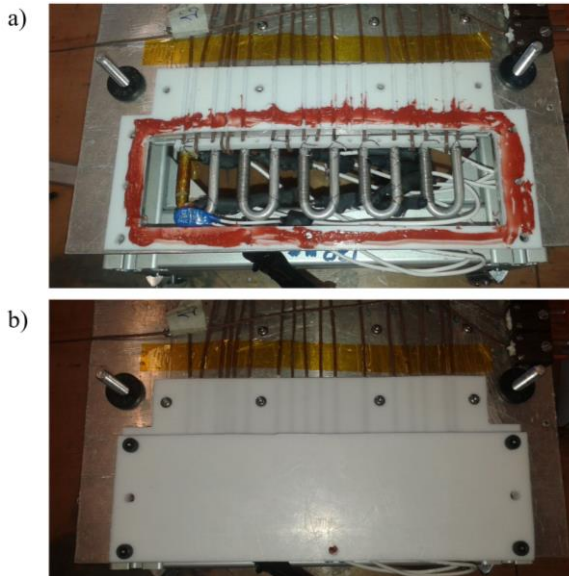


Figure 5.6 a) The evaporator zone: bottom view, open. Silicon paste able to resist up to 200 °C is spread to seal the double containment; b) The evaporator zone: bottom view, closed using the PTFE.

The transparent section at the condenser zone is the one where the risks of a leakage is higher due to the presence of the connections glued between them and the glass tube itself; for this reason the second containment around the transparent tube is sealed by means of silicon paste. The double containment for the transparent section has to be of course transparent as well, to permit to visualize the two-phase flow motion during tests. It is made by 4 mm of Lexan plates, to allow fluid flow visualization, as shown in Figure 5.7.

## 5. ESA Parabolic Flight Campaigns and rack design

---



Figure 5.7 Double containment in the transparent section.

Finally, in the condenser section, it is the heat sink and the aluminium back plate the double containment of the device, as shown in Figure 5.8:

## 5. ESA Parabolic Flight Campaigns and rack design

---

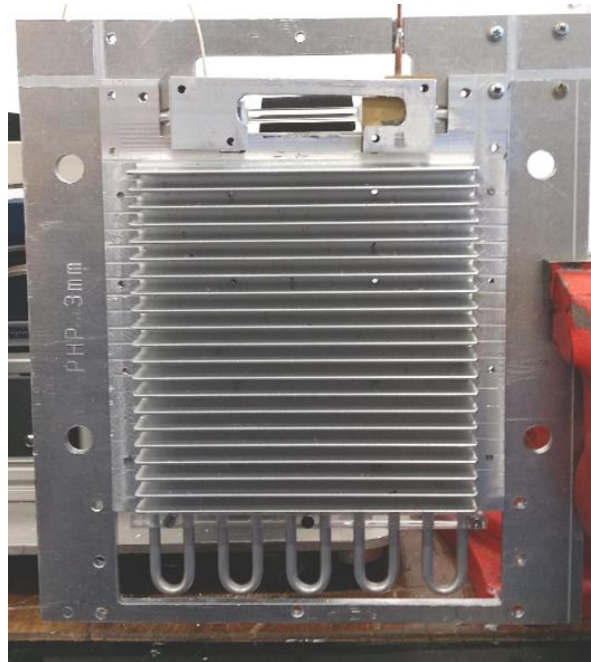


Figure 5.8 Heat sink and aluminum back plate that create the double containment in the condenser section.

### 5.4.1 Test cell protection cage

The test cell is covered with a metal cage in order to avoid contact with the fan propellers and with the hot parts and to protect the experiment during flights. It is composed by Item<sup>®</sup> 20x20 profiles and perforated aluminum plates.

It is connected to the base plate, spaced from it of 5 mm by spacers (thick washers) in order to allow better air passage from below. The spacers also host the nuts used to keep the connection bolt on the base plate when the cage is removed.

## 5. ESA Parabolic Flight Campaigns and rack design

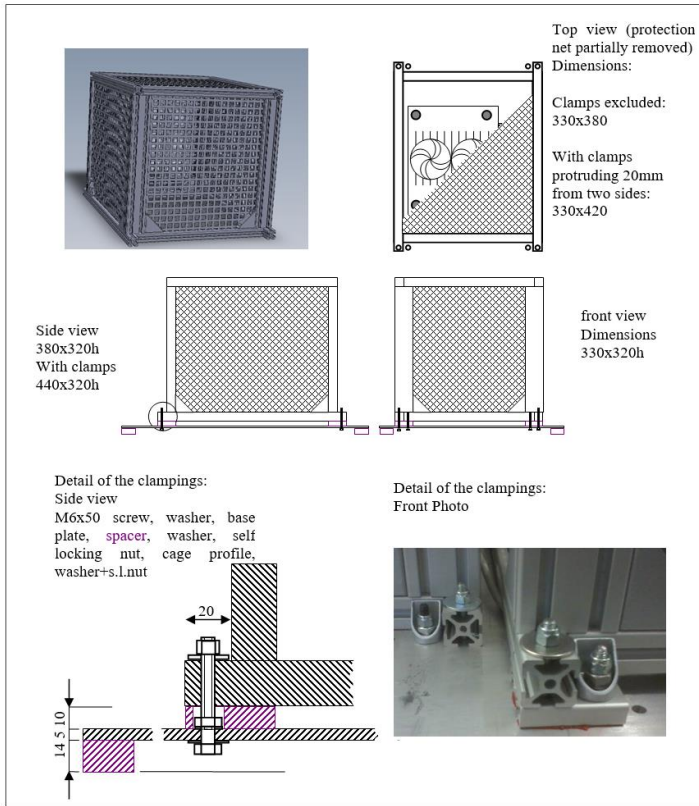


Figure 5.9 The cage that covers the test cell during parabolic flights.

### 5.4.2 Test cell vertical and horizontal support

The test cell is permanently connected to two item 30x30 profiles with two rods (aluminum profiles mm 270x25x5) that contribute to the rigidity of the assembly. The test cell can be connected to the structure vertically (Figure 5.10a) or horizontally (Figure 5.10b), permitting to test it in both of the directions on flight.



## 5. ESA Parabolic Flight Campaigns and rack design

---

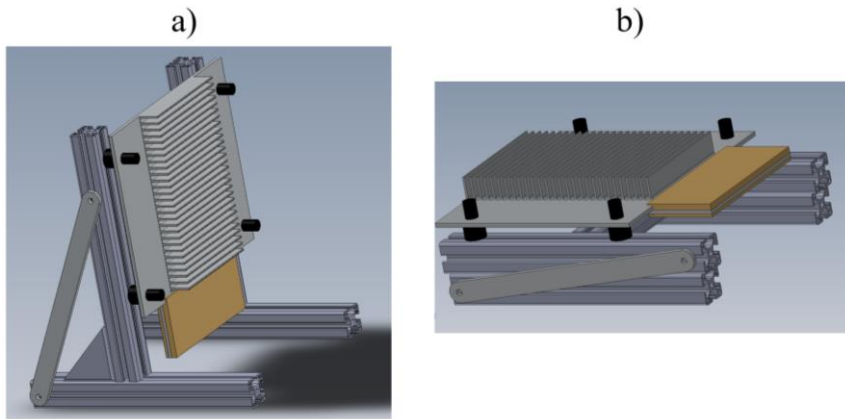


Figure 5.10 Test cell connected a) vertically and b) horizontally

The test assembly is held through four vibration insulating bushes, designed to withstand at least 15 times the assembly weight in any direction (XYZ) during normal flight and parabolic maneuvers, permitting also to insulate electrically the device with respect to the rack.

## 5. ESA Parabolic Flight Campaigns and rack design

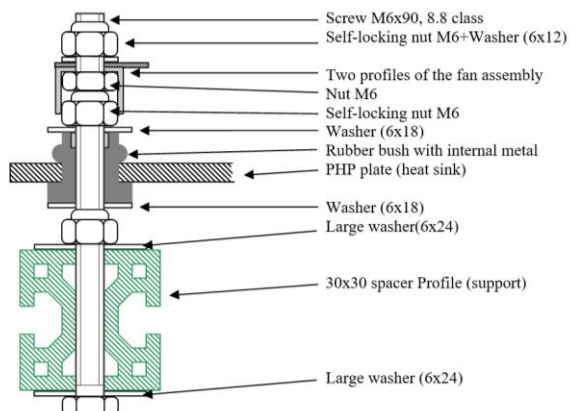


Figure 5.11 The anti-vibrating bush scheme and the connection between the device and the item support.

### 5.4.3 Cage to protect the power supply, the DAQ system and the laptop

Not only the test has to be protected by possible human contact by means of a cage properly designed, but also the power supply, the DAQ acquisition system and the laptop utilized to collect data during experiments. For safety reasons, since the power supply can provides up to 180 W, reaching an ampere output of approximately 5 A, the cage is designed to avoid any possibility of contact between the experimenters, the power supply and the wires that provide the power to the heating elements, as shown in Figure 5.12 a and b.

The Laptop is protected by possible human impacts with an external cage that holds it in the rack. The experimenters can modify the different

## 5. ESA Parabolic Flight Campaigns and rack design

---

parameters on flight, since they have a direct access to the keyboard, as shown in Figure 5.12c and d.

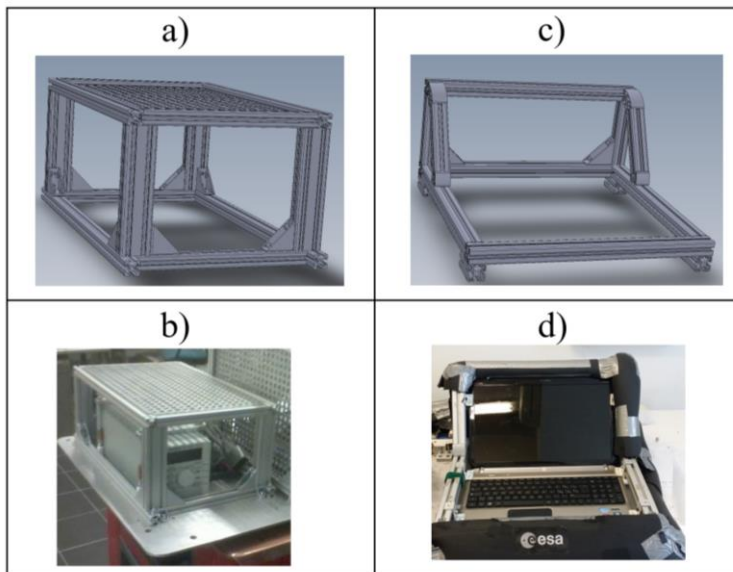


Figure 5.12 Power supply and DAQ cage: a) CAD view; b) real picture; Laptop cage: c) CAD view; d) real picture.

### 5.5 Electrical system

Novespace provides a connection block which includes a ground fault interrupter, a fast blow fuse and an emergency stop button. This device represents the electrical interface between experiment and aircraft. On the experimental rack itself, good practice measures must be adopted in every step of electrical design:

## **5. ESA Parabolic Flight Campaigns and rack design**

---

- 220 V electrical connections must be single strand wire, while multi strand wire must be connected using crimp-type terminals to ensure a reliable connection and no risk of micro-arcing between the single strands;
- The experiment itself must be properly grounded by ensuring a good connection with the ground connector of the electrical plug that draws from the aircraft power supply;
- Electrical cables must have a minimum cross section, proportional the current they are designed to carry;
- Fuses must be selected with a rating much lower than the cable carrying capacity, because they must always be the first to trip if necessary;
- Batteries (of laptops, cameras etc) need to be no more than 3 years old and have no recall history by the manufacturer. Some batteries, such as off-the-shelf Li-ion units, are forbidden due to the hazard involved.

For our experiment, the power supply to the heaters was limited to 36 V to prevent any risk of electrical shock to the operators.

The global electrical system is shown in Figure 5.13:

## 5. ESA Parabolic Flight Campaigns and rack design

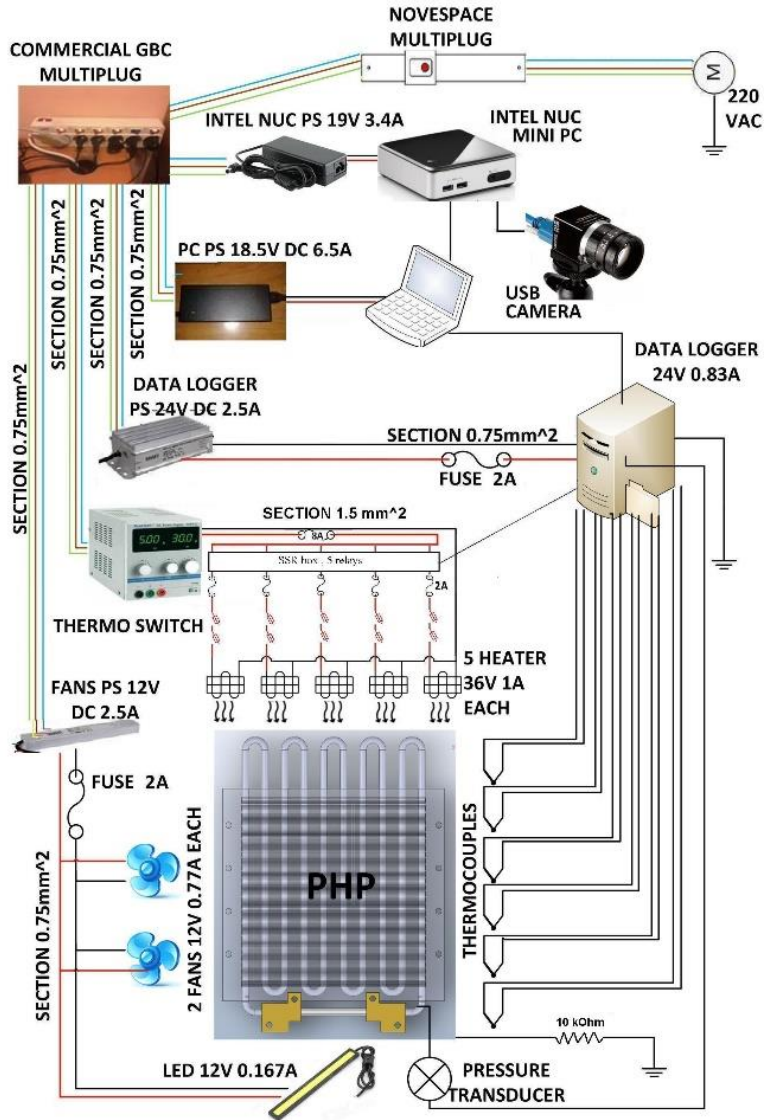


Figure 5.13 General schematic of the electrical system.

Different electrical fuses are positioned in the electrical system: if it is present an unexpected electrical overload, the fuses will open the circuit,

## **5. ESA Parabolic Flight Campaigns and rack design**

---

preventing any possible damage both to the experiment and to the experimenters. The fuses and the fuse holders are transparent. In this way, the operators can easily detect where the circuit is opened in case of broken fuse.

Additionally, the heating elements are directly in contact with thermal switches (DMP<sup>®</sup> 11MP150H046E), which will cut power supply in the event that temperatures above the given limit are sensed by the switch (Figure 5.14). Two thermal switches, connected in series to avoid any kind of risk if there is a failure of one of them, are directly mounted on each heating elements, to prevent unexpected over-temperatures on the entire evaporator section.

## 5. ESA Parabolic Flight Campaigns and rack design

---

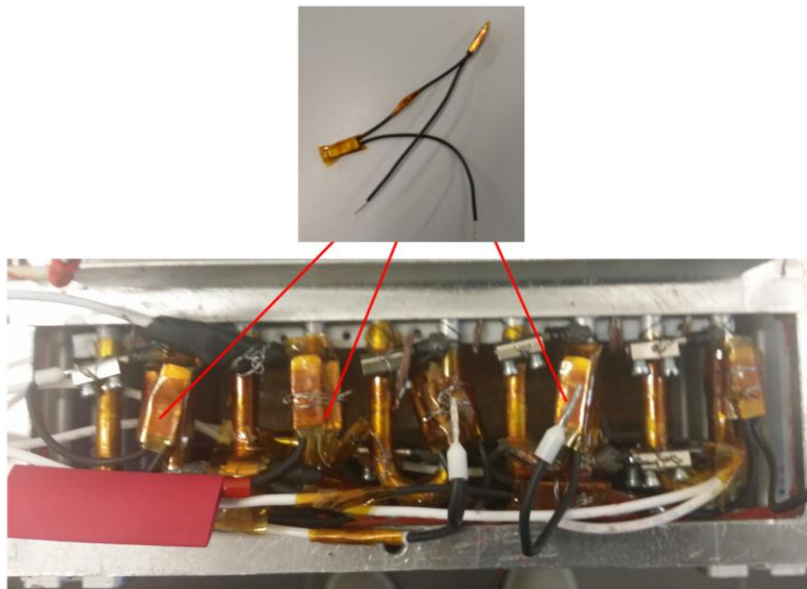


Figure 5.14 Thermal switches directly in contact to the heating elements utilized to open the electrical circuit in case of unexpected overtemperatures (above 150 °C) at the evaporator zone.

# Chapter 6

## 6. Results obtained in hyper and micro- gravity conditions: 61<sup>th</sup> ESA PFC

The more relevant results obtained in hyper and micro-gravity conditions during the 61<sup>th</sup> ESA PFC performed in October 2014 at Novespace, Bordeaux are pointed out in this chapter. The device is tested both in BHM (during the first day of flight) and horizontally (during the second and the third day of flight).



## 6.1 Experimental procedure during the 61th ESA PFC

During the Parabolic flight, the experimental parameters are:

- The global heat input level: from 10 W to 160 W for the bottom heat mode orientation and from 10 W to 80 W for the horizontal orientation. All the heating elements dissipate the same heat power input, since they are not controlled independently: electrically they are all connected in parallel. Therefore, the Amperes provided by the power supply are splitted between them homogeneously.
- The gravity field: Normal gravity (1 g) during the test on ground and during the straight flight trajectory; hyper-gravity (1.8 g) before and after the parabola during the ascending and descending maneuvers (duration: 20/25 s each); micro-gravity during the parabola (duration: 20-21 s).
- The orientation: Bottom Heated mode (BHM), tested during the first day of flight and horizontal position, tested during the second day of flight.

While, the measured quantities are:

- Tube wall temperatures: 10 measuring points in the evaporator zone, 6 in the condenser zone and 1 measuring point that monitors the ambient air temperature (for the thermocouple position: Figure 3.4).
- Local fluid pressure in the condenser zone, by means of the pressure transducer mounted directly in contact to the two-phase flow.

- Acceleration: the gravity field variation during each parabola is monitored by means of a three-axis accelerometer.

Additionally, it is recorded a video (80 s at 450 fps) during each parabola, starting 10 s before the maneuver and stopping around 10 s after the second hyper-gravity period<sup>5</sup>.

Table 6-1 Global heat power during flight days. Since the heating elements are connected electrically in parallel, each one dissipates one fifth of the global heat power input.

<b>Flight test procedure</b>		
<i>Parabola N.</i>	<i>PF-I (Vertical, BHM)</i>	<i>PF-II (Horizontal)</i>
Parabola 0	10 W (2 W each one)	10 W (2 W each one)
Parabola 1-5	20 W (4 W each one)	20 W (4 W each one)
Parabola 6-10	30 W (6 W each one)	30 W (6 W each one)
Parabola 11-15	40 W (8 W each one)	40 W (8 W each one)
Parabola 16-20	80 W (16 W each one)	50 W (10 W each one)
Parabola 21-25	120 W (24 W each one)	60 W (12 W each one)
Parabola 26-30	160 W (32 W each one)	80 W (16 W each one)

One flying day has been devoted to each of the two experiments summarized in Table 6-1 (PF-I and PF-II, respectively). Finally, the third day of the campaign is devoted to ensure the repeatability of the horizontal

---

<sup>5</sup> Supplementary video related to this article can be found at:  
<http://dx.doi.org/10.1016/j.ijthermalsci.2015.04.001>.

test. The heat input level is changed during the 5 min pause at normal g between each sequence of parabola, in order to reach the pseudo-steady state before the beginning of the successive 5 parabolic trajectories (1 g, 1.8 g, 0 g, 1.8 g, 1 g). This procedure is followed in all of the six sequences, ensuring data repeatability.

## 6.2 Results in vertical orientation

Focusing on Figure 6.1, it is recognizable the thermal response of the device during the gravity field variations. As shown previously in the Chapter 4, during the ground tests in vertical position, at 10 W and 20 W, the heat power is not sufficient to pump the liquid batches in the condenser zone. Therefore, during the parabolic flight experiments, the temperatures appear stable in the normal and the hyper-gravity conditions with such global heat power inputs. In addition, the pressure does not show any fluctuation and the transparent section remains dry. Nevertheless, when the micro-gravity period is achieved during the maneuver, a slug/plug flow is suddenly observed in the transparent condenser section, the inner pressure starts to oscillate and the temperature values at the evaporator zone decrease rapidly. The liquid phase is indeed able to reach more easily the condenser zone when the body force becomes negligible during the microgravity period, and the slug/plug flow activation is detectable in the transparent section.

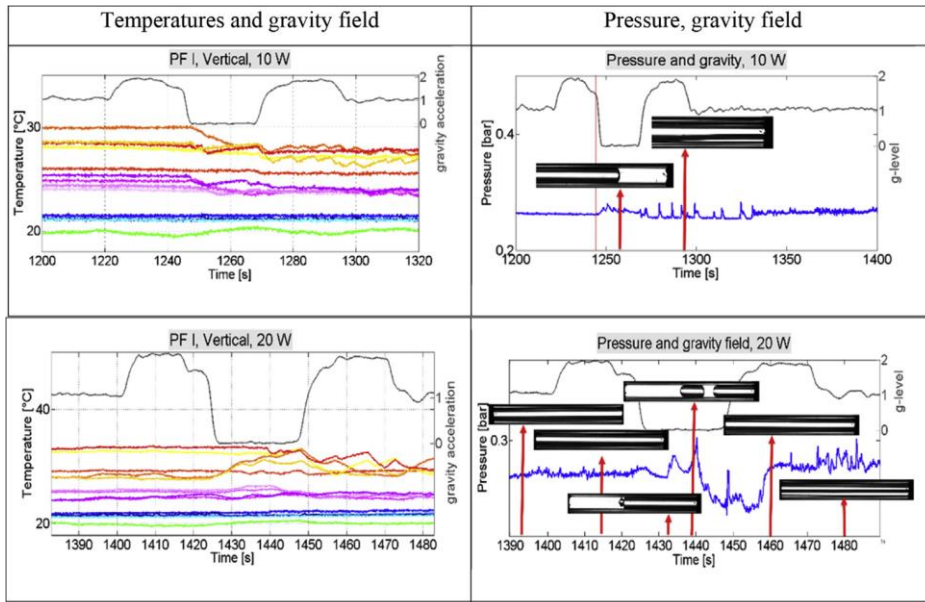


Figure 6.1 Flight tests in vertical position using a global heat power input of 10 W and 20 W; first column: temperatures and gravity field; second column: pressure and gravity field synchronized with visual images (red arrows identify the exact timing of each image).

For all the other higher heat power inputs tested (from 30 W up to 160 W), as shown in Figure 6.2, when the device reaches the standard operating conditions as TS, the gravity certainly assists the device, giving a net contribution to the fluid momentum, improving the heat exchange. The beginning of micro-gravity, activating the slug/plug flow regime, makes the device to work as a PHP, increasing the temperatures at the evaporator zone, since without gravity the two-phase flow return from the condenser to the evaporator section is hindered through the down-comers. In fact, the

non-heated branches are no more “down-comers” in micro-gravity, in the sense that without a gravity field, the two-phase flow motion is guaranteed only by phase transitions along the circuit.

## 6. Results obtained in Hyper and micro-gravity conditions: 61<sup>th</sup> ESA PFC

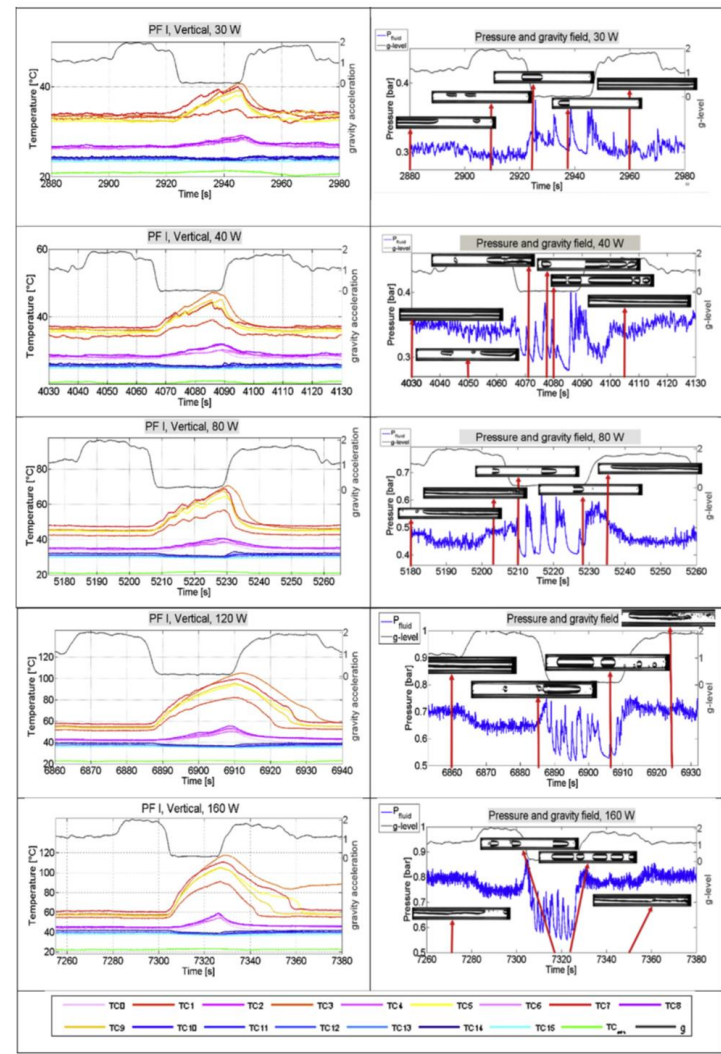


Figure 6.2 Flight tests in vertical position using a global heat power input of 30 W (first line), 40 W (second line), 80 W (third line), 120 W (fourth line), 120 W (fifth line) and 160 W (last line); first column: temperatures and

gravity field; second column: pressure and gravity field synchronized with visual images (red arrows identify the exact timing of each image).

However, interestingly to note is that the fluid motion does not stop completely in micro-gravity: the temperatures do not exhibit an ever-increasing trend, but the oscillating slug/plug flow motion, increasing the convection, tends to stabilize the temperatures also in such conditions.

Figure 6.3 focuses on the fluid dynamic between the hyper and micro-gravity transition, showing that during micro-gravity, the sudden absence of the buoyancy forces allows the surface tension of the liquid phase to create liquid/vapor interfaces perpendicular to the flow path (i.e. menisci). The vapor phase, filling completely the tube section, creates an alternation of vapor plugs and liquid slugs, enabling the device to start working as a PHP.

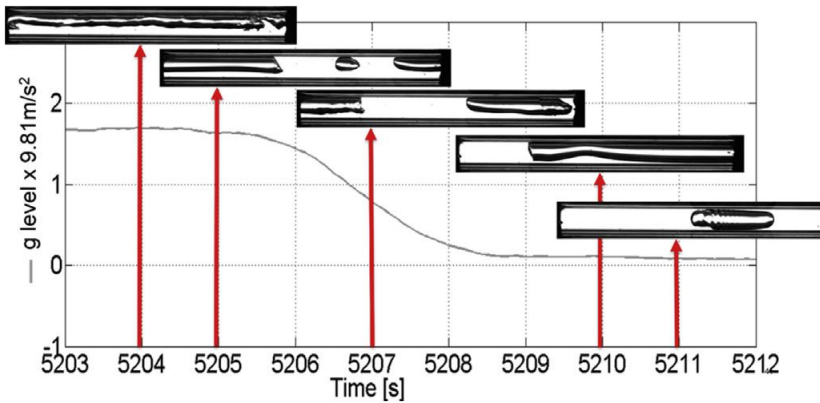


Figure 6.3 Gravity field transition from hyper to micro-gravity: activation of a slug/plug flow regime [66].

After the slug/plug flow regime activation in micro-gravity conditions, the fluid is no more circulating in a preferential direction, but it is characterized by pulsations (typical of a PHP) as shown in Figure 6.4, where fluid oscillation can be detected both from the pressure transducer readings as well as from the corresponding images.



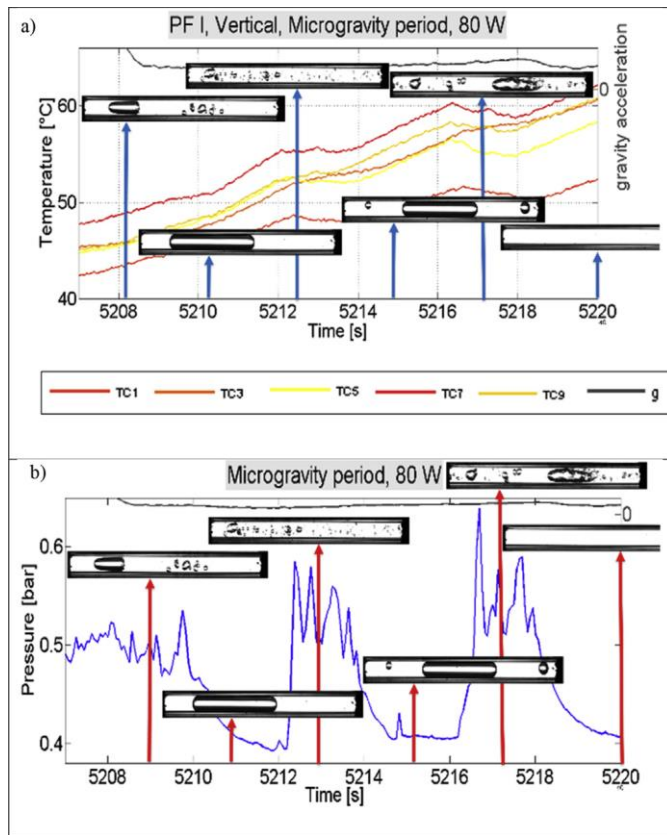


Figure 6.4 Microgravity period at 80 W; a) temperatures recorded at the evaporator zone and b) the synchronized pressure signal and images [66].

When the pressure is nearly constant, the fluid in the condenser zone is not moving, the vapor plugs inside the transparent section of the condenser remain at the same position and the temperatures at the evaporator tends to increase (Figure 6.4a). Such short stop-over periods, in which the heat exchange is hindered, are followed by vigorous fluid pulsations: as shown in Figure 6.4a, as soon as the fluid starts to oscillate in the condenser

transparent section, an abrupt decrease of the evaporator temperatures is also recognizable, increasing this time the heat exchange in micro-gravity between the evaporator and the condenser.

The beneficial effect of gravity, when the device works in TS mode, is recognizable especially at the highest heat power input tested (160 W). In some case for example, after a parabola, the temperature recorded by one thermocouple close one of the heating elements (TC3 in the example of Figure 6.5) sets at approximately 90 °C, probably due to a partial dry-out. The consecutive hyper-gravity period is able to eliminate such partial dry-out, restoring the correct operation until the occurrence of the next microgravity period.

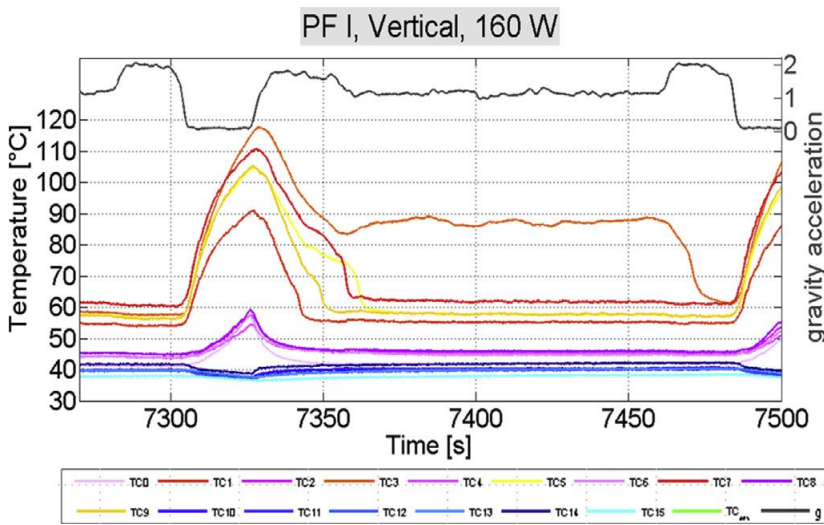


Figure 6.5 Hyper-gravity effect on partial dry-out occurred at 160 W.

### **6.3 Results in horizontal orientation**

During micro-gravity, the inclination of the device does not play an important role, since there is no a gravity field. As a consequence, the temperatures and the pressure measurements are similar to the micro-gravity case during the BHM test (PF-I), previously highlighted in the Section 6.2. The vapor plugs, generated during the absence of gravity field, are similar to a piston that pumps the liquid columns through the condenser, due to their expansion in the evaporator section. This kind of fluid motion is of course beneficial regarding the thermal performance of the device: as soon as the slug/plug flow is activated, the evaporator temperatures start to oscillate, as it is observable in the second column of Figure 6.6. This is however not possible on ground, since the flow is stratified and the liquid phase fills completely the lowest half part of the tube. In this case, there is no possibility to pump the flow in the condenser zone, since the device acts like a TS on ground, as previously mentioned in Section 4.2.

## 6. Results obtained in Hyper and micro-gravity conditions: 61<sup>th</sup> ESA PFC

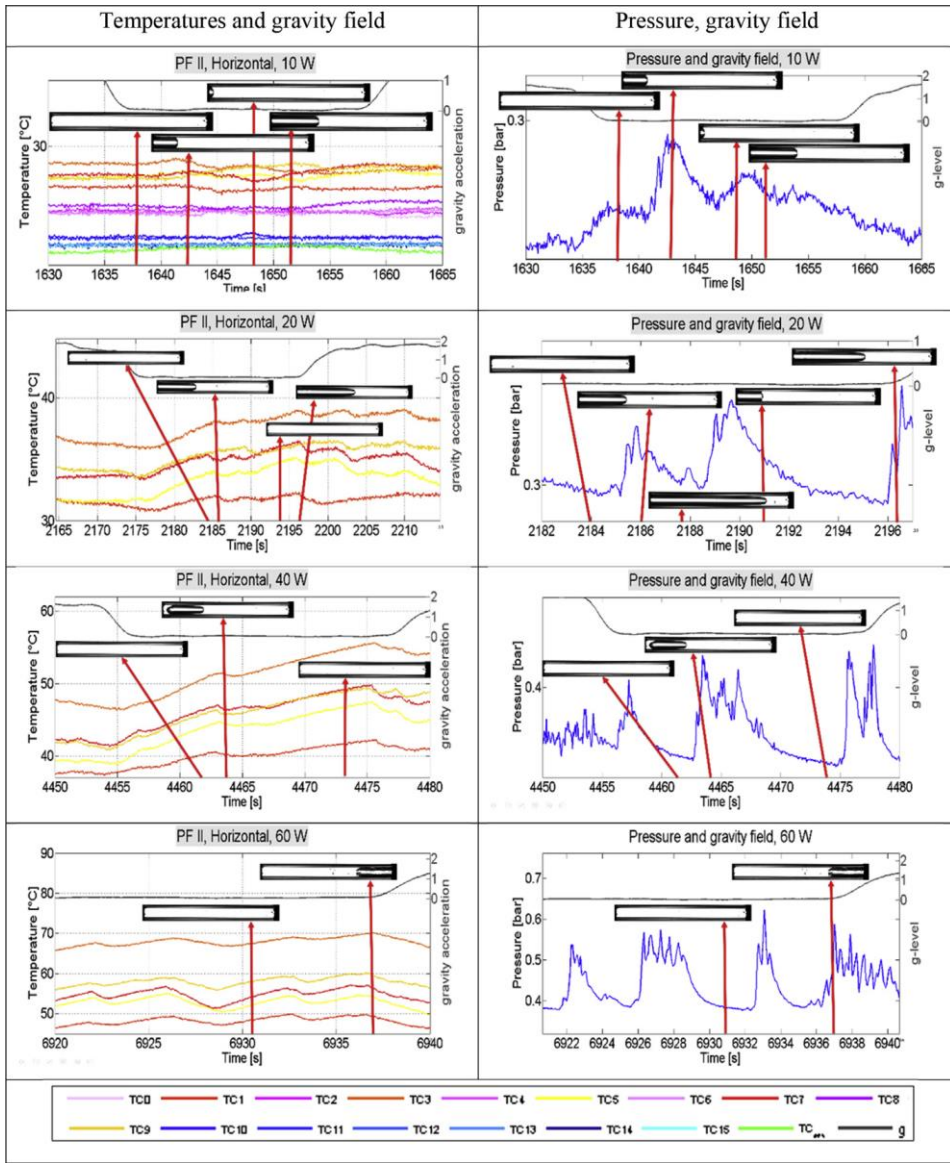


Figure 6.6 Microgravity period for different heat inputs tested in horizontal orientation; first column: evaporator temperatures, gravity field and images; second column: pressure, gravity field and images [66].

Carefully observing the Figure 6.6, it can be noticed that the fluid motion is often activated during the first hyper-gravity period, causing a sudden decrease in the evaporator temperatures. Nevertheless, this does not occurred during the second hyper-gravity period. This can be explained observing the acceleration components plotted in Figure 6.7. The activation during the first hyper-gravity period is not due to the acceleration in the  $z$ -direction, but to the “spurious” force in the  $x$  direction (green line in Figure 6.7b). During the first hypergravity period, the generated inertia force causes the fluid to move in the opposite direction due to  $g_x$  component orientation, improving the beneficial effect due to the thermal non-symmetry. However, during the second hyper-gravity period,  $g_x$  is negative inhibiting this preferential fluid motion due to the peculiar position of the heating elements. This also affects the successive microgravity period: evaporator temperatures are decreasing during the first hypergravity period (Figure 6.7c) since the fluid is already moving inside the device as witnessed by the fluid oscillations recorded by the pressure transducer (Figure 6.7d).

However, during micro-gravity, all the gravity vector components are close to zero. Therefore, the fluid motion is mainly due to the slug/plug motion.

## 6. Results obtained in Hyper and micro-gravity conditions: 61<sup>th</sup> ESA PFC

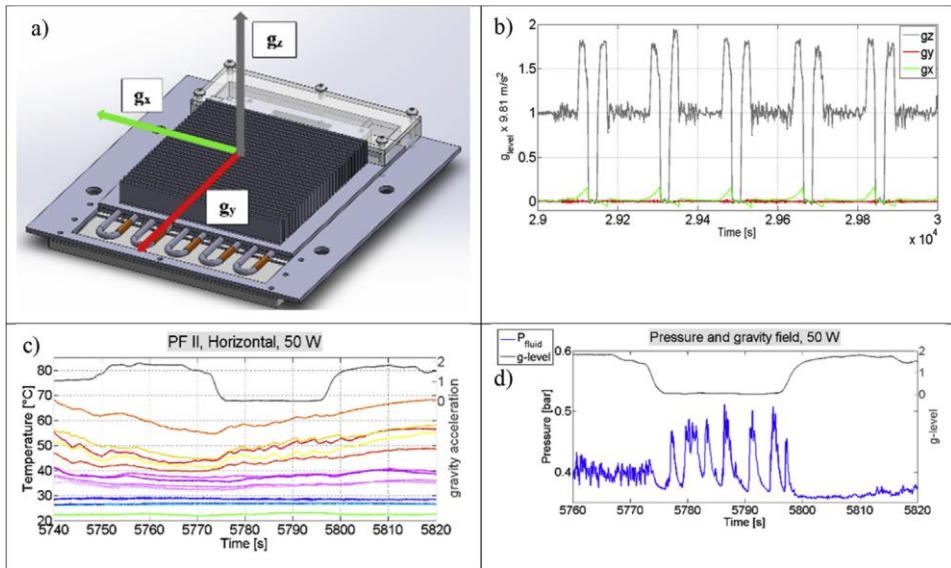


Figure 6.7  $g_x$ ,  $g_y$ ,  $g_z$  acceleration components and time evolution during parabolic maneuvers in horizontal orientation: a) Layout and directions; b)  $g_x$ ,  $g_y$ ,  $g_z$  acceleration over time; c) effect on temperatures; d) effect on fluid pressure [66].

---

# Chapter 7

## 7. Results obtained in hyper and micro- gravity conditions: 63<sup>th</sup> ESA PFC

Chapter 6 has shown that in micro-gravity, the sudden absence of buoyancy forces allows to activate a slug/plug flow motion, and the device is able to work as a PHP even if the ID dimension is higher than the capillary limit on ground.

## 7. Results obtained in hyper and micro-gravity conditions: 63<sup>th</sup> ESA PFC

The pressure signals, the images recorded in the transparent section, together with the temporal evolution of the temperatures, have been demonstrated experimentally the idea to have an hybrid two-phase heat transfer device able to work as a Multi-Evaporator loop Thermosyphon (MELT) on ground and as a PHP only in microgravity, opening the frontier to a new kind of Pulsating Heat Pipe able to work only in the Space (SPHP).

Nevertheless, in weightlessness the two-phase flow motion had an intermittent behavior when all the heating elements dissipate the same heat power input: vigorous pulsations are followed by period of inactivity, i.e. stop-over periods (see also Figure 6.4). During such no-motion periods, the two-phase flow does not pulsate and the temperatures at the evaporator zone increase abruptly, assuming an ever-increasing trend.

As already discussed in the Chapter 4.4, peculiar non-uniform heating configurations allow to a better two-phase flow stabilization in a preferential direction, thus improving also the overall thermal performance. Improving the non-uniform thermal boundary layers at the evaporator, could be beneficial to stabilize the two-phase flow also when the device is not anymore gravity assisted. For instance, if one can control all the five heating elements independently, there will be the possibility to test the device with non-uniform heating configurations at the evaporator. Creating this additional unbalance in the thermal boundary the stop-over periods in micro-gravity should be hindered or avoided. Therefore, the device is tested in the a subsequent PFC (63<sup>th</sup> ESA PFC) in October 2015 controlling all the five heating elements independently by means of the electronic control



## 7. Results obtained in hyper and micro-gravity conditions: 63<sup>th</sup> ESA PFC

system already presented in the section 3.4, thus permitting to test the device with non-uniform configurations at the evaporator.

The aim of this PFC is to prove that, positioning non-symmetrically the heating elements in the heated zone and providing to the SPHP appropriate heating distributions, it is possible to reduce stop-over periods in microgravity, permitting to establish a slug/plug flow motion that continuously oscillate also when the gravity field is absent.

### **7.1 Experimental apparatus and procedure**

The experiment proposed is the same tested during the 61<sup>th</sup> ESA PFC (see Chapter 4). However, the electronic power control system is the same proposed in the section 3.4, in such a way to control the five heating elements independently, thus heating up the device non-uniformly at the evaporator.

The experimental parameters are:

- The total heat input levels, 50 W, 70 W or 90 W which is the sum of all the power levels provided by each of the five heaters.
- The different heating distributions among the five heaters at the evaporator zone. All the heating configurations are pointed out in Figure 7.1.
- The gravity field: normal gravity (1g) during the test on ground and during the straight flight trajectory; hyper-gravity (1.8g) before and after the parabola during the ascending and descending maneuvers

## 7. Results obtained in hyper and micro-gravity conditions: 63<sup>th</sup> ESA PFC

(duration: 20-25 s each); microgravity during the parabola (duration: 20-21 s).

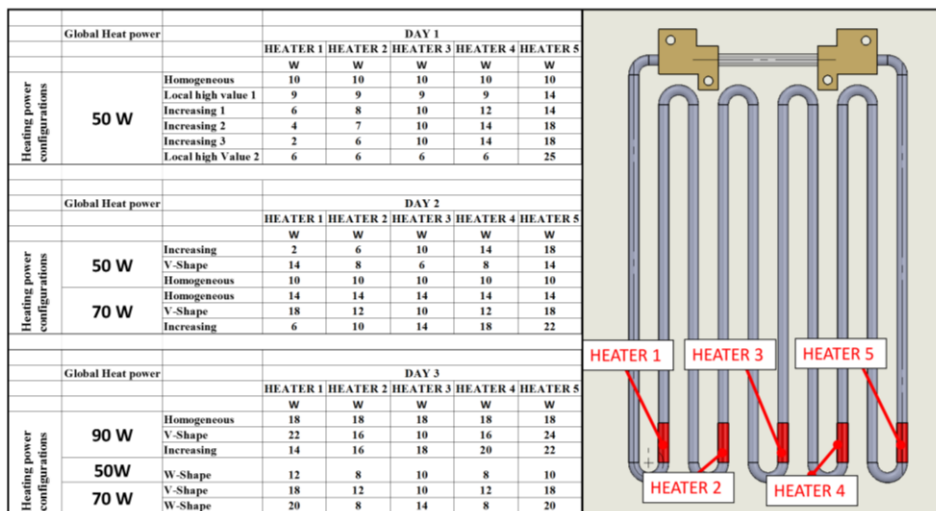


Figure 7.1. Heating configurations tested during the three days of flight.

The measured quantities are:

- the tube wall temperatures, recorded at 10 Hz (see Figure 3.4);
- the local fluid pressure in the condenser zone, recorded at 200 Hz;
- Acceleration: the gravity field variation during each parabola is monitored by means of a three-axis accelerometer, recorded at 10 Hz.

In addition, a video at 200 fps synchronized with the pressure signal, is recorded for 80 seconds during each parabolic maneuver and for 30 seconds during tests on ground after reaching steady state conditions.

## 7. Results obtained in hyper and micro-gravity conditions: 63<sup>th</sup> ESA PFC

On flight, the movie starts approximately ten seconds before the maneuver and stopping around ten seconds after the second hyper-gravity period. The bubble velocity is after measured with an open source PIV software [109] partially modified to detect the vapor phase motion along the transparent section.

### 7.2 Experimental results during the 63<sup>th</sup> PFC

In the three days of flight, tests are performed varying the configuration of the heat power input at the evaporator zone. The different heat power distributions at the evaporator zone tested (listed in Figure 7.1) are changed in the five minutes pause at earth-gravity level between one set of parabola to the next one, to allow reaching a pseudo-steady state conditions before the beginning of the next parabolic trajectories. All the different heat power input distributions are kept constant for the entire set of five parabola to ensure repeatability. Being in total 18 different configurations for the 3 days of flight, only the most relevant results obtained in hyper/microgravity conditions are resumed in the experimental result section. The procedure described above is followed and repeated in all the three days of flight. The device is tested in Bottom Heated Mode.

The global heat power input is maintained constant during flights, changing its distribution between the five heating elements. Three levels of global heat power input are tested:

- 50 W,
- 70 W;

## 7. Results obtained in hyper and micro-gravity conditions: 63<sup>th</sup> ESA PFC

- 90 W

The results obtained providing to the device these three levels of global heat power input are now pointed out in detail.

### **7.2.1 Results obtained providing 50 W of global heat power input**

In microgravity, when each of the five heaters dissipates 10 W (Figure 7.2), the thermofluid behavior is “intermittent”: oscillating periods, in which the pressure signal exhibits fluctuations (green sections, Figure 7.2b) and slug/plug flow motion is observable in the transparent section, are followed by prolonged stop-over (red sections in Figure 7.2b and in Figure 7.2c). During stop-over periods, the pressure is nearly constant, while the bubbles in the transparent section are stopped at the same position. This stagnant situation has a negative impact on the heat exchange. As shown in Figure 7.2b, during each stop-over, the temperatures at the evaporator exhibit an ever-increasing trend. When the fluid starts again to oscillate, the temperatures stabilize, proving the importance of the flow motion on the heat exchange. It is worthwhile to note that these results are very similar with respect to the ones obtained during the 61<sup>th</sup> ESA PFC (see section 6.2).

7. Results obtained in hyper and micro-gravity conditions: 63<sup>th</sup> ESA PFC

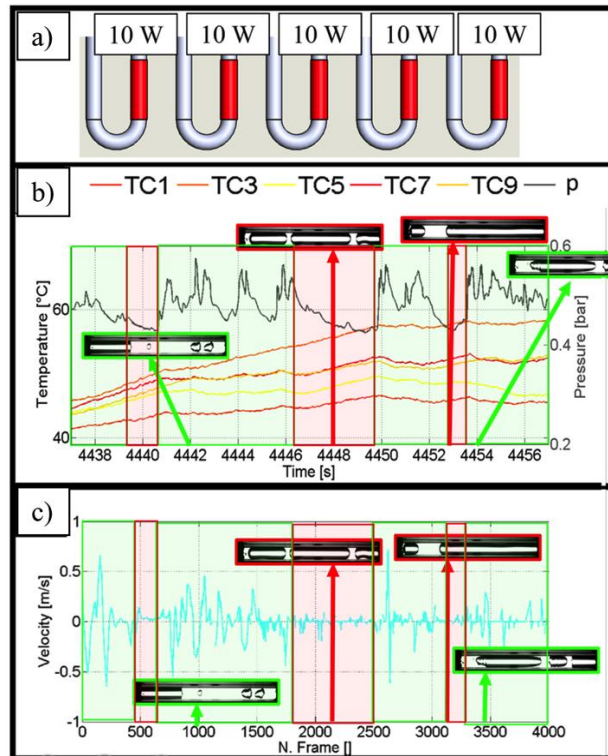


Figure 7.2 a) Power supplied by the five heating elements (Global heat power input: 50 W); Uniform heating pattern; b) Temperatures at the evaporator and pressure during microgravity; c) Bubble velocity measured in microgravity. The stop-over periods do not occurs providing to the SPHP a peculiar non-uniform heating distributions (Figure 7.3a).

## 7. Results obtained in hyper and micro-gravity conditions: 63<sup>th</sup> ESA PFC

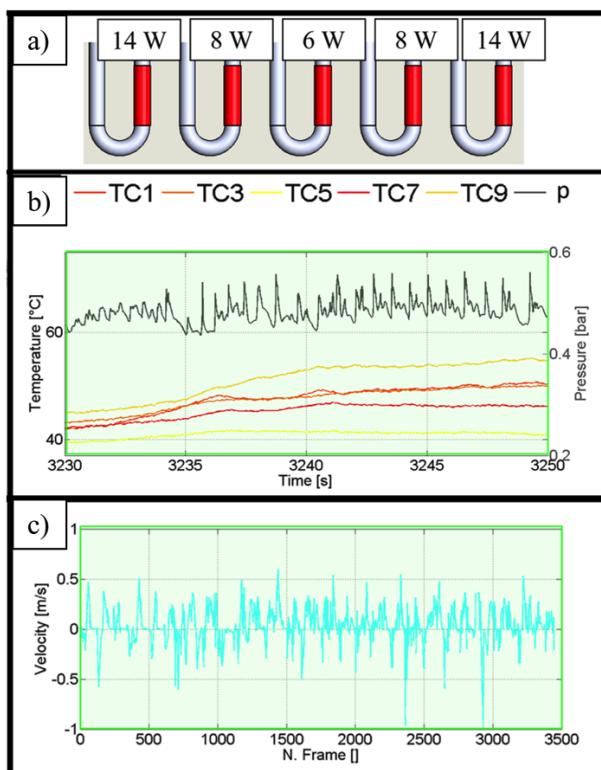


Figure 7.3 a) Power supplied by the five heating elements: non-uniform heating pattern; b) Temperatures at the evaporator and pressure during microgravity; c) Bubble velocity measured in microgravity.

Increasing the power at the lateral up-headers and decreasing it at the center (V-Shape Configuration), the pressure signal fluctuates continuously in microgravity (Figure 7.3b), while the bubble velocity measurements point out an oscillating flow (Figure 7.3c). The constant flow oscillations have a positive effect also in the heat exchange: even if the lateral up-headers dissipates a heating power 40% higher than the

## 7. Results obtained in hyper and micro-gravity conditions: 63<sup>th</sup> ESA PFC

uniform case, the maximum temperatures approaches 60 °C at the end of the micro-gravity period, that it is approximately the same value reached heating up the device uniformly. Increasing the heat power inputs at the lateral up-headers, the larger heat exchange area at the condenser permits to dissipate a higher amount of power.

When the device works as TS, the gravity certainly assists the flow motion, giving a net contribution to the fluid momentum. The gravity force is like an interconnection component between the different up-headers, permitting to the liquid phase to fall down through the down-comers and refreshing continuously the evaporator. As a consequence, even if the up-headers are heated up with non-uniform power levels, the temperatures at the evaporator resides in a narrow range: the fluid circulation keeps constant each ones. Nevertheless, in microgravity, the sudden absence of a gravity field “disconnects” hydro-dynamically all at once the five heating elements: in such condition, the expansions and contractions of the vapor phases are the principal responsible of the flow motion. The non-heated branches are not anymore “down-comers”, since in microgravity the liquid phase returns at the evaporator only if it is properly pushed back by vapor bubble expansions and contractions. Therefore, after the transition from hyper-gravity to micro-gravity the evaporator temperatures tend to spread in a wider range, from 35 °C to 70 °C, depending on the heating power provided to each element (Figure 7.4). As soon as the second hyper-gravity is achieved, the sudden return of the gravity field, linking again the heated

## 7. Results obtained in hyper and micro-gravity conditions: 63<sup>th</sup> ESA PFC

zone and permitting to the liquid phase to be pushed again in the heated zone, decreasing immediately all the temperatures at the evaporator.

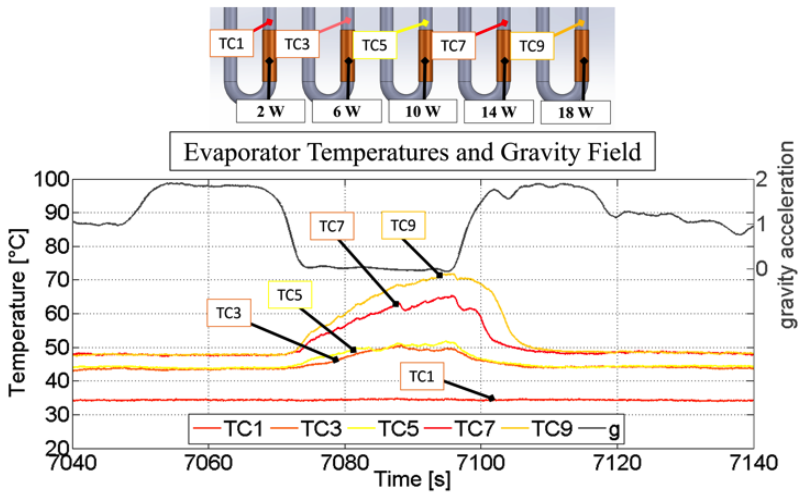


Figure 7.4 Temperature evolution at the evaporator during parabola.

### 7.2.2 Results obtained providing 70 W of global heat power input

Providing to the SPHP a global heat power of 70 W, again, an intermittent working mode is recognizable when the SPHP is uniformly heated up (Figure 7.5a): stop-over periods, that last up to six seconds (highlighted with a red rectangle in Figure 7.5a), are followed by sudden peaks in terms of pressure. Increasing the power value at the lateral up-headers and decreasing it at the center, stop-over periods are another time limited (Figure 7.5b): the pressure signal oscillates continuously, pointing out a continue flow pulsating slug/plug motion.



7. Results obtained in hyper and micro-gravity conditions: 63<sup>th</sup> ESA  
PFC

7. Results obtained in hyper and micro-gravity conditions: 63<sup>th</sup> ESA PFC

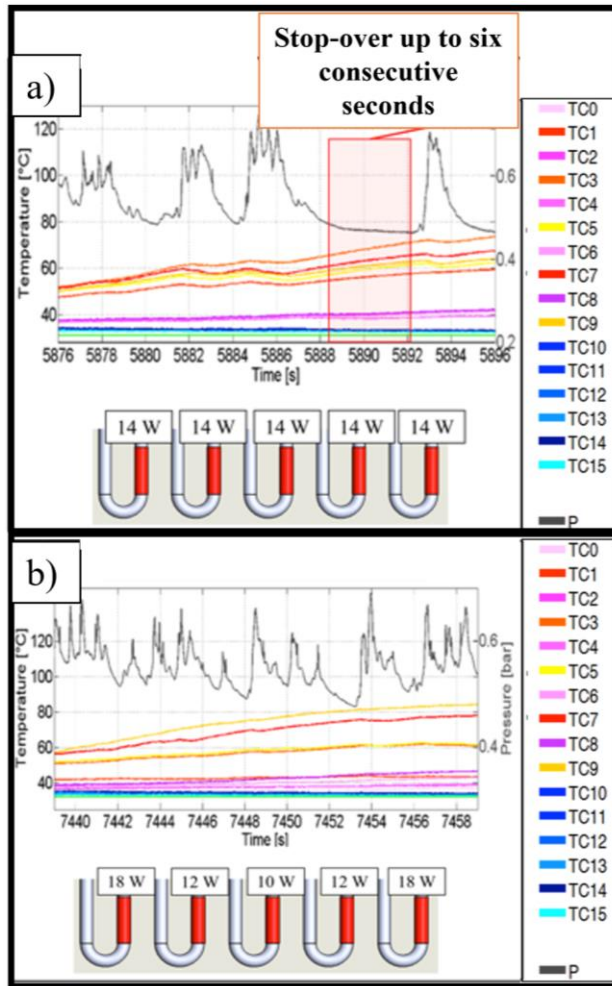


Figure 7.5 Pressure and temperatures during microgravity providing a global power of 70 W in a) uniform heating and b) non-uniform heating configuration.

**7.2.3 Results obtained providing 90 W of global heat power input**

Increasing the global heat power input up to 90 W, the homogeneous

## 7. Results obtained in hyper and micro-gravity conditions: 63<sup>th</sup> ESA PFC

heating configuration another time alternates stop-overs and intervals in which both the pressure signals and the bubble velocity point out a pulsating motion in microgravity (Figure 7.6a). Nevertheless, the non-uniform heating configurations tested in microgravity (V-Shape Configuration in Figure 7.6b and “Increasing” Configuration in Figure 7.6c) hinder this time the overall thermo-fluid dynamic behavior of the device. During the last seconds of microgravity, the pressure does not oscillate anymore, while the temperatures at the evaporator exhibit an increasing trend, reaching 95 °C at the end of the 20 seconds of microgravity, as if dry out conditions are

## 7. Results obtained in hyper and micro-gravity conditions: 63<sup>th</sup> ESA PFC

reached for both the tested non-uniform configurations.

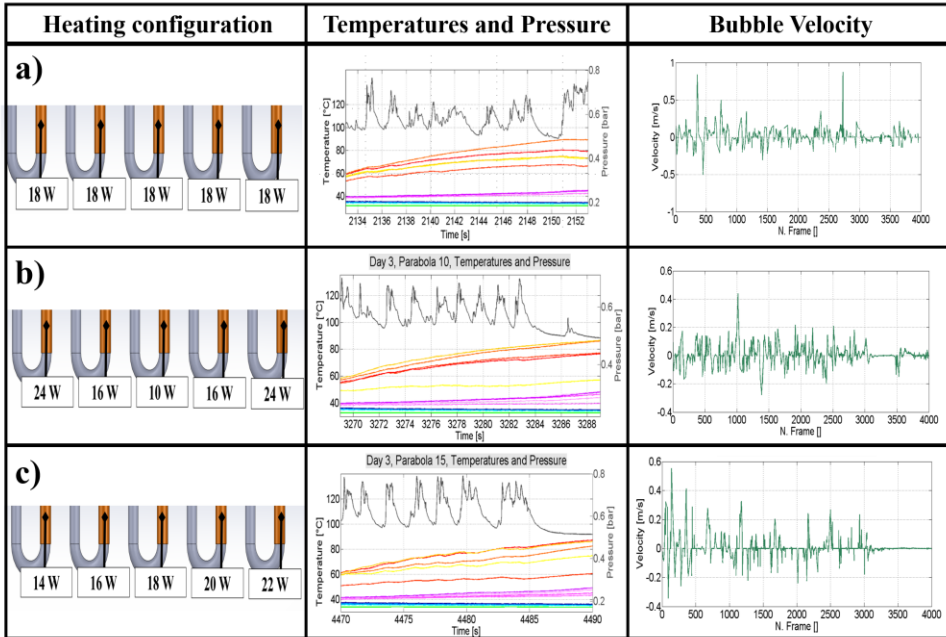


Figure 7.6 Results in microgravity conditions providing to the device a global heat power input of 90 W for (a) the homogeneous heating configuration; increasing the global heat power input at the most lateral branches (b), continuously increasing the heating power from the heater 1 to the heater 5 (c).

These results seem to be in contradiction with respect to what is pointed out providing to the SPHP similar non-uniform heating configurations for the 50 W and the 70 W case. However, dry-out conditions are observable only for the channels in which is provided the highest values of heating power.

## 7. Results obtained in hyper and micro-gravity conditions: 63<sup>th</sup> ESA PFC

Indeed, a local heating power of 20 W, corresponding to a heat flux of 13 W/cm<sup>2</sup>, seems to represent the limit of the SPHP in such conditions for all the configurations, even if further experiments in prolonged weightlessness conditions are necessary to prove the assumption.

Similar results are achieved for instance by providing to the device a global power of 50 W and a “Local High Value” Configuration (Figure 7.7). In this case, only the TC9, positioned just above the heating element that dissipates locally 26 W, shows an increasing trend during the 20 seconds of microgravity, while all the other channels, heated up with only 6 W, appear

7. Results obtained in hyper and micro-gravity conditions: 63<sup>th</sup> ESA PFC

stable.

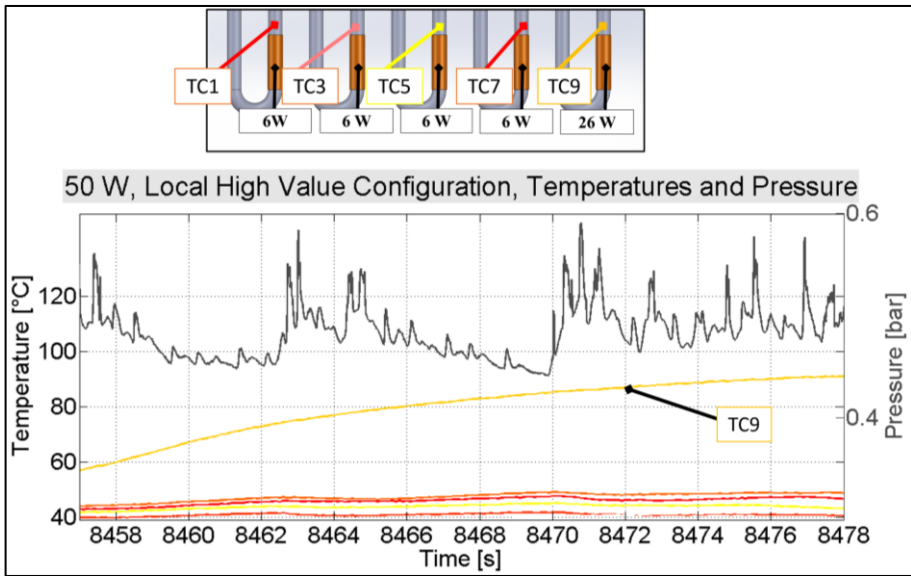


Figure 7.7. Temporal evolution of the temperatures at the evaporator zone and the inner pressure during the 20 seconds of microgravity providing to the device a Local High Value Configuration (Global heat power input: 50 W).

---

# Chapter 8

## 8. Conclusions and future developments

The work proposed in the previous chapters describes in detail the design, the physical realization and subsequent tests on ground and in micro/hyper-gravity conditions of a novel two-phase passive heat transfer

## Acknowledgments

device able to work as a Multi-Evaporator Loop Thermosyphon on ground and as a Pulsating Heat Pipe only in micro-gravity. In particular, the thesis pursues two main objectives:

1. the stabilization of the two-phase flow motion on ground and to decrease stop-over period time in micro-gravity using peculiar heating arrangements.
2. providing information about the influence that a reduced gravity field has on the capillary limit, in order to develop a “hybrid” two-phase passive heat transfer device operating as a Multi-Evaporator Loop Thermosyphon on ground (MELT) and as a PHP only in the space (SPHP).

### **8.1 Effect of peculiar heating distributions**

In order to fulfil the first aim, experimental campaigns have been conducted in various gravity conditions on a novel-type of “hybrid” closed loop thermosyphon operating with the “bubble lift principle” on ground and as a PHP in micro-gravity. A peculiar heating distribution, non-symmetric with respect to the gravity field is tested changing the ambient temperature, the position of the heating elements, the heat power input, the inclination and the gravity field.

#### **8.1.1 Main results on ground**

A novel concept of advanced multi-evaporator closed loop thermosyphon (MELT) is tested for two different heating patterns (symmetrical and non-



## Acknowledgments

symmetrical), in several orientations and varying the ambient temperature between  $-20\text{ }^{\circ}\text{C}$  and  $30\text{ }^{\circ}\text{C}$  in order to assess the beneficial effects of the induced fluid circulation and testify its reliability and very promising thermal performance. The main outcomes are:

- The non-symmetrical heating distribution promotes a stable circulation of fluid in a preferential direction more effectively than the symmetrical case. This is observable locally from the glass tube that closes the loop in the condenser zone and confirmed by the fluid pressure and the wall temperature trends.
- The vertical operation in BHM shows the best performance, both in terms of equivalent thermal resistance and heat flux capability. In particular, for the non-symmetrical case the maximum dissipated heat flux is 75% higher than the Critical Heat Flux for pool boiling of FC-72.
- The device thermal performance and heat power capability is negatively affected by its inclination, highlighting the importance of gravity assistance. Nevertheless, the dry-out condition are reached at higher heat flux levels for the non-symmetrical case with respect to the symmetrical case.
- There is a direct relationship between tilting level and the heat flux level required for the full activation.
- The dry-out heat input level is linked to the orientation both for the symmetric and the non-symmetrical case: increasing the tilting level

## Acknowledgments

towards the horizontal results in a lower value on the heat input capability.

- The system is able to recover from the dry-out condition decreasing the heat power, but the crisis phenomenon usually persists at the lower heat input levels, and the heat flux must be decreased to some extent more, in order to restore the correct device operation.
- Peculiar non-uniform heating distribution, stabilizing better the two-phase flow motion in a preferential direction, are able to decrease the  $R_{eq}$  values up to 10% with respect to the uniform case. This is more evident for the lowest global heat power input tested (50 W and 70 W).
- Lower the ambient temperature, higher will be the heat flux level to start-up the device.
- For the lowest ambient temperature tested, the two-phase flow seems to be hindered because of the increase of the liquid viscosity. However, even if it is clearly demonstrated that the ambient temperature affects the start-up and the two-phase flow motion within the device, further additional tests need to be performed to better understand physically this aspect.

Additionally, the Table 8-1 points out the main advantages and drawbacks of the MELT with respect to other two-phase passive heat transfer technologies such as PHPs and LTSs:

## Acknowledgments

Table 8-1 Advantage (green) and drawbacks (red) of the wickless heat pipe technologies.

	<b>Closed Thermosyphon (LTS)</b>	<b>Multi-Evap. Loop Thermosyphon (MELT)</b>	<b>Pulsating Heat Pipe (PHP)</b>
<b>3D space adaptability</b>	LOW	HIGH	VERY HIGH
<b>Thermally controlled surface</b>	MEDIUM	HIGH	VERY HIGH
<b>Dependency on gravity assistance</b>	VERY HIGH	HIGH	LOW
<b>Heat flux capability</b>	MEDIUM	VERY HIGH	MEDIUM
<b>Reliability</b>	VERY HIGH	HIGH	MEDIUM
<b>Modeling/Design tools</b>	HIGH	LOW	LOW
<b>Cost</b>	LOW	LOW	LOW

Concluding, the advantages of the MELT such as the high 3D space adaptability, combined with the extremely high heat flux capability in comparison to other two-phase passive heat transfer devices, the low production costs and the design simplicity could make this new technology a suitable tool to dissipate heat from electronic components. In particular, the application of this thermally driven two-phase technology, that does not need electrical energy to work being completely passive, could represent the future candidate to cool down electronic components in data centers. In fact, nowadays the 50% of the total energy is required in the data center for

## Acknowledgments

their electronic thermal management, essentially because heat dissipation is mainly achieved by “active systems”, such as forced liquid loops or fans that need electrical energy to work. The implementation of two-phase passive heat transfer device able to cool down high value of heat fluxes in an extremely low volume, like the MELT could represents a breakthrough solution, since there is no need of further electrical power.

### **8.1.2 Main results obtained in micro-gravity**

For the very first time, a novel concept of hybrid Thermosyphon/Pulsating Heat Pipe with an inner diameter bigger than the static threshold level on ground is tested both on ground and in hyper/micro gravity conditions during the 61<sup>th</sup> and 63<sup>th</sup> ESA Parabolic Flight Campaigns. According to the author’s best knowledge, this is the first attempt in literature that such a hybrid device is tested.

Summarizing, the parabolic flight tests have demonstrated that a transition from the Thermosyphon to the PHP working modes occurs during the microgravity periods.

On ground the device acts as a Multi-Evaporator Thermosyphon operating with the bubble lift principle, able to reach stable performance. However, the device is not able to work horizontally when gravity assisted, since the flow is stratified on ground. In micro-gravity, the sudden absence of the buoyancy forces activate a slug/plug flow motion typical of a PHP, permitting to the device to work also when it is horizontally oriented (Figure 8.2).

## Acknowledgments

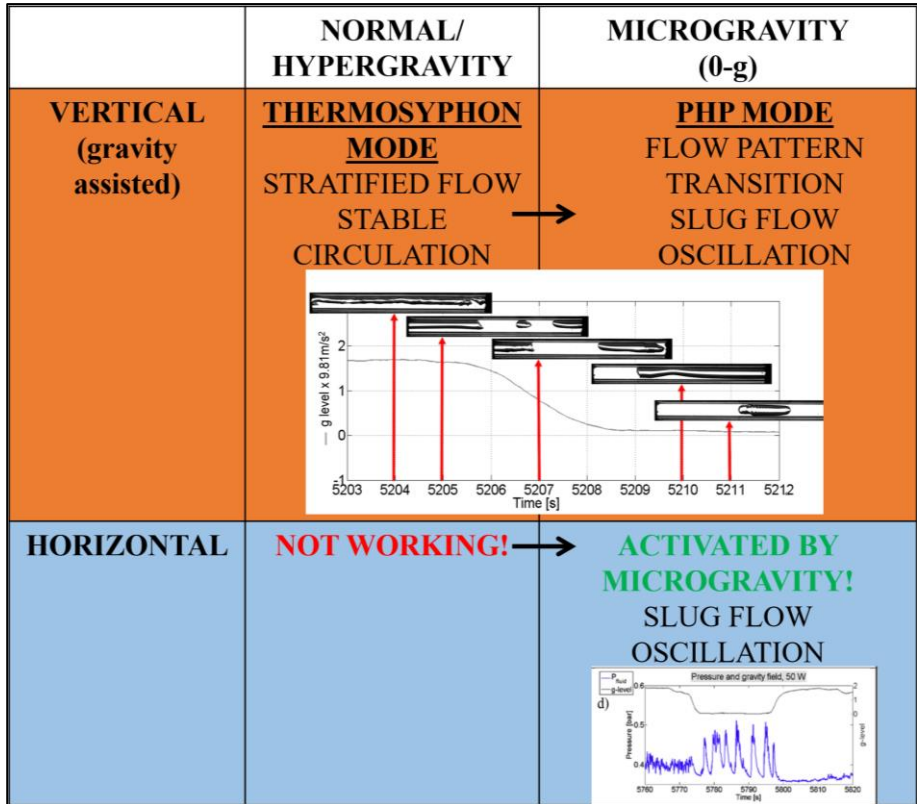


Figure 8.1 Results obtained during the 61th ESA PFC summarized.

Some important conclusions that comes from the 61th ESA PFC are listed here below:

- The parabolic flight tests reveal that the device operates in a complete different way when micro-gravity is reached: the images recorded in the transparent section, together with the pressure signal shows a transition from the Thermosyphon mode to the PHP working mode.

## Acknowledgments

- The flight test in vertical position points out a start-up also at the lowest heat power input levels in microgravity. The vapor plugs, expanding in the evaporator zone, permits to the adjacent liquid column to reach the condenser zone, promoting the heat exchange also at 10 W and 20 W.
- During micro-gravity, a slug/plug pulsating flow is observed also when the PHP is in the horizontal position
- In micro-gravity, the two-phase flow motion is intermittent when all the heating elements dissipate the same heat power input: vigorous pulsations are followed by stop-over periods, in which it is observed a two-phase flow stop in the condenser section, while temperatures at the evaporator tends to increase.
- For the highest heat power input tested in microgravity, i.e 120W and 160 W, the hyper-gravity period is able to eliminate partial dry-outs restoring the correct operation until the occurrence of the next microgravity period.
- heating up the device non-uniformly has a beneficial impact in microgravity for peculiar configurations: the homogeneous heating distribution causes an intermittent working mode when the device is not gravity assisted. Stop-over periods are spaced out by vigorous two-phase flow oscillations. The non-uniform heating distribution, creating an additional imbalance on the thermal boundary layers, establishes a pulsating motion also when gravity is absent, decreasing abruptly the stop-over periods.

## Acknowledgments

The non-uniform heating distribution, creating an additional imbalance on the thermal boundary layers, establishes a pulsating motion also when gravity is absent, decreasing abruptly the stop-over periods. The stabilization of the two-phase flow motion occurs especially in the configurations with partial asymmetries, as pointed out in Table 8-2, where all the configurations tested in microgravity are divided in three main categories. Configurations in which alternated stop-over periods and vigorous pulsations are observed, like the homogeneous ones, are colored in orange. Configurations with a dry-out are highlighted in red, while configurations with a flow stabilization are in green. Only particular heating configurations are beneficial on the stabilization of the two-phase flow motion in microgravity. The “V-shape” configurations, providing only small asymmetries at the evaporator, are the most effective ones in micro-gravity conditions. Either increasing locally the heating power with value higher than 20 W, or varying too much the heating power from the different heaters, causes a local dry-out.

Table 8-2 Thermo-fluid dynamic response of the device in microgravity.

## Acknowledgments

		DAY 1					
Global Heat power		HEATER 1	HEATER 2	HEATER 3	HEATER 4	HEATER 5	
		W	W	W	W	W	
Heating power configurations	50 W	Homogeneous	10	10	10	10	10
		Local high value 1	9	9	9	9	14
		Increasing 1	6	8	10	12	14
		Increasing 2	4	7	10	14	18
		Increasing 3	2	6	10	14	18
		Local high Value 2	6	6	6	6	25
		DAY 2					
Global Heat power		HEATER 1	HEATER 2	HEATER 3	HEATER 4	HEATER 5	
		W	W	W	W	W	
Heating power configurations	50 W	Increasing	2	6	10	14	18
		V-Shape	14	8	6	8	14
		Homogeneous	10	10	10	10	10
	70 W	Homogeneous	14	14	14	14	14
		V-Shape	18	12	10	12	18
		Increasing	6	10	14	18	22
		DAY 3					
Global Heat power		HEATER 1	HEATER 2	HEATER 3	HEATER 4	HEATER 5	
		W	W	W	W	W	
Heating power configurations	90 W	Homogeneous	18	18	18	18	18
		V-Shape	22	16	10	16	24
		Increasing	14	16	18	20	22
	50W	W-Shape	12	8	10	8	10
	70 W	V-Shape	18	12	10	12	18
		W-Shape	20	8	14	8	20

- The sudden absence of gravity, hindering the return of the two-phase flow through the down-comers, also establishes dry-out phenomena when just a single branch is heated up with high values of power. Finally, increasing locally the heating power, the subsequent rapid expansion of the vapor bubbles hinders the return of the cooled flow from the condenser, increasing the temperatures and establishing a typical dry-out condition.
- As a practical conclusion, heating up the channels locally with higher values of heat power at the most lateral branches where the



## Acknowledgments

transversal conduction along the condenser plate is lower, in such a way to create a non-symmetric thermal condition at the evaporator, is effective to stabilize the two-phase flow in microgravity. However, increasing excessively the non-symmetric heating configuration, for instance providing the SPHP with the “High Local Value” configuration, the dry-out conditions are more probable than the pumping of the flow into the condenser.

## 8.2 Future developments

Even if Parabolic flights have clearly evidenced a transition from a Loop Thermosyphon working mode to a PHP working mode when microgravity is achieved during parabolic trajectories, 20 s without a gravity field are not sufficient to reach pseudo-steady state conditions, and thus it is not possible to evaluate the thermal performance of such device without gravity. Therefore, further prolonged test in micro-gravity conditions are needed to fully thermally characterized such device in these conditions. For instance, testing the device using suborbital flights or installing it in the International Space Station (ISS) for a prolonged period could be extremely useful to quantify its thermal performance in such conditions.

Indeed, the non-symmetric heating distribution have clearly indicate a stabilization of the two-phase flow motion in a preferential direction only when the device is gravity assisted. When the device is no more gravity assisted, the two-phase flow pulsates within the device, as evidenced by the local fluid flow visualization and the pressure signal. Consequently, an

## Acknowledgments

additional unbalance in the thermal boundary layer conditions is needed to stabilize the two-phase flow also when the device is not anymore affected by gravity.

Results in this thesis pointed out that for peculiar non-uniform heating configurations, there is a stabilization of the two-phase flow motion also in micro-gravity. One possible idea to better stabilize the thermo-fluid dynamic behavior of such device could be designing also the condenser section with an additional non-symmetric thermal boundary layer condition. For instance, thermally insulating alternatively the branches just above the heating elements in the condenser section, should improve the bubble condensation in the non-heated channels, recalling more fluid from the heated section and thus promoting flow circulation. This arrangement could be beneficial in micro-gravity, without precluding the design simplicity of such device, as show in Figure 8.2.

## Acknowledgments

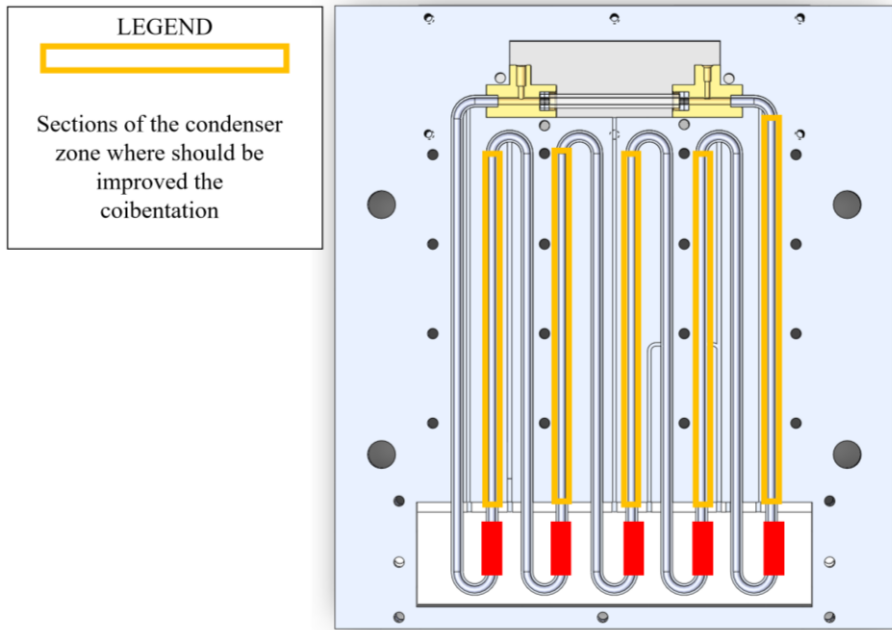


Figure 8.2 Coibentation of the branches just above the heating elements in order to improve non-symmetric thermal boundary conditions at the condenser.

Another possibility could be creating a hydraulic non-symmetry varying the wettability of the inner diameter. Imposing respectively hydrophilic and superhydrophobic features, the stabilization of the two-phase flow could be achieved. In order to better understand how the micro-channel wettability affects the overall performance of such device, the author of this PhD thesis is designing and assembling in this moment a novel PHP having transparent and interchangeable tubes between the evaporator and the condenser. The transparent tubes can be functionalized

## Acknowledgments

before tests, in such a way to decrease the inner wettability of the tube making it superhydrophobic, allowing to test different wettability configurations. The PHP is designed in a Single Loop geometry: the two transparent sections connect directly the heated and the cooled zone, simplifying the geometrical complexity. Two pressure transducers will be installed just before and after one of the transparent tubes, allowing to quantify also the pressure drop in that section, with a global accuracy of 70 Pa. A scheme description of this new experiment is pointed out in Figure 8.3. Since the design, the realization and the further test of this novel PHP is not a part of the PhD thesis, results are not included here.

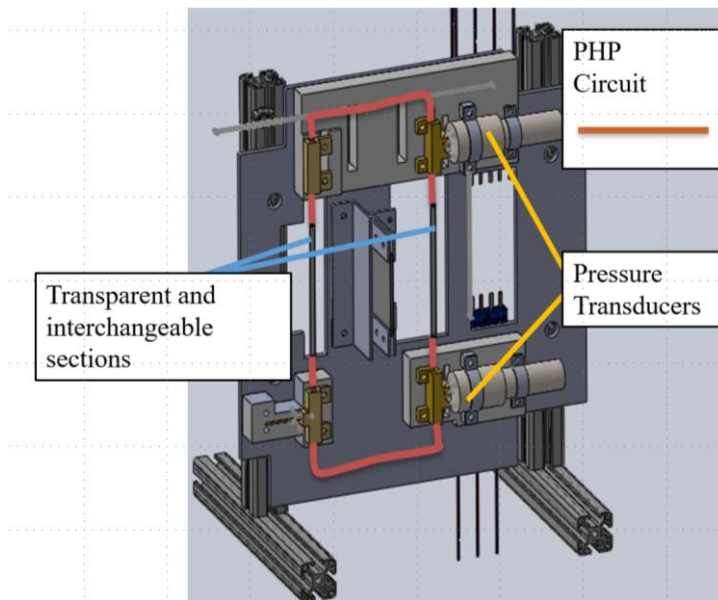


Figure 8.3 Single-Loop PHP scheme

# Acknowledgements

The present work has been carried out in the framework of two projects: the ESA-AO-2009 “*Microgravity investigations of a novel two phase thermal management device for the International Space Station*” financed by the Italian Space Agency (ASI-DOLFIN-II) and the ESA MAP Project INWIP, coordinated by Prof. Raffaele Savino.

The author would like to thank Ing. Battaglia for his administrative support; the NOVESPACE team in Bordeaux and Dr. V. Pletser for his support and encouragement in the parabolic flight campaign.

A grateful thanks is needed to the MSc thesis student G.F. Vanoli for his help in the experimental characterization of the device on ground. A sincerely thought also to Prof. Filippeschi for the fruitful discussion on the two-phase passive heat transfer devices and to Davide Fioriti, for his great

## Acknowledgments

help on the design of electronic components successfully implemented to the system during the 63th ESA PFC.

Thank to Dr. O. Minster and Dr. B. Toth for their interest in PHP activities and to all the members of the Pulsating Heat Pipe International Scientific Team, led by Prof. M. Marengo, for their contribution in pushing the PHP technology for real space applications.

The author acknowledges Prof. M. Mantelli and Prof. Paiva for the research activities performed during the 3 months period spent at the Federal University of Santa Catarina, Brazil from January 2015 to April 2015.

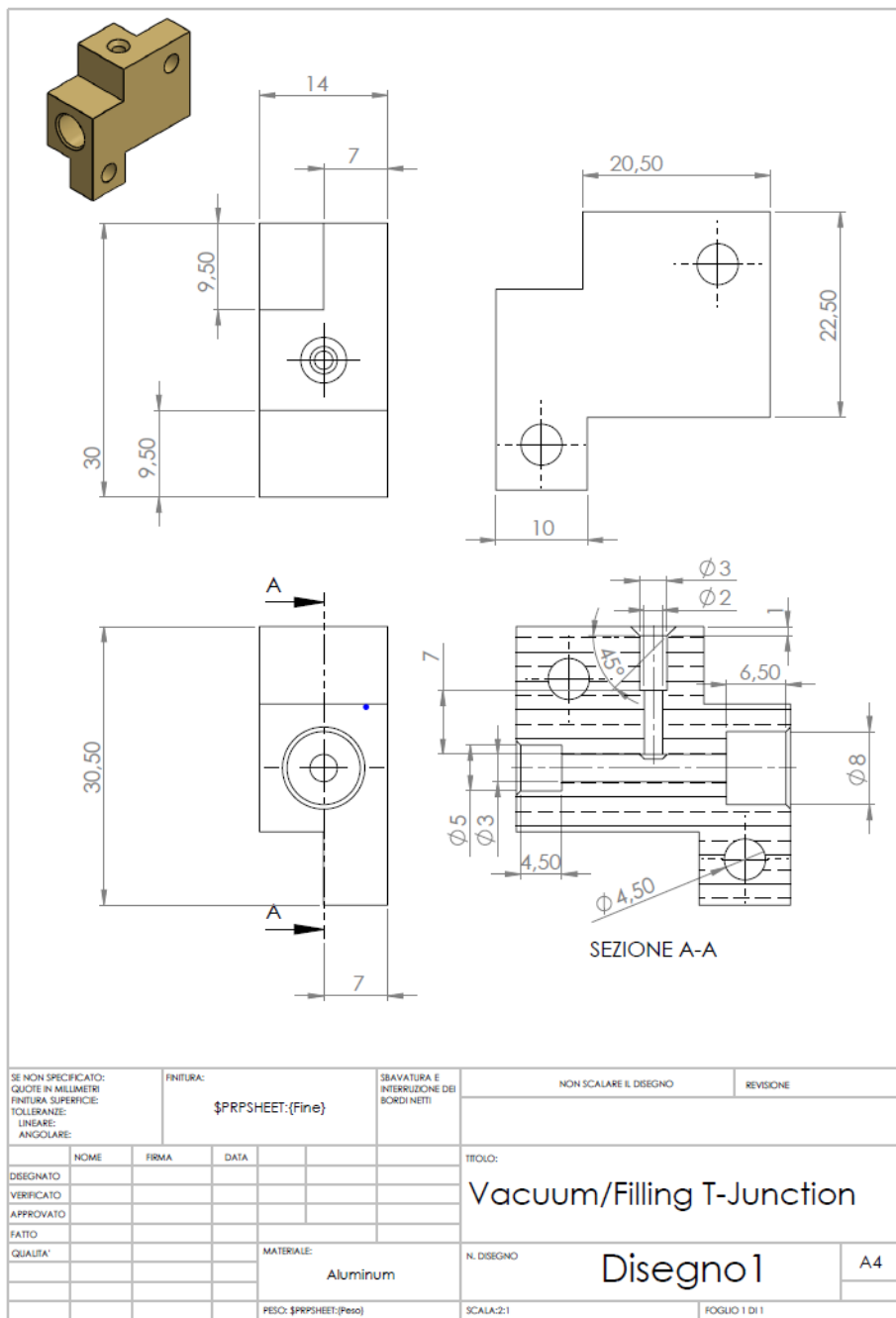
## Appendix

# Appendix

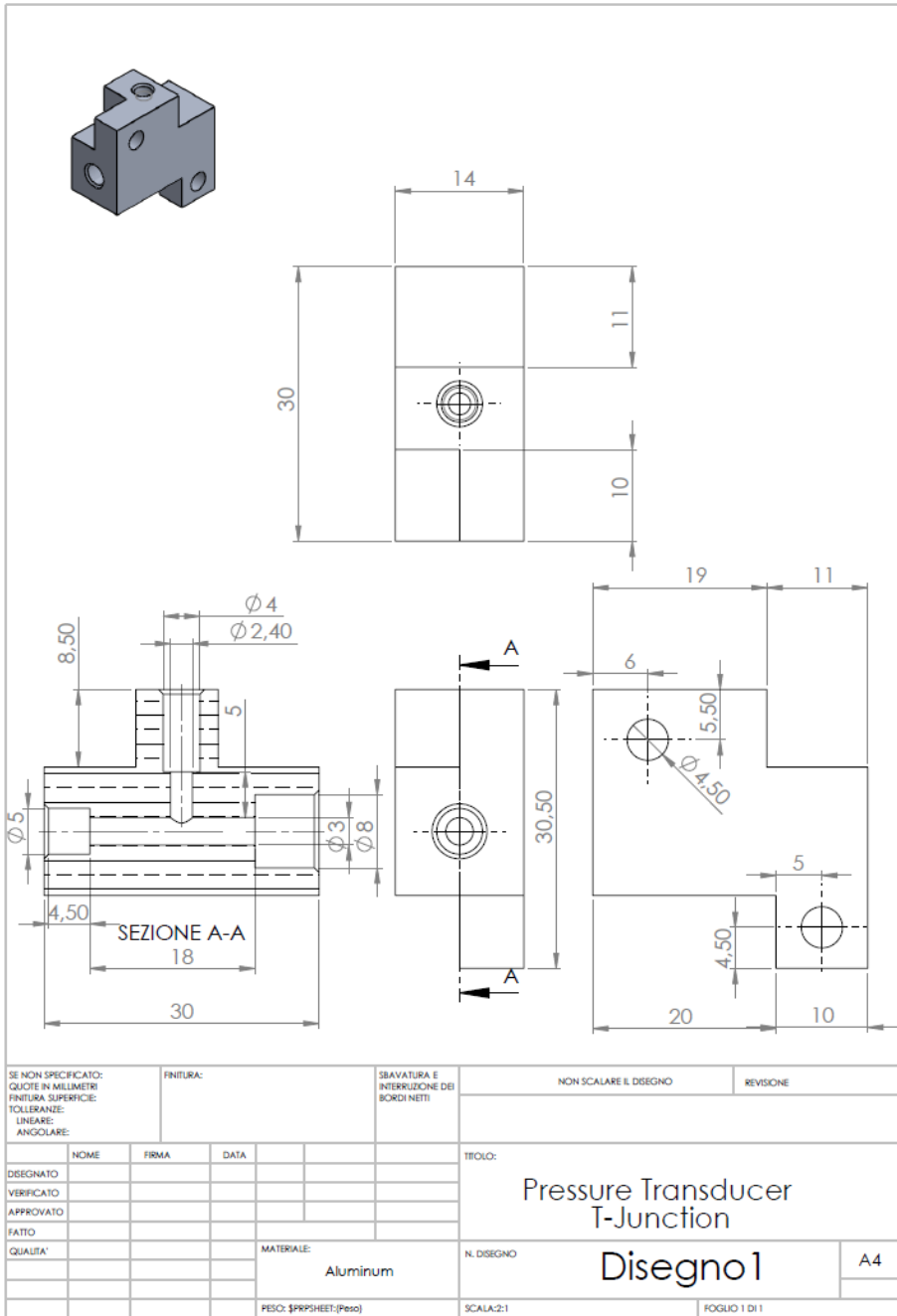
Since the most of the components are designed and realized in the Thermal Physics Laboratory of the University of Bergamo directly by the author, in the next pages are reported the drawings of the most relevant part of the device.



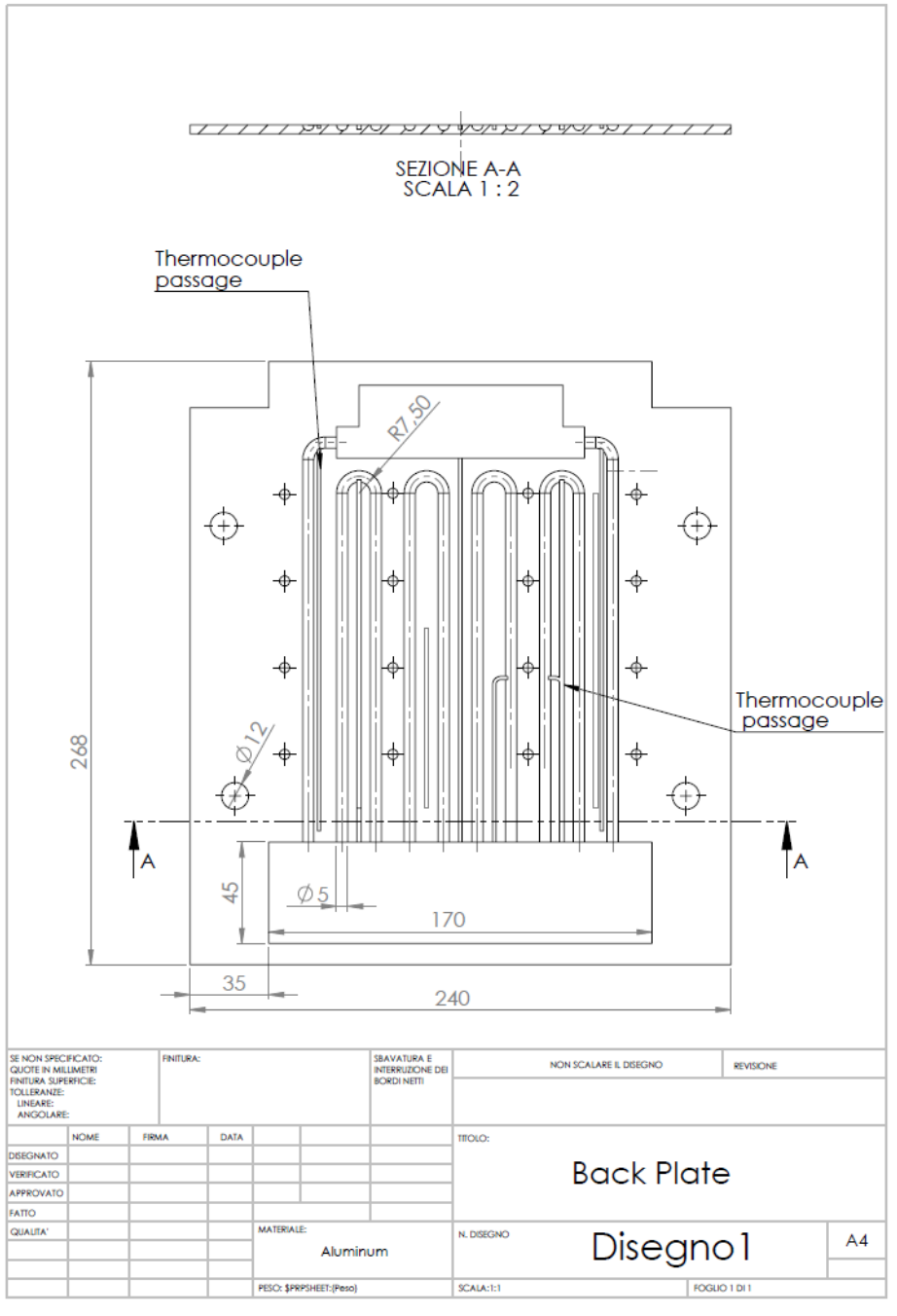
# Appendix



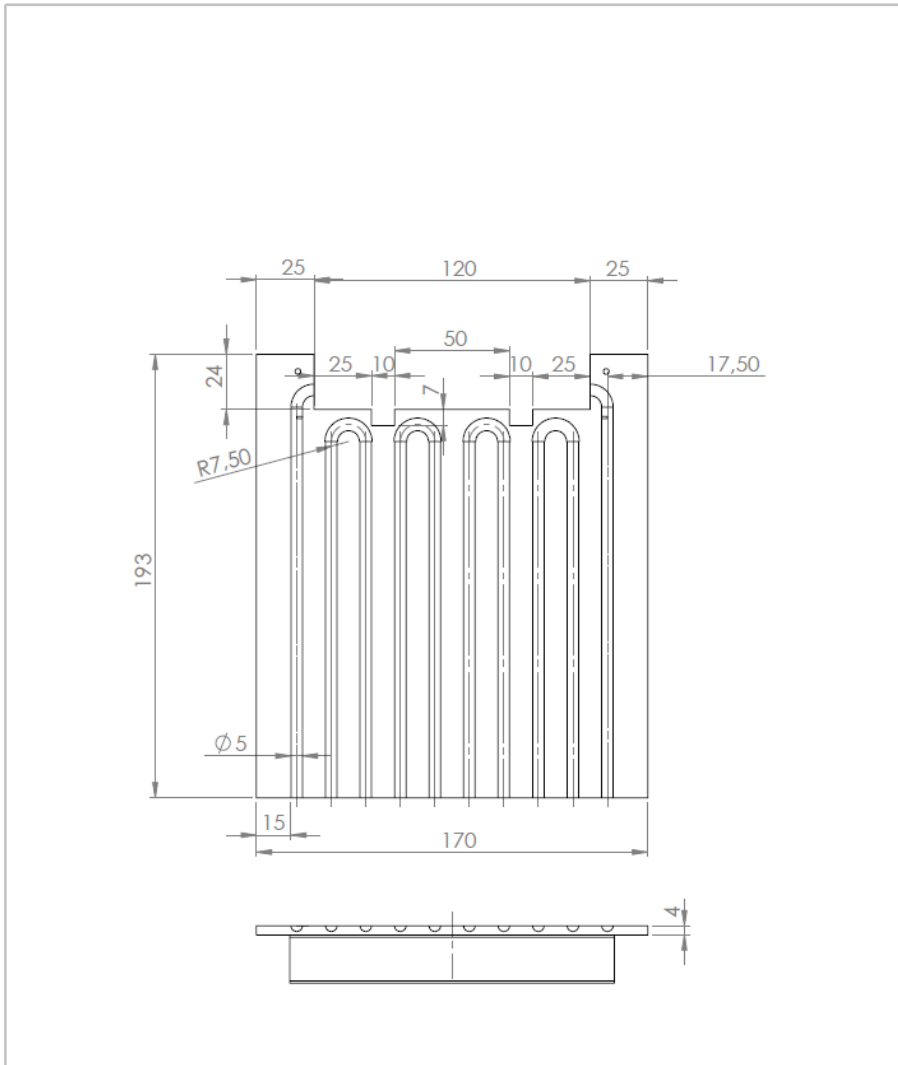
# Appendix



# Appendix

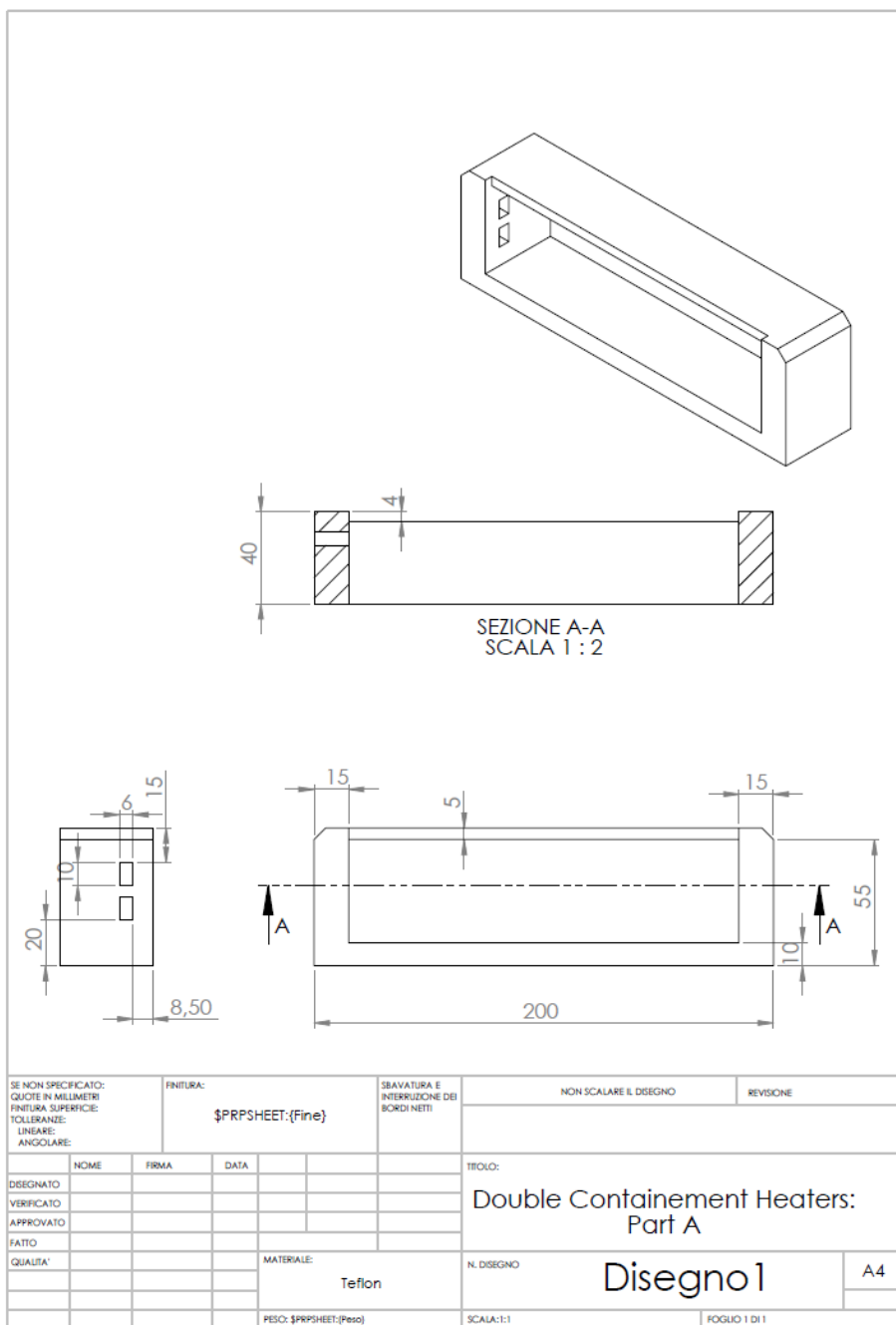


# Appendix

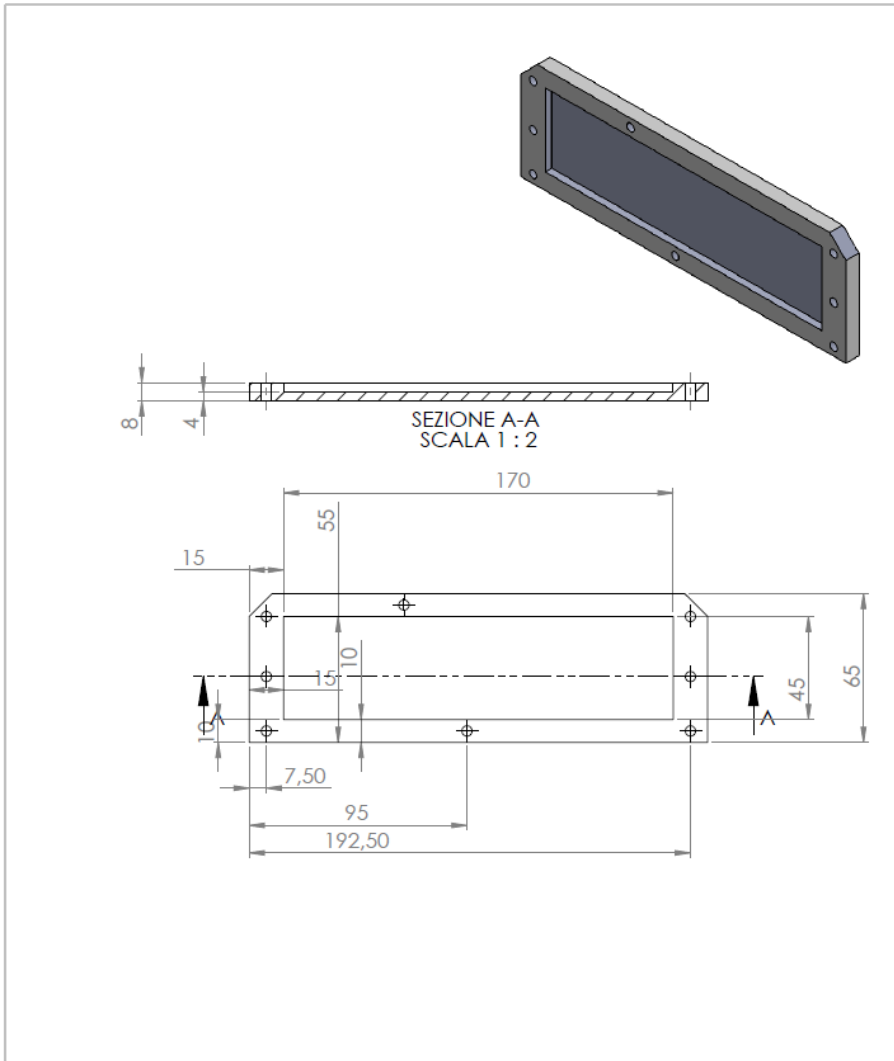


SE NON SPECIFICATO: QUOTE IN MILLIMETRI FINITURA SUPERFICIE: TOLLERANZE: LINEARE: ANGOLARE:		FINITURA:		SBAVATURA E INTERRUZIONE DEI BORDI NETI		NON SCALARE IL DISEGNO		REVISIONE	
DISEGNATO	NOME	FIRMA	DATA			TITOLO:			
VERIFICATO						Heat Sink			
APPROVATO									
FATTO						N. DISEGNO			
QUALITA'					MATERIALE: Aluminum	Disegno 1			A4
					PESO: \$PRPSHEET:Peso	SCALA: 1:1		FOGLIO 1 DI 1	

# Appendix

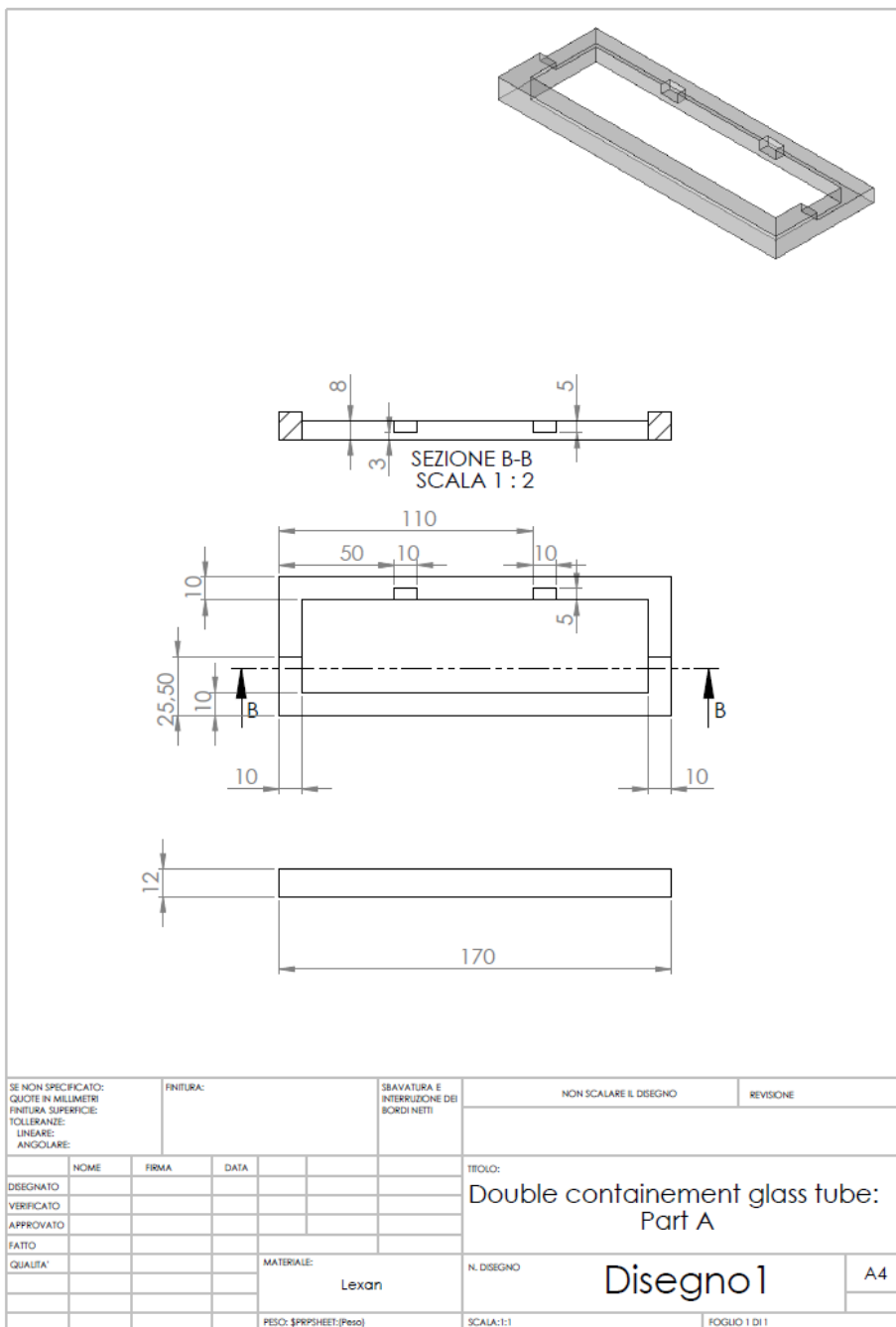


# Appendix



SE NON SPECIFICATO: QUOTE IN MILLIMETRI FINITURA SUPERFICIE: TOLLERANZE: LINEARE: ANGOLARE:		FINITURA:  \$PRPSHEET:(Fine)		SBAVATURA E INTERRUZIONE DEI BORDI NETTI		NON SCALARE IL DISEGNO		REVISIONE	
DISEGNATO	NCOME	FIRMA	DATA			TITOLO: Double Containment Heaters: Part B			
VERIFICATO						N. DISEGNO Disegno 1			
APPROVATO						A4			
FATTO					MATERIALE: Teflon				
QUALITA'					PESO: \$PRPSHEET:(Peso)	SCALA:1:1		FOGLIO 1 DI 1	

# Appendix







# List of publications

## **International journals**

1. Mangini, D., Antonini, C., Amirfazli, A., Marengo, M., Runback ice formation mechanism on hydrophilic and superhydrophobic surfaces, Cold Regions Science and Technology, Vol. 109, pp. 53-60, 2015.
2. Mangini, D., Mameli, M., Georgoulas, A., Araneo, L., Filippeschi, S., Marengo, M., A pulsating heat pipe for space applications: Ground and microgravity experiments, International Journal of Thermal Sciences, Vol. 95, pp. 53-63, 2015.

3. Mameli, M., Mangini, D., Vanoli, G.T., Araneo, L., Filippeschi, S., and Marengo, M., Advanced multi-evaporator loop thermosyphon. *Energy*, Vol. 112, pp. 562-573, 2016.
4. Mangini, D., Mameli, M., Fioriti, D., Filippeschi, S., Araneo, L., Marengo, M., Hybrid Pulsating Heat Pipe for Space Applications with Non-Uniform Heating Patterns: Ground and Micro-Gravity experiment, Sent to Applied Thermal Engineering (Under Review).
5. L. A. Betancur, Mangini, D., Mameli, M., Slongo, L.K., De Paiva, K., Mantelli, M., Marengo, M., Effect of the Condenser Temperature on the Start-up of a Pulsating Heat Pipe, Sent to Heat Pipe Science and Technology, An International Journal (Under Review).

### **Conference proceedings**

1. Mangini, D., Mameli, M., Vanoli, G.T., Araneo, L., Filippeschi, S., Marengo, M., A Novel Type of Multi-Evaporator Closed Loop Two Phase Thermo-syphon: Thermal Performance Analysis and Fluid Flow Visualization , *Proc. of the 14<sup>th</sup> UK Heat Transfer Conference*, Edinburgh, UK, 7-8 September 2015.
2. Mangini, D., Mameli, M., Vanoli, G.T., Araneo, L., Filippeschi, S., Marengo, M., Multi-Evaporator Closed Loop Thermosyphon, *Proc. of the 7<sup>st</sup> European-japanese two-phase flow group meeting*, Zermatt, 10-15 october, 2015.
3. Mangini, D., Mameli, M., Fioriti, D., Araneo, L., Filippeschi, S., Marengo, M. (2016). Pulsating Heat Pipe for space applications with

- non-uniform heating patterns: ground and micro-gravity experiments. *Proc. of the 18<sup>th</sup> IHPC and 12<sup>th</sup> IHPS*, Jeju-Do, South Korea, 10-15 June 2016.
4. Betancur, L. A., Mangini, D., Mameli, M., Slongo, L.K., dePaiva, K., Mantelli, M., Filippeschi, S., and Marengo, M. (2015). Condenser Temperature Effect on the Transient Behavior of a Pulsating Heat Pipe. *Proc. of the 18<sup>th</sup> IHPC and 12<sup>th</sup> IHPS*, Jeju-Do, South Korea, 10-15 June 2016.
  5. Araneo, L., Mangini, D., Mameli, M., Filippeschi, S., and Marengo, M., Effect of the Ambient Temperature on the Start-Up of a Multi-Evaporator Loop Thermosyphon, *Proc. of the 11<sup>th</sup> International Conference on Two-Phase flow systems for Ground and Space Applications*, Marseille, France, 2016.



# List of figures

Figure 1.1 General schematic view of the capillary driven heat transfer device (Mameli, 2012) [7]. .....	9
Figure 1.2. Order of magnitude of heat transfer coefficient ( $\text{W}/\text{m}^2\text{K}$ ) depending on cooling technology [8]. .....	11
Figure 1.3. Schematic representation of a TS and its working principle. ....	13
Figure 1.4 Wickless Heat Pipes working principles in the light of the confinement criteria [48].....	17
Figure 1.5. Closed Loop Thermosyphon with small cross section operating with the “bubble lift principle”.....	18
Figure 1.6. The reverse thermosiphon (Filippeschi, 2006).....	20

Figure 1.7 a) Heat Pipe schematization, where it is highlighted the liquid-vapor interface variation; b) pressure variations for the liquid and the vapor phase from the heat sink to the heat source..... 23

Figure 1.8. Qualitative heat pipe performance map [14]..... 25

Figure 1.9 Wick structures usually found in a Heat Pipe..... 26

Figure 1.10. Loop Heat Pipe [12]..... 30

Figure 1.11: Basic scheme of a closed loop PHP; on the right, zoom of the internal flow patterns. .... 31

Figure 1.12. Expansion of a vapor bubble in the evaporator section and subsequent push of the adjacent two-phase flow in the condenser section. .... 32

Figure 2.1 LTS working principle [-]..... 37

Figure 2.2 Operating mode of Closed Loop Two-Phase Thermosyphons [24]..... 46

Figure 2.3 Fundamental transport processes in a PHP, Khandekar and Groll 2008 [50]..... 58

Figure 2.4 Pressure-Enthalpy diagram of a working fluid control volume in non equilibrium conditions [51]..... 60

Figure 2.5 PHP configurations tested by Gu et al. [57] [56]..... 73

Figure 2.6 Flight tests in BHM [63], testing the device with 50 W. Temperatures at the evaporator are highlighted in red-yellow colors; temperatures at the condenser in blue colors. The ambient temperature is in green. The gravity field is pointed out by means of a black line. .... 76

Figure 2.7 Air–water flow patters along a 10 mm diameter tube in micro-gravity (first line) terrestrial gravity (second line), and hyper-gravity (third line) adapted from Choi et al. [78] varying the gas velocity ( $J_g$ ) and the fluid velocity ( $J_f$ ).....	79
Figure 2.8 Images of representative bubbles at varying accelerations and drift velocities: (a) $a/g = 0.01$ , $U_d = 20$ mm/s, $Bo = 0.48$ , $L = 17$ mm; (b) $a/g = 0.01$ , $U_d = 41$ mm/s, $Bo = 0.48$ , $L = 18$ mm; (c) $a/g = 0.34$ , $U_d = 94$ mm/s, $Bo = 16.6$ , $L = 13$ mm; (d) $a/g = 1$ , $U_d = 106$ mm/s, $Bo = 48.7$ , $L = 13$ mm; (e) $a/g = 1.8$ , $U_d = 214$ mm/s, $Bo = 87.7$ , $L = 13$ mm [79]......	81
Figure 2.9 Sudden decrease of temperatures at the evaporator when circulation is established [80]. .....	84
Figure 2.10 Scheme of a Check Valve [82]. .....	85
Figure 2.11 Heat Tranfer rate for all the working fluids and the evaporator temperature tested using a CLOHP and a CLOHP/CV [83]. .	86
Figure 2.12 Schematic of the liquid slug proposed in the simplified model with a non-constant ID.....	88
Figure 2.13. Schematic of the PHP configuration used in the numerical simulation done by C.M. Chiang et al. [86].....	89
Figure 2.14. The PHP tested with a different inner diameter along the tube [89]. .....	91
Figure 3.1 Qualitative plot in which is shown the capillary limit varying the gravity level.....	102
Figure 3.2 Qualitative representation of the two-phase flow passive heat transfer devices varying the ID dimensions and the gravity field. ....	103

Figure 3.3 Geometry of the device.....104

Figure 3.4 Thermocouple locations along the serpentine.....107

Figure 3.5 Exploded view of the test cell with all its main components.  
.....108

Figure 3.6 a) The two fans mounted above the heat sink; b) CAD view  
of the milled heat sink. ....109

Figure 3.7 Vacuum test of the device.....110

Figure 3.8 The filling system and the valve connected to the system.  
.....112

Figure 3.9 Heater and thermocouples arrangements, a) symmetrical, b)  
non-symmetrical.....114

Figure 3.10 Experimental layout. ....117

Figure 4.1 Temperature, pressure and power input diagram in  
vertical position, a) symmetrical heating; b) non-symmetrical heating;  
c) Legend. ....125

Figure 4.2 Wall temperature and fluid pressure: a) partial startup at  
20W; b) Complete activation at 40W. ....126

Figure 4.3 Symmetrical, a) visualization of oscillating motion 45 fps;  
b) Temperature and Pressure measurements at the transparent section ends;  
Non-Symmetrical, c) visualization of oscillating motion 45 fps; d)  
Temperature and Pressure measurements at the transparent section ends.  
.....128

Figure 4.4 Fluid circulation scheme with up-headers (red arrows) and  
down-comers (blue-arrows).....130



---

Figure 4.5 Equivalent thermal resistance for the various inclinations. The first power-up: a) symmetrical case, b) non-symmetrical case; the subsequent power-down: c) symmetrical case, d) non-symmetrical case.....	136
Figure 4.6 a) $R_{eq}$ values for the configurations tested on ground providing a global power of 50 W; b) Temperatures and Pressure evolutions during test. ....	146
Figure 4.7 a) Bubble velocity when the device is heated up uniformly; b) the heating configuration provided; c) Bubble direction and $R_{eq}$ value. ....	148
Figure 4.8 a) Bubble velocity when the device is heated up non uniform; b) the heating configuration provided; c) Bubble direction and $R_{eq}$ value. ....	149
Figure 4.9. Temperatures and pressure for the configurations tested providing 90 W to the device.....	151
Figure 4.10. $R_{eq}$ values for the main heating configurations tested providing to the device a global heat power input of 50 W, 70 W, 90 W. ....	152
Figure 4.11 . a) Test with $T_{amb}$ of $-20\text{ }^{\circ}\text{C}$ : temperatures and pressure and Flow oscillations at 50 fps; b) Test with $T_{amb}$ of $20\text{ }^{\circ}\text{C}$ : temperatures and pressure and Flow oscillations at 50 fps. ....	156
Figure 5.1 a) Airbus A300 “ZERO-G” aircraft internal side and upper views and b) the experimental area during a parabolic flight, with tests rack being mounted and the scientific crew perform tests.....	161

Figure 5.2: On the left, time schedule of the parabolas performed during each parabolic flight; on the right, the Airbus A300 Zero-G during a pull-up phase. ....164

Figure 5.3: Parabolic flight maneuver profile.....164

Figure 5.4 a) Test rig and main components and b) its scheme, in which are pointed out: the rack plate with the test cell cage covering the test cell assembly, PS=Heater power supply DL=data logger, notebook PC with its protective cage, PS and multiplug; NUC= compact laptop connected to the high speed camera. ....169

Figure 5.5 a) the test cell and b) its exploded view (highlighted the double containment).....172

Figure 5.6 a) The evaporator zone: bottom view, open. Silicon paste able to resist up to 200 °C is spread to seal the double containment; b) The evaporator zone: bottom view, closed using the PTFE. ....173

Figure 5.7 Double containment in the transparent section.....174

Figure 5.8 Heat sink and aluminum back plate that create the double containment in the condenser section. ....175

Figure 5.9 The cage that covers the test cell during parabolic flights. ....176

Figure 5.10 Test cell connected a) vertically and b) horizontally.....177

Figure 5.11 The anti-vibrating bush scheme and the connection between the device and the item support. ....178

Figure 5.12 Power supply and DAQ cage: a) CAD view; b) real picture; Laptop cage: c) CAD view; d) real picture. ....179

---

Figure 5.13 General schematic of the electrical system. ....	181
Figure 5.14 Thermal switches directly in contact to the heating elements utilized to open the electrical circuit in case of unexpected overtemperatures (above 150 °C) at the evaporator zone.....	183
Figure 6.1 Flight tests in vertical position using a global heat power input of 10 W and 20 W; first column: temperatures and gravity field; second column: pressure and gravity field synchronized with visual images (red arrows identify the exact timing of each image). ....	188
Figure 6.2 Flight tests in vertical position using a global heat power input of 30 W (first line), 40 W (second line), 80 W( third line), 120 W(fourth line), 120 W(fifth line) and 160 W(last line); first column: temperatures and gravity field; second column: pressure and gravity field synchronized with visual images (red arrows identify the exact timing of each image). ....	190
Figure 6.3 Gravity field transition from hyper to micro-gravity: activation of a slug/plug flow regime [66]. ....	192
Figure 6.4 Microgravity period at 80 W; a) temperatures recorded at the evaporator zone and b) the synchronized pressure signal and images [66]. ....	193
Figure 6.5 Hyper-gravity effect on partial dry-out occurred at 160 W. ....	194
Figure 6.6 Microgravity period for different heat inputs tested in horizontal orientation; first column: evaporator temperatures, gravity field and images; second column: pressure, gravity field and images [66]....	197

Figure 6.7  $g_x$ ,  $g_y$ ,  $g_z$  acceleration components and time evolution during parabolic maneuvers in horizontal orientation: a) Layout and directions; b)  $g_x$ ,  $g_y$ ,  $g_z$  acceleration over time; c) effect on temperatures; d) effect on fluid pressure [66].....198

Figure 7.1. Heating configurations tested during the three days of flight. ....202

Figure 7.2 a) Power supplied by the five heating elements (Global heat power input: 50 W); Uniform heating pattern; b) Temperatures at the evaporator and pressure during microgravity; c) Bubble velocity measured in microgravity. The stop-over periods do not occurs providing to the SPHP a peculiar non-uniform heating distributions (Figure 7.3a).....205

Figure 7.3 a) Power supplied by the five heating elements: non-uniform heating pattern; b) Temperatures at the evaporator and pressure during microgravity; c) Bubble velocity measured in microgravity. ....206

Figure 7.4 Temperature evolution at the evaporator during parabola. ....208

Figure 7.5 Pressure and temperatures during microgravity providing a global power of 70 W in a) uniform heating and b) non-uniform heating configuration. ....210

Figure 7.6 Results in microgravity conditions providing to the device a global heat power input of 90 W for (a) the homogeneous heating configuration; increasing the global heat power input at the most lateral branches (b), continuously increasing the heating power from the heater 1 to the heater 5 (c).....212

Figure 7.7. Temporal evolution of the temperatures at the evaporator zone and the inner pressure during the 20 seconds of microgravity providing to the device a Local High Value Configuration (Global heat power input: 50 W).  
..... 214

Figure 8.1 Results obtained during the 61th ESA PFC summarized.  
..... 221

Figure 8.2 Coibentation of the branches just above the heating elements in order to improve non-symmetric thermal boundary conditions at the condenser. .... 227

Figure 8.3 Single-Loop PHP scheme ..... 228



# List of tables

Table 1-1 General classification of HPs depending on the wick structure.....	26
Table 2-1 Thermophysical properties of the various fluids at atmospheric pressure .....	43
Table 2-2 Characteristic values of limit diameters for the fluids usually found in literature utilizing a temperature of 25 °C.....	45
Table 2-3 Experimental results in CLTPT experimental devices from 1999.....	48
Table 2-4: Main numerical, theoretical and experimental works of PHPs in micro-gravity.....	63

## List of tables

Table 2-5 Critical Diameters for HFE-7100 on ground and in micro-gravity calculated by the Bond Number at 20 °C.....	80
Table 2-6 Confinement diameters for FC-72 at 20 °C accordingly to static and dynamic criteria for FC-72.....	83
Table 3-1 Capillary limit in static and dynamic conditions on ground and reduced gravity conditions for FC-72.....	101
Table 3-2 FC-72 properties .....	105
Table 3-3. Pressure transducer Kulite® XCQ-093 specs .....	106
Table 3-4. Heater layouts characteristics .....	115
Table 4-1. Critical Heat Flux Correlations for FC72.....	131
<b>Table 4-2.</b> Comparison between different technologies. ....	133
Table 4-3 Flow pattern maps: a) Symmetrical case; b) Non-symmetrical case.....	140
Table 4-4. Heating configurations tested on ground providing to the device a global heat power input of 50 W. ....	144
Table 4-5 Flow pattern map for all the configurations. The full activation is highlighted with red lines.....	155
Table 4-6 FC-72 thermo-fluid properties between -20 °C to 30 °C.	157
Table 6-1 Global heat power during flight days. Since the heating elements are connected electrically in parallel, each one dissipates one fifth of the global heat power input.....	186
Table 8-1 Advantage (green) and drawbacks (red) of the wickless heat pipe technologies. ....	219



## List of tables

Table 8-2 Thermo-fluid dynamic response of the device in microgravity.....	223
--	-----



# Bibliography

- [1] T. Stocker, "Contribution of Working Group I to the Fifth Assessment Report of the Intergovernmental Panel on Climate Change," Cambridge University Press., cambridge, 2013.
- [2] R. Iyengar., M. Schmidt, "Thermodynamics of Information Technology Data Centers," *J. Res and Dev*, vol. 53, 2009.

## Bibliography

- [3] H. Akachi, "Structure of a heat pipe". USA Patent 4921041. 1990, 1 May 1990.
- [4] Y. Zhang and A. Faghri, "Advances and unsolved issues in Pulsating Heat Pipes," *Heat Transfer Engineering*, vol. 29, no. 1, pp. 22-44, 2008.
- [5] H. Akachi, "Structure of micro-heat pipe". USA Patent 5219020. 1993, 15 June 1993.
- [6] K. P. Reay D.A., Heat Pipes, Fifth ed., Butterworth-Heinemann, Burlington, USA: Butterworth-Heinemann, 2006.
- [7] Chisholm, Two-phase Flow in Pipelines and Heat Exchangers, New York: Chemie Ingenieur Technik, 1983.
- [8] M. A. Gibson, Thermosyphon Flooding in reduced gravity environments, Glenn Research Center, Cleveland, Ohio: NASA/TM—2013-216536, 2013.
- [9] A. Faghri, M.-M. Chen and M. Morgan, "Heat Transfer Characteristics in Two-Phase Closed Conventional And Concentric Annular," in *National Heat Pipe Conference*, Houston, 1988.
- [10] S. Filippeschi and A. Franco, "Closed Loop Two-Phase Thermosyphon of Small Dimensions: a Review of the," *Microgravity Science and Technology*, vol. 24, pp. 165-179, 2012.

## Bibliography

- [11] S. Filippeschi, "On Periodic Two-phase Thermosyphons Operating Against Gravity," *International Journal of Thermal Sciences*, vol. 45, pp. 124-137, 2006.
- [12] A. Faghri, "Review and Advances in Heat," *Journal of Heat Transfer*, vol. 134, 2012.
- [13] G. Gilmore, *Spacecraft Thermal Control Handbook*, California: The Aerospace Press, El Segundo, 2002.
- [14] K. P. Reay D.A., *Heat Pipes Theory Design and Applications*, Elsevier, 5th Edition, 2006.
- [15] S. Thomas. and A. Faghri, "Performance Characteristics of a Concentric Annular Heat Pipe: Part I- Experimental Prediction and Analysis of the Capillary Limit," *ASME Journal of Heat Transfer*, vol. 4, pp. 844-850, 1989.
- [16] A. Faghri, "Performance Characteristics of a Concentric Annular Heat Pipe: Part II- Vapor Flow Analysis," *ASME Journal of Heat Transfer*, vol. 4, pp. 851-857, 1989.
- [17] Y. F. Maidanik, Fershtater. Y., K. A. Goncharov, "Capillary Pump Loop for the Systems of Thermal Regulation of Spacecraft," in *4th European Symposium on Space Environment and Control Systems*, Florence, Italy, 1991.
- [18] T. Cooter, "Principles and Prospects for Micro Heat Pipes," in *Proceedings of 5th International Heat Pipe Conference*, Tsukuba, Japan, 1984.

## Bibliography

- [19] D. Hopkins and D. Khrustalev, "Flat Miniature Heat Pipes with Micro Capillary Grooves," *ASME Journal of Heat Transfer*, vol. 121, pp. 438-445, 1999.
- [20] S. Kandlikar, "Fundamental issues related to flow boiling in minichannels and microchannels," *Experimental Thermal and Fluid Science*, vol. 26, pp. 389-407, 2002.
- [21] D. Brauner, "Identification of the range of "small diameters" conduits, regarding two-phase flow pattern transitions," *International Journal of Heat and Mass Transfer*, vol. 19, pp. 29-39, 1992.
- [22] K. Kew, "Correlations for the prediction of boiling heat transfer in small diameter channels," *Applied Thermal Engineering*, vol. 17, pp. 705-715, 1997.
- [23] A. Franco. and S. Filippeschi, "Experimental analysis of heat and mass transfer in small dimension, two phase loop thermosyphons," *Heat Pipe Science and technology*, vol. 2, pp. 163-182, 2010.
- [24] Y. Dobriansky, "Concepts of self-acting circulation loops for downward heat transfer (reverse thermosyphons)," *Energy Conversion and Management*, vol. 52, pp. 414-425, 2011.
- [25] I. S. Kyung and S. Y. Lee, "Periodic flow excursion in an open two-phase natural circulation loop," *Nuclear Engineering and Design*, vol. 162, pp. 233-244, 1996.

## Bibliography

- [26] F. Rossi, "Thermal Control of Electronic Equipment by Heat Pipes and Two-Phase Thermosyphons," in *1999*, Tokio, 11th International Heat Pipe Conference.
- [27] R. E. Simons, G. M. Chrysler, R. C. Chu, "Experimental investigation of a Enhanced Thermosyphon Heat Loop for Cooling of a High Performance Electronics Module," in *Proc. of the 15th IEEE SEMI-THERM Symposium*, 1999.
- [28] M. K. Na, J. Jeon., K. H. Kwak., S. Nam, "Experimental study on Closed-Loop Two-Phase Thermosyphon Devices for Cooling MCMs," *Heat Transfer Engineering*, vol. 22, pp. 29-39, 2001.
- [29] J. Y. B. M. P. C. W. T. Pal. A., "Design and Performance Evaluation of a Compact Thermosyphon," *IEEE Transactions on Components And Packaging Technologies*, vol. 25, pp. 601-607, 2002.
- [30] S. M. I. Mukhejee, "Pumpless Loop for Narrow Channel and Micro-Channel Boiling," *ASME Journal of Electronic Packaging*, vol. 125, pp. 431-441, 2003.
- [31] H. Z. Z. T. N. Honda, "Flow and Heat Transfer Characteristics of a Natural Circulation Evaporative Cooling System for Electronic Components," *ASME Journal of Electronics Packaging*, vol. 126, pp. 1225-1239, 2004.

## Bibliography

- [32] R. Khodabandeh, "Heat Transfer in the evaporator of an advanced two-phase thermosyphon loop," *International Journal of refrigeration*, vol. 28, pp. 190-202, 2005.
- [33] R. F. R. Khodabandeh, "Instability, heat transfer and flow regime in a two-phase flow thermosyphon loop at different diameter evaporator channel," *Applied Thermal Engineering*, vol. 30, pp. 1107-1114, 2010.
- [34] X. C. L. T. Y. K. T. Huo, "Flow Boiling and Flow Regimes in Small Diameter Tubes," *Applied Thermal Engineering*, vol. 24, pp. 1225-1239, 2004.
- [35] C. Y. B. P. Y. Kim, "An experimental study of a Two-Phase Closed loop Thermosyphon with Dual Evaporator in Parallel Arrangement," *Journal of Mechanical Science and Technology*, vol. 19, pp. 189-198, 2005(2).
- [36] M. H. C. K. S. Tsai, "Experimental Study of a Loop Thermosyphon Using Methanol as Working Fluids," in *14th International Heat Pipe Conference*, Florianopolis, Brazil, 2007.
- [37] P. Tuma, "Evaporator/Boiler Design for Thermosyphon utilizing Segregated Hydrofluoroether Working Fluids," in *22th IEEE SEMI-THERM Symposium*, Dallas, 2007.



## Bibliography

- [38] P. K. G. M. R. Garrity, "A Flow Boiling Microchannel Evaporator Plate for Fuel Cell Thermal Management," *Heat Transfer Engineering*, vol. 28, pp. 877-844, 2007.
- [39] P. K. G. J. M. R. Garrity, "Instability Phenomena in a two-phase microchannel thermosyphon," *International Journal of Heat and Mass Transfer*, vol. 52, pp. 1701-1708, 2009.
- [40] A. Franco, "Heat Transfer and Flow pattern in Two-Phase Loops: an Experimental Investigation," in *Eurotherm*, Eindhoven, 2008.
- [41] S. Filippeschi, "Experimental analysis of boiling in saturated FC72 confined pools: preliminary results," in *7th Experimental and Heat Transfer, fluid Mechanics and Thermodynamics conference*, Krakow, 2009.
- [42] R. Khodabandeh, "Instability, heat transfer and flow regime in a two-phase flow thermosyphon loop at different diameter evaporator channels," *Applied Thermal Engineering*, vol. 30, pp. 1107-1114, 2010.
- [43] K. Dincera, Y. Yilmaza. A. Berbera, S. Baskaya, "Experimental investigation of single-phase and two-phase closed thermosyphon solar water heater systems," *Scientific Research and Essays*, vol. 6, pp. 688-693, 2011.

## Bibliography

- [44] M. Mameli., D. Mangini, G. Vanoli, L. Araneo, S. Filippeschi. M. Marengo, "Advanced Multi-Evaporator loop Thermosyphon," *Energy*, 2016.
- [45] M. Mameli, D. Mangini, G. Vanoli, L. Araneo, S. Filippeschi. M. Marengo, "Advanced Multi-Evaporator Loop Thermosyphon," *Energy*, 2016.
- [46] Z. J. Zuo, M. T. North and L. Ray, "Combined pulsating and capillary heat pipe mechanism for cooling of high heat flux electronics," in *Proceedings of ASME Heat Transfer Device Conference*, Nashville, Tennessee, USA, 1999.
- [47] Z. J. Zuo, M. T. North and K. L. Wert, "High heat flux heat pipes for cooling of electronics," *IEEE Transactions on Components and Packaging Technologies*, vol. 24, no. 2, p. 220–225, 2001.
- [48] J. Kim. N. Bui, J. Kim, H. Kum, "Flow Visualization Experiment on Oscillating Heat Pipes," in *149-153*, Tokyo, 1999.
- [49] Z. Zhang, "Experimental Study of a Pulsating Heat Pipe using FC-72, Ethanol, and Water as a Working Fluids" *Experimental heat transfer*, vol. 17, pp. 47-67, 2004.
- [50] S. Khandekar and M. Groll, "Roadmap to realistic modeling of closed loop Pulsating Heat Pipes," in *Proceedings of 9th*

## Bibliography

*International Heat Pipe Symposium*, Kuala Lumpur, Malaysia, 2008.

- [51] G. Karimi, "Review and assessment of pulsating heat pipe mechanism for high heat flux electronic cooling," *Thermal and Thermomechanical Phenomena in Electronic Systems*, vol. 2, pp. 52-59, 2004.
- [52] M. Delil, "Microgravity two-phase flow and heat transfer," Nationaal Lucht- en Ruimtevaartlaboratorium, 1999.
- [53] M. Delil, "Thermal-gravitational modelling and scaling of heat transport systems for applications in different gravity environments: super-gravity levels & oscillating heat transfer devices," ationaal Nationaal Lucht- en Ruimtevaartlaboratorium, 2000.
- [54] M. Delil, "Pulsating & oscillating heat transfer devices in acceleration environments from microgravity to supergravity," Nationaal Lucht- en Ruimtevaartlaboratorium, 2001.
- [55] M. Kawaji, "Studies of vibration-induced multi-phase fluid phenomena and pulasating heat pipe performance under microgravity," in *Proceeding of the ASME FEDSM'03 - 4th ASME\_JSME Joint Fluids Engineering Conference*, Honolulu, Hawaii, USA, 2003.
- [56] J. Gu, M. Kawaji and R. Futamata, "Effects of gravity on the performance of Pulsating Heat Pipes," *Journal of*

## Bibliography

- Thermophysics and Heat Transfer*, vol. 18, no. 3, pp. 370-378, 2004.
- [57] J. Gu, M. Kawaji and R. Futamaca, "Microgravity performance of micro pulsating heating pipe," *Microgravity Science and Technology*, vol. 16, no. 1, 2005.
- [58] K. V. de Paiva, M. B. H. Mantelli, L. K. Slongo and S. J. Burg, "Experimental tests of mini Heat Pipe, Pulsating Heat Pipe and Heat Spreader under microgravity conditions aboard suborbital rockets," in *Proceedings of the 15th International Heat Pipe Conference*, Clemson, South Carolina, USA, 2010.
- [59] K. De Paiva, R. Gaur, M. Mantelli, "Mini Heat Pipe Experiments under Microgravity conditions. What have we learned?" in *17th International Heat Pipe Conference*, Kanpour, India, 2013.
- [60] M. Maeda, A. Okamoto, H. Kawasaki and H. Sugita, "Development of Flat Plate Heat Pipe and the project of on-orbit experiment," in *Proceedings of the 41st International Conference on Environmental Systems*, Portland, Oregon, USA, 2011.
- [61] M. Mameli, "Pulsating Heat Pipes. Numerical Modeling and Experimental Assessment," in *PhD Thesis*, 2012.
- [62] V. Ayel, F. Thevenot, Y. Bertin and C. Romestant, "Analyse thermo-hydraulique expérimentale d'un caloduc oscillantsous

## Bibliography

- champ de gravité variable," in *Proceedings of the Congrès Français de Thermique SFT 2013*, Gerardmer, France, 2013.
- [63] M. Mameli, L. Araneo, R. Testa, S. Filippeschi, M. Marengo "Thermal response of a closed loop Pulsating Heat Pipe under a variable gravity force," *International Journal of Thermal Sciences*, vol. 80, pp. 11-22, 2014.
- [64] B. Taft, S. Laun, M. Smith, "Microgravity Performance of a Structurally Embedded Oscillating Heat Pipe," *Journal of Thermophysics and heat Transfer*, vol. 29, no. 2, 2015.
- [65] V. Ayel, L. Araneo, A. Scalambra, M. Mameli, C. Romestant, A. Piteau, M. Marengo, S. Filippeschi and Y. Bertin, "Experimental study of a closed loop flat plate pulsating heat pipe under a varying gravity force," *International Journal of Thermal Sciences*, vol. 96, pp. 23-34, 2015.
- [66] D. Mangini, M. Mameli, A. Georgoulas, L. Araneo, S. Filippeschi and M. Marengo, "A pulsating heat pipe for space applications: Ground and microgravity experiments," *International Journal of Thermal Sciences*, vol. 95, pp. 53-63, 2015.
- [67] F. Creatini et al., "Thermal response of a Pulsating Heat Pipe on board the Rexus 18 sounding rocket: PHOS experiment chronicles," in *14th UK Heat Transfer Conference*, Edimburgh, 2016.

## Bibliography

- [68] V. Ayel, et al., "Visualizations of the flow patterns in a closed loop flat plate PHP with channel diameter above the critical one and tested under microgravity," in *18th IHPC and 12th IHPS*, Jeju-do, South Korea, 2016.
- [69] D. Mangini, M. Mameli, D. Fioriti, L. Araneo, S. Filippeschi, M. Marengo, "Hybrid Pulsating Heat Pipe for Space Applications with Non Uniform Heating Patterns: Ground and Microgravity Experiments," in *18th IHPC and 12th IHPS*, Jeju-Do, South Korea, 2016.
- [70] M. Manzoni, M. Mameli, L. Araneo, S. Filippeschi, M. Marengo "Advanced Numerical Method for a Thermally Induced Slug flow: Application to a Capillary Closed Loop Pulsating Heat Pipe," *International Journal of Numerical Methods in fluids*, p. in press, 2016.
- [71] S. Khandekar and M. Groll, "Pulsating Heat Pipes: Progress and Prospects," in *roc. International Conference on Energy and the Environment*, Shangai, China, 2003.
- [72] K. Tong et al., "Closed-Loop Pulsating Heat Pipe," *Applied Thermal Engineering*, vol. 21, pp. 1845-1862, 2001.
- [73] S. Khandekar and M. Groll, "An Insight into Thermo-Hydraulic Coupling in Pulsating Heat Pipes," *International Journal of Thermal Sciences*, vol. 43, pp. 13-20, 2004.

## Bibliography

- [74] S. Khandekar et al., "Closed Loop Pulsating Heat Pipes, Part B: Visualization and Semi-Empirical Modeling," *Applied Thermal Engineering*, vol. 23, no. 16, pp. 2012-2033, 2003.
- [75] S. Khandekar et al., "Pulsating Heat Pipes: Thermo-fluidic characteristics and Comparative Study with Single Phase Thermosyphon," in *12th International Heat Transfer Conference*, Grenoble, France, 2002.
- [76] M. Mameli, L. Marelli, M. Manzoni, L. Araneo, S. Filippeschi and M. Marengo, "Closed loop pulsating heat pipe: ground and microgravity experiments," in *Proceedings of the 9th International Conference on two-phase systems for ground and space applications*, Baltimore, USA, 2014.
- [77] D. Hepner et al., "Zero gravity experiments in two-phase fluids flow regime," in *ASME Intersociety Conference of Environmental systems*, San Francisco, 1975.
- [78] B. Choi, "A study of gas-liquid two-phase flow in a horizontal tube under microgravity," *Ann. N.Y. Acad. Sci.*, vol. 94, pp. 316-327, 2002.
- [79] A. Scammell, J. Kim., M. Magnini, J. R. Thome, "A study of gravitational effects on single elongated vapor bubbles," *International Journal of Heat and Mass Transfer*, vol. 99, pp. 904-917, 2016.

## Bibliography

- [80] S. Khandekar and M. Groll, "Understanding Operational regimes of closed loop pulsating heat pipes:an experimental study," *Applied Thermal Engineering*, vol. 23, pp. 707-719, 2002.
- [81] S. Rittidech, "Heat-transfer characteristics of a closed-loop oscillating heat-pipe with check valves," *Applied Energy*, vol. 84, p. 565, 2007.
- [82] P. Supirattanakul et al., "Application of a closed-loop oscillating heat pipe with check valves (CLOHP/CV) on performance enhancement in air conditioning system," *Energy and Buildings*, vol. 43, no. 7, pp. 1531-1535, 2011.
- [83] P. R. S. Meena, ", Comparisons of heat transfer performance of a closed-looped oscillating heat pipe and closed-looped oscillating heat pipe with check valves heat exchangers," *American Journal of Engineering and applied Sciences*, vol. 1, pp. 7-11, 2008.
- [84] S. Rittidech et al., "Thermal performance of horizontal closed-loop oscillating heat-pipe with check valves," *Journal of Mechanical Science and Technology*, vol. 24, pp. 545-550, 2010.
- [85] B. Holley and A. Faghri, "Analysis of pulsating heat pipe with capillary wick and varying channel diameter," *International Journal of Heat and Mass Transfer*, vol. 48, pp. 2635-2651, 2005.



## Bibliography

- [86] C. Chiang et al., "Theoretical study of oscillatory phenomena in a horizontal heat pipe with asymmetrical arrayed minichannel," *International journal in heat and mass transfer*, vol. 39, p. 923, 2012.
- [87] K. Chien et al., "A novel design of pulsating heat pipe with fewer turns applicable to all orientations," *International Journal of Heat and Mass Transfer*, vol. 55, pp. 5722-5728, 2012.
- [88] D. Jang et al., "Experimental investigation on the thermal performance of pulsating heat pipes with asymmetric channels," in *18 IHPC and 12 IHPS*, Jeju-do, South Korea, 2016.
- [89] K.-S. Tseng et al., "Investigation of the performance of pulsating heat pipe subject to uniform/alternating tube diameters," *Experimental and fluid science*, vol. 54, pp. 85-92, 2014.
- [90] S. M. H. Thompson, "Effect of localized heating on three-dimensional flat-plate oscillating heat pipe," *Advances in Mechanical engineering*, 2010.
- [91] J. O'Conner et al., "Gas-saturated pool boiling heat transfer," *Journal of Heat Transfer*, vol. 188, pp. 662-667, 1996.

## Bibliography

- [92] B. T. Taft, "Non-condensable gases and oscillating heat pipe operation," *Frontiers in Heat Pipes*, vol. 4, 2013.
- [93] J. Henry et al., "Heater size and heater aspect ratio effects on sub-cooled pool boiling heat transfer in low-g," in *3rd International Symposium on Two-Phase Flow Modeling and Experimentation*, Pisa, Italy, 2004.
- [94] D. Mangini, M. Mameli, G. Vanoli., L. Araneo, S. Filippeschi. M. Marengo, "Multi-Evaporator Closed Loop Thermosyphon," in *7th European-Japanese Two-Phase Flow Group Meeting*, Zermatt, Switzerland, 2015.
- [95] D. Mangini., G. F. Vanoli, L. Araneo, S. Filippeschi. M. Marengo, "A Novel Type of Multi-Evaporator Closed Loop Thermosyphon: Thermal Performance Analysis and Fluid Flow Visualization," in *UK Heat Transfer Conference*, Edimburgh, 2015.
- [96] D. Mangini, M. Mameli, D. Fioriti, L. Araneo, S. Filippeschi, M. Marengo, "Hybrid Pulsating Heat Pipe for Space Applications with Non Uniform Heating," in *18th International Heat Pipe Conference and 12th Heat Pipe Symposium*, Jeju-do, South Korea, 2016.
- [97] L. Araneo, D. Mangini, M. Mameli, M. Marengo, "Effect of the Ambient Temperature on the Start-Up of a Multi-Evaporator Loop Thermosyphon," in *Eleventh International*

## Bibliography

*Conference on Two-Phase Systems for Ground and Space Applications*, Marseille, 2016.

- [98] I. G. B. Golobic, "Corresponding States Correlation for Maximum Heat Flux in Two Phase Closed Thermosyphon," *International Journal of Refrigeration*, vol. 20, no. 6, pp. 402-410, 1997.
- [99] S. Kutateladze, "Hydrodynamic Theory of Changes in the Boiling Process Under Free Convection Condition," *Izv. Akad. Nauk.*, vol. 4, pp. 529-536, 1951.
- [100] N. Zuber, "Hydrodynamic Aspects of Boiling Heat Transfer," AEC Report No. AECU-4439, Physics and Mathematics, 1959.
- [101] Y. Katto, "Generalized Correlation for Critical Heat Flux of the Natural Convection Boiling in Confined Channels," *Japan Society of Mechanical Engineering*, vol. 44, pp. 3908-3911, 1978.
- [102] I. V. M. V. Piro, "Rascetnoe Opređenje Predelnogo Teplovogo Potoka Pri Kipienii Zidkosteĵ v Dvuhfaznih Termosifonah," *Inz. Fiz. Journal*, vol. 53, pp. 376-383, 1987.
- [103] J. Jung, "Observations of the Critical Heat Flux Process During Pool Boiling of FC-72," *Journal of Heat Transfer*, p. 136, 2014.

## Bibliography

- [104] H. R. A. J. Johuara, "Experimental Investigation of Small Diameter two-phase closed thermosyphons charged with water, FC-84, FC-77 and FC-3283," *Applied Thermal Engineering*, vol. 20, pp. 201-211, 2010.
- [105] M. Mameli, L. Araneo, S. Filippeschi, L. Marelli, R. Testa and M. Marengo, "Thermal response of a closed loop pulsating heat pipe under variable gravity field," *International Journal of Thermal Sciences*, vol. 80, pp. 11-22, 2014.
- [106] L. Betancur, D. Mangini, L.K. Slongo, M. Mameli, K. De Paiva, M. Mantelli, M. Marengo, "Condenser Temperature Effect on the Transient Behavior of a Pulsating Heat Pipe," in *18th IHPC and 12th IHPS*, Jeju-do, South Korea, 2016.
- [107] Novespace, "A300 Zero-G Rules and Guidelines, RG-2009-2," France, 2009.
- [108] "Novespace Experiment design guidelines in parabolic flight," 11 May 2015. [Online]. Available: [http://www.esa.int/Our\\_Activities/Human\\_Spaceflight/Research/Parabolic\\_flights\\_guidelines](http://www.esa.int/Our_Activities/Human_Spaceflight/Research/Parabolic_flights_guidelines).
- [109] Z. Taylor, R. Gurka, G. Kopp and A. Liberzon, "Long-Duration Time-Resolved PIV to Study Unsteady Aerodynamics, Instrumentation and Measurement," *Instrumentation and Measurement, IEEE Transactions*, vol. 59, pp. 3262-3269, 2010.

## Bibliography

- [110] F. P. Incropera and D. P. DeWitt, "Chapter 8: internal flow," in *Fundamentals of Heat and Mass Transfer*, Wiley, 2007, pp. 485-558.
- [111] Y. Miyazaki and H. Akachi, "Heat transfer characteristics of looped capillary heat pipe," in *Proceeding of 5th International Heat Pipe Symposium*, Melbourne, Australia, 1996.
- [112] Y. Miyazaki and H. Akachi, "Self excited oscillation of slug flow in a micro channel," in *Proceedings of 3rd International Conference on Multiphase Flow*, Lyon, France, 1998.
- [113] Y. Miyazaki and M. Arikawa, "Oscillatory flow in the oscillating heat pipe," in *Proceeding of 11th International Heat Pipe Conference*, Tokyo, Japan, 1999.
- [114] S. Khandekar and A. Gupta, "Embedded Pulsating Heat Pipe radiators," in *Proceedings of 14th International Heat Pipe Conference*, Florianopolis, Brazil, 2007.



# Nomenclature

## Latin symbols

$a$	Acceleration, [ $\text{ms}^{-2}$ ]
$Bo$	Bond criterion number, []
$c_V$	Specific heat constant volume, [ $\text{Jkg}^{-1}\text{K}^{-1}$ ]
$d_{in}$	Diameter, [m]
$g$	Gravity acceleration, [ $\text{ms}^{-2}$ ]
$k$	Thermal conductivity, [ $\text{Wm}^{-1}\text{K}^{-1}$ ]
$k_{eq}$	Equivalent thermal conductivity, [ $\text{Wm}^{-1}\text{K}^{-1}$ ]
$L$	Length, [m]
$m$	Mass, [kg]
$\dot{m}$	Mass flux, [kg/s]
$Pr$	Prandtl, []
$Q$	Heat power, [W]
$T$	Temperature, [K]

$t$	Time, [s]
$V$	Volume, [m <sup>3</sup> ]
$x$	Axial coordinates, [m]
$y$	Axial coordinates, [m]

Greek

$\vartheta$	Inclination between gravity and flow path,
$\mu$	Viscosity, [m <sup>2</sup> /s]
$\rho$	Density, [kgm <sup>-3</sup> ]
$\sigma$	Surface tension, [Pa s]

Subscripts

$f$	Fluid
$l$	Liquid
$sat$	Saturated conditions
$v$	Vapor

**Acronyms**

DAQ	Data Acquisition System
ESA	European Space Agency
ID	Inner Diameter
ISS	International Space Station
JAXA	Japan Aerospace Exploration Agency
LS	Liquid Slug or Slice
MELT	Multi-Evaporator Loop Thermosyphon
OD	Outer Diameter
PET	PolyEthylene Terephthalate
PHP	Pulsating Heat Pipe
PFC	Parabolic Flight Campaign
SPHP	Space Pulsating Heat Pipe



TRL

Technological Readiness Level

